Corso di dottorato di ricerca in

SCIENZE BIOMEDICHE E BIOTECNOLOGICHE

Ciclo 33°

Titolo della tesi

Role of post-translational modification in *KRAS* expression: interplay between PARP1, Reactive Oxygen Species and G-quadruplex DNA

Dottorando

CINQUE GIORGIO

Supervisore

Prof. LUIGI E. XODO

Co-supervisore

ANNALISA FERINO, PhD

Anno 2021

“Pain is inevitable.

Suffering is optional.”

Haruki Murakami

“*What I Talk About When I Talk About Running”*

Summary

1 Abstract 4

2 Pancreatic Cancer 7

3 RAS 10

3.1 KRAS signalling in pancreas 13

3.2 Targeting KRAS 16

4 G-Quadruplex, a non canonical DNA/RNA structure 21

4.1 G4 presence in genomes 23

4.2 G4s as therapeutic target 24

5 Oxidation 27

5.1 ROS and cancer 28

5.2 8-oxo-7,8-dihydroguanine 31

5.3 8-OG and G-quadruplex 32

6 PARP1 and PARylation 34

6.1 PARP1 role in cells 37

6.2 PARP1 and cancer 38

6.3 PARP1 vs oncogene G4s 39

6.3.1 PARP1 vs *CKIT* G4 40

6.3.2 PARP1 vs *CMYC* G4 40

6.3.3 PARP1 vs telomeres G4 41

6.3.4 PARP1 vs *KRAS* G4 42

7 Aim of the work 43

8 Results and discussion 46

9 Conclusions 88

10 References 91

11 Acknowledgments 108

1 Abstract

More than 90 % pancreatic ductal adenocarcinomas (PDACs) carry mutations in exon 1 of the *KRAS* gene causing the malignant transformation of the cells. One main function of mutant *KRAS* is to reprogram the metabolism in PDAC to generate biomass and reducing power to fuel a high rate of proliferation.

Previous studies have demonstrated that the *KRAS* promoter contains a G-rich sequence located immediately upstream of the transcription start site (TSS). Our laboratory reported for the first time that this sequence (called 32R or G4 near) can fold in a non-canonical DNA structure, called G-quadruplex (or G4) under physiological conditions. This discovery was done in 2006 and since then many questions about the biological functions of this unusual G4 structure have been raised. Two years later, our laboratory reported that the *KRAS* G4 is recognized by several transcription factors (TFs) including MAZ, hnRNP A1, Ku70 and PARP1. We therefore hypothesized that the G4 structure could play a role in the mechanism controlling the transcription of the *KRAS* oncogene.

PDAC cells having a high metabolic rate produce more reactive oxygen species (ROS) than healthy cells. Higher intracellular levels of ROS are toxic as they promote the oxidation of lipids, proteins and DNA. Among the four nucleobases, guanine, having the lowest redox potential, is prone to oxidation to 7,8-dihydro-8-oxoguanine (8OG). In fact, previous data from our laboratory revealed that an increase of oxidative stress results in a higher level of 8OG in the promoter region containing the G4 structure than in non-G4 guanine-rich genomic regions. This guanine lesion is likely to behave as an epigenetic mark for the recruitment of MAZ and hnRNP A1 to the promoter. An important observation reported in this thesis is the existence of a strict correlation between *KRAS* and oxidative stress, as an increase of ROS significantly stimulates the expression of the gene. An insight into the mechanism activating *KRAS* transcription was obtained when we focused on PARP1, as this protein was seen to be associated to the KRAS promoter region encompassing the G4 motif. We reasoned that this protein could be involved in the mechanism controlling transcription because when ROS are enhanced in PDAC cells, PARP1 is recruited to the KRAS promoter in the region near to TSS.

PARP1 (Poly-ADP-Ribose Polymerase 1) is a nuclear protein that catalyses the transfer of poly ADP-ribose units (a post translation modification called PARylation) or mono ADP-ribose unit

(MARylation) onto target proteins, including itself. PARP1 is known to take part to the base excision repair (BER) mechanism by which an oxidized base is recognized, excised and repaired.

In addition to its involvement in BER, the data accumulated during my PhD work clearly indicate that PARP1 plays also an important function in the KRAS promoter as a transcription factor. We found that PARP1 tightly binds to the critical G4 structure formed by the 32R G4 motif. We foundthat PARP1 forms two DNA-protein complexes of stoichiometry 1:1 and 1:2 with a cooperative type of binding. In addition, as PARP1 contains multiple Trp residues in its DNA-binding domain, we followed its binding to G4 by measuring the quenching of the Trp fluorescence upon addition of G4 to a PARP1 solution. The fluorescence data confirmed a 1:2 stoichiometry.

We also observed that upon binding to the folded G4, but not a linear DNA strand, PARP1 undergoes auto PARylation, acquiring a net negative charge. We reasoned that PARylated PARP1 may behave as an anionic platform for the recruitment of nuclear factors that are cationic in nature under physiological conditions like MAZ (pI = 8.1) and hnRNP A1 (pI = 9.2). According to this model, G4 and PARP1 play together a key role in activating the transcription of *KRAS*. The G4 structure near to TSS attracts, via PARP1, the transcription factors for the formation of the transcription pre-initiation complex. This is indeed confirmed by pulldown experiments carried out with biotinylated G4s and a nuclear extract from PDAC cells. We found that the G4 baits pulled down indeed all the proteins forming the multiprotein complex: a finding corroborating the initial hypothesis that the G4 upstream TSS behaves as an antenna for the recruitment of transcription factors. This idea is supported by the fact that when the cells are treated with an oligonucleotide mimicking the *KRAS* G4, the expression of *KRAS* is strongly inhibited because the exogenous G4 molecules sequester the transcription factors essential for *KRAS* transcription.

The key role played by PARP1 in the *KRAS* promoter is evidenced by the fact that when the PARP1 gene is silenced by a specific siRNA, or when the catalytic activity of PARP1 is inhibited by a small molecule (Veliparib) we found that the *KRAS* expression was dramatically reduced. Taken together, these results provide evidence that PARP1 inhibition is a validated strategy to arrest PDAC cell proliferation.

Besides elucidating the role played by PARP1 in activating KRAS transcription, we addressed also the issue about the recognition of PARP1 by the G4 formed by the 32R motif. A recent NMR study

reported that 32R folds in two structurally different G4 conformers (namely G25T and G9T) that are in slow equilibrium one another. We found by EMSA that both conformers interact with PARP1, forming stable DNA-protein complexes. However, pulled down assays showed that G25T has a higher capacity than G9T to form a multiprotein complex. Further experiments are required to clarify the role, if any, of G9T.

2 Pancreatic Cancer

The pancreas is an abdominal glandular organ whose major part is located behind the bottom half of the stomach (Figure 1, [1]). Morphologically and functionally it can be divided into an exocrine (composed of acinar and ductal cells) and an endocrine (made of islets of Langerhans) pancreas. Exocrine pancreas displays digestive functions: acinar cells secret lipases, proteinases and amylases into pancreatic duct and finally reach small intestine to break down fats, proteins, and carbohydrates for absorption [2]. Endocrine pancreas is composed of five different Langerhans islets that synthesizes and secretes a specific hormone: insulin (β-cells), glucagon (α-cells), somatostatin (δ-cells), pancreatic polypeptide (PP cells), and ghrelin (ε-cells) [2].

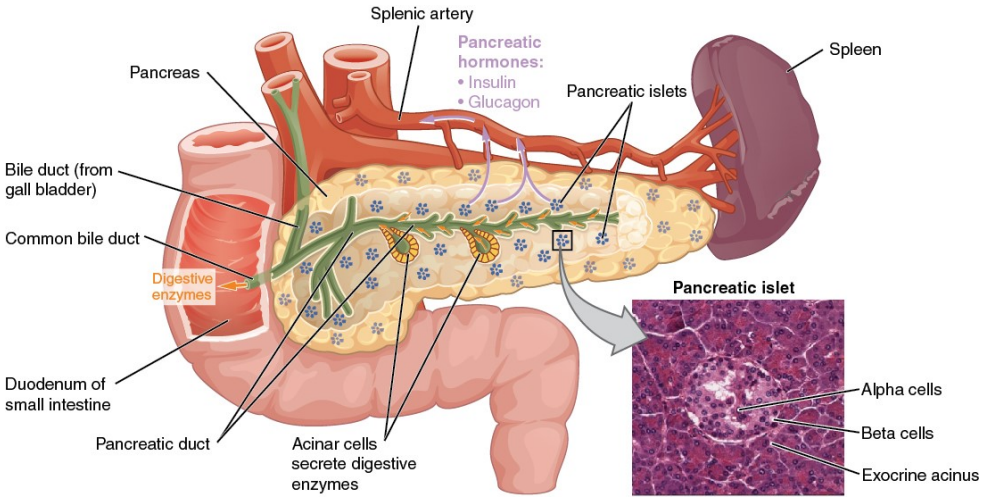

Figure 1. A view of the pancreas. Bottom right: a micrograph of the pancreatic islets (Betts, J. G., Young, K. A., Wise, J. A., Johnson, E., Poe, B., Kruse, D. H., … De Saix, P. (2013). The endocrine pancreas. In Anatomy and Physiology. OpenStax.)

When malignancies occur, this organ can give rise to three different tumour types: pancreatic neuroendocrine tumour (PNET) from the endocrine portion, pancreatic ductal adenocarcinoma (PDAC) and acinar cell carcinoma from the exocrine one [3]. PDACs are originated from five distinct precursor lesions: pancreatic intraepithelial neoplasias (PanINs), intraductal papillary mucinous neoplasms (IPMNs), intraductal tubulopapillary neoplasms (ITPNs), intraductal oncocytic papillary neoplasms (IOPNs), and mucinous cystic neoplasms (MCNs). All of them

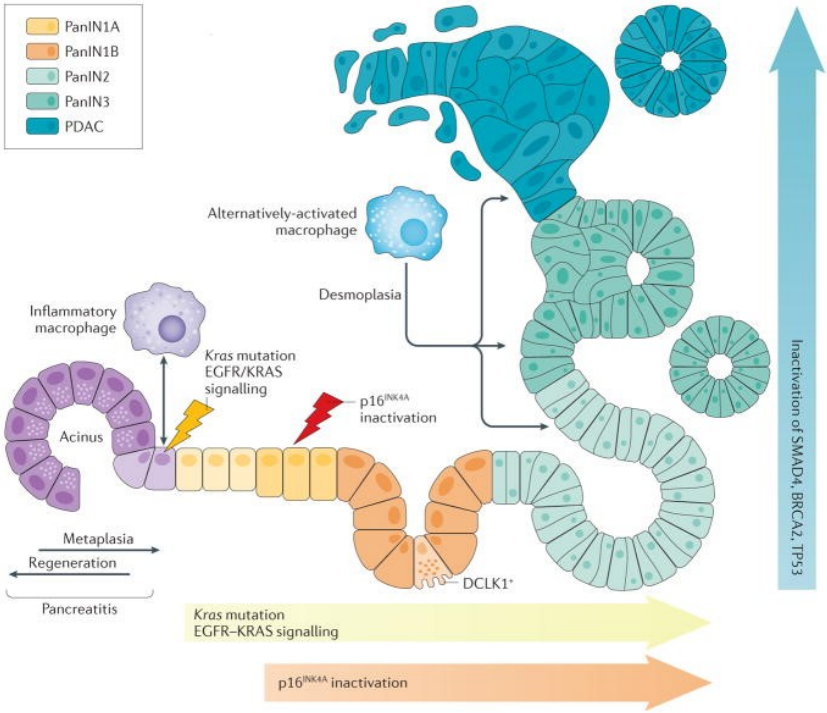

Figure 2. Schematic representing how inflammatory macrophages and genetic alterations contribute to ADM and further cell progression toward pancreatic cancer cells (Storz, 2017)

harbour different histological features, as well as mucin glycoprotein expression pattern and genetic alterations [4]. PanINs are the best known PDACs precursor lesions. The early step is known as acinar-to-ductal metaplasia (ADM), a process in which acinar cells regress to a more embryonic progenitor cell state in which they express ductal markers [5]. Despite the common reversibility of the process during pancreatitis or injury, murine acinar cells driven by oncogenic $KRAS^{G12D}$ not only are impaired in redifferentiation, but also further progress to duct-like cells that form precancerous PanIN 1A or 1B (early dysplastic) or PanIN 2 lesions (increasing levels of dysplasia). High-grade dysplasia PanIN 3 and PDAC phenotypes are achieved through further factors including: loss of cyclin-dependent kinase inhibitor 2A, inactivation of tumour suppressor genes (i.e. Tp53, Brca2, Smad 4) and inflammation (Figure 2, [5]).

PDAC is the fourth most frequent cause of cancer-related deaths worldwide with a 5-year overall survival of less than 8% [6]. In the last decades, several attempts have been made for a proper PDACs classification (reviewed in [7]), which led to the important conclusion that pancreatic cancer can't be managed as one disease [7]; consequently, there's a urgent demand of tailored cures. In 2016, Bailey and co-workers provided a classification of PDACs starting from 456 samples collected after surgical resection [8]. They described four subtypes with distinct genes programs.

- *The Squamous subtype*. Gene reprogramming is addressed to networks involved in inflammation, hypoxia response, metabolic reprogramming, TGF-β signalling, MYC pathway activation, autophagy and upregulated expression of TP63ΔN and its target genes;
- *The Pancreatic Progenitor subtype*. Transcriptional networks containing transcription factors pivotal for cell-fate determination towards a pancreatic lineage and those linked to fatty acid oxidation, steroid hormone, drug metabolism and glycosylation;
- *The Immunogenic subtype*. Associated immune gene programmes included B cell signalling pathways, antigen presentation, CD4+ T cell, CD8+ T cell and Toll-like receptor signalling pathways.
- *The Aberrantly Differentiated Endocrine Exocrine (ADEX) subtype*. Key genes in their network are those involved in acinar cell differentiation, pancreatitis/regeneration and endocrine differentiation.

Currently, four genes resulted to be directly involved in the development of PDAC with different frequency through pancreatic cancer samples: *KRAS* (90%), *CDKN2A* (90%), *Tp53* (70%) and *SMAD4* (55%) [9]. *KRAS* is a GTPase proto-oncogene that will be discussed in the next section. The other three critical genes are tumour suppressor genes implicated in the control of cell cycle regulation (CDKN2A), in cellular stress response (Tp53) and in signalling mediated by transforming growth factor β, TGF-β (SMAD4).

3 RAS

The RAS oncogene proteins are the founding members of GTPases superfamily, which is divided into five major branches on the basis of sequence and functional similarities: RAS, Rho, Rab, Ran and Arf [10]. RAS family is composed of 36 members, among which Kirsten Ras (KRAS) (included isoforms KRAS4A and KRAS4B), Neuroblastoma Ras (NRAS) and Harvey Ras (HRAS) are the main components.

Investigation of RAS started in 1960s from the isolation of transforming retroviruses able to induce sarcomas in mice, rats, cats, monkeys, chickens, turkeys and potentially transform cells in culture [11]. First sarcoma viruses were isolated in 1964 by Jennifer Harvey [12] and three years later by Werner Kirsten [13], from whom they were named Harvey and Kirsten sarcoma viruses, respectively (Ha-MSV and Ki-MSV). In 1974 Scolnick and colleagues found that these viruses held rat sequences within their genomes, hence suggesting that sarcoma formation might be related to normal cells that underwent malignant transformation [14]; at that time, genes we now know to be *Ras* were named as variants of *src* genes. Further studies performed by Scolnick proved the cellular origin of Harvey and Kirsten viruses (hereafter called *HRAS* and *KRAS*, from rat sarcoma); furthermore, these genes encode 21 kDa proteins that bind GDP and GTP, they are associated with the plasma membrane; when overexpressed, these proteins can turn cells into malignant counterpart and the key event is the GTP preferential binding (summarized in the review [11]). In 1982 a report by Cooper and colleagues stated that the transforming genes of human bladder and lung carcinoma cell lines are homologous to the transforming genes of Harvey and Kirsten sarcoma viruses [15]. Finally, in 1983 sequences of both normal and transformed HRAS and KRAS were provided.

RAS-related proteins can be distinguished from the rest of the GTPases superfamily for the “G-domain” that undergoes conformational change upon GDP-GTP switch [16]. Structure of KRAS4B is shown in Figure 3 [17].

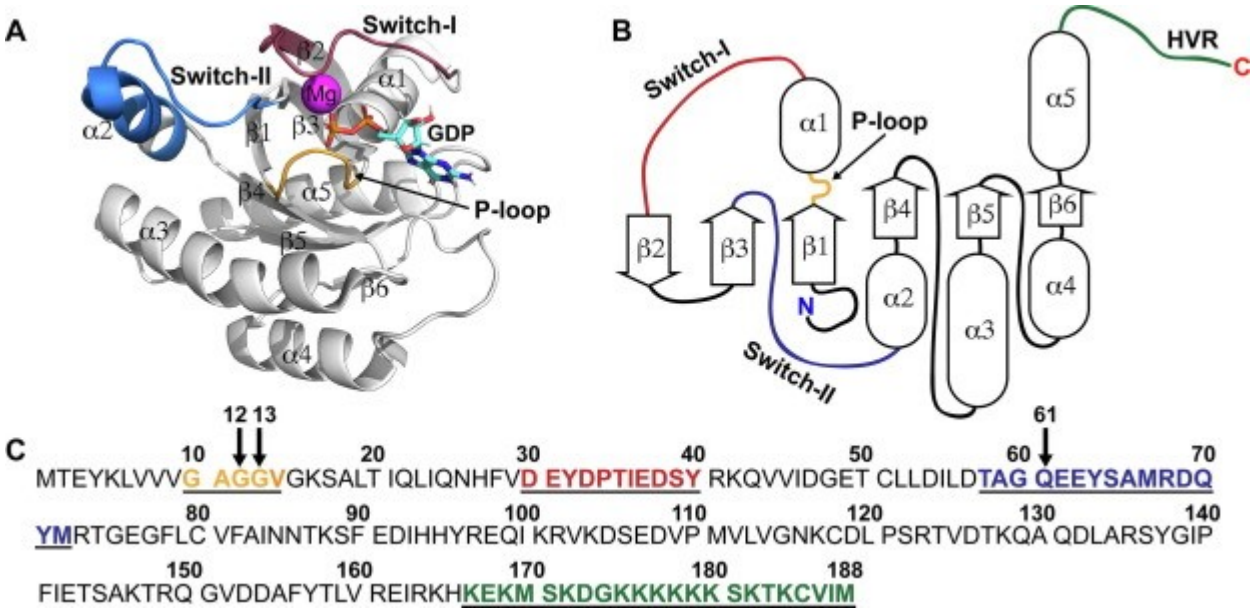

Figure 3. A) GDP-bound KRAS 4B crystal structure ; B) 2D representation of KRAS 4B secondary motifs; C) Linear sequence of KRAS 4B. Arrows indicate the most common mutational hotspots. Structural regions in all panels are highlighted with the following colour scheme: P-loop (residues 10–14), orange; switch-I (residues 30–40), red; switch-II (residues 58–72), blue; HVR (residues 167–188), green (Pantsar, 2020).

H-, N- and KRAS genes encode for 188-89 residues proteins that share almost 90% of homology sequence, with some differences in the primary structure [16]. The most important common features among these proteins are the membrane targeting domain and the G domain.

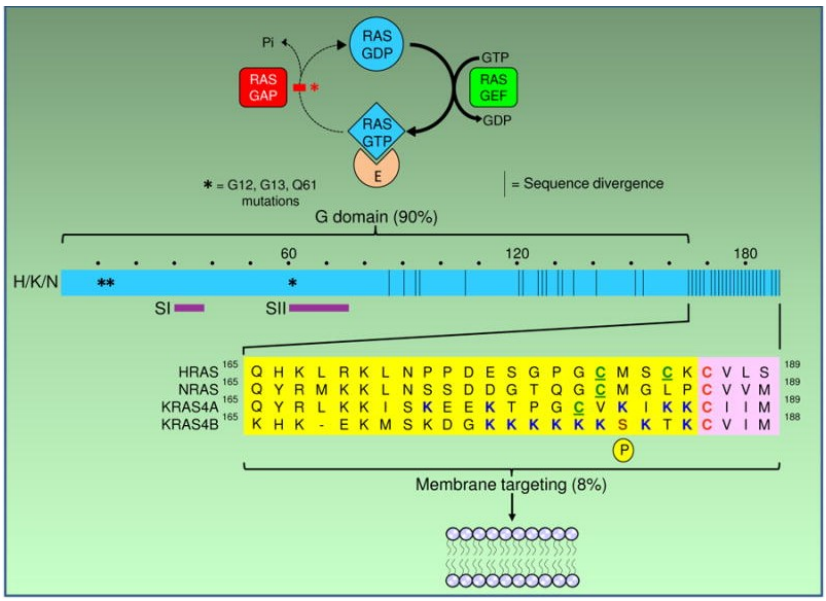

Figure 4. Top: molecular insight of KRAS switch mechanism. When bound to GTP, it interacts with effectors (E) for downstream signaling. Middle: overall sequence of Ras proteins. G-domain displays the highest homology degree among Ras members. Asterisks label most common mutational hotsposts. SI = switch region 1; SII = switch region 2. Bottom: detailed sequences of hypervariable C-terminus where lipid post-translational modification occurs. Pink box: CAAX motif. (Cox et al., 2015)

C-terminus is the site where a crucial post-translational modification occurs to keep KRAS anchored to the cytosolic site of plasmatic membrane: the addition of a lipid anchor. C-terminus is a hypervariable region (illustrated in Figure 4, bottom); despite RAS proteins here display lowest homology degree, they share a common pattern in the last four residues, known as "CAAX motif" (C = cysteine, A = aliphatic amino acid, X = any amino acid, but commonly serine or methionine) [18]. Once translated, RAS undergoes farnesylation: briefly, farnesyltransfeRase (FTase) catalyzes the thioether linkage formation between a 15-carbon farnesyl polyisoprene unit and the cysteine of the CAAX motif. Farnesylated-RAS displays higher affinity toward endoplasmic reticulum whereas it undergoes cleavage of AAX amino acids by RAS converting CAAX endopeptidase 1, also known as RAS converting enzyme 1 (RCE1); finally, the carboxy end of cysteine gets methylesterified by isoprenylcysteine carboxylmethyltransfeRase (LCMT). This final reaction results in mature Ras with higher affinity toward plasma membrane where it migrates.

G domain is where GTP-GDP switch occurs. Secondary structure encompasses six β-strands, forming the protein core, surrounded by five α-helices (Figure 3). G domain harbours two regions referred to as Switch 1 (SW1) and Switch 2 (SW2), that change conformation when γ-phosphate is released upon GTP hydrolysis [19] and contain crucial residues for nucleotide and Mg^{2+} coordination [20]. The P-loop, also known as Walker A motif, is located between the 10^{th} and the 17^{th} residue and is shared among ATPases and GTPases [21], [22]. P-loop wraps tightly around the GTP β-phosphate group [23]. Mutations in this sequence dramatically affect RAS behaviour, leaving the protein in a constitutive GTP-bound active state.

GTP-bound KRAS indicates signalling pathway is on, whereas the GDP-bound points out signalling is switched off. Two proteins promote this transition: GTPase Exchange Factor (GEF), which aids the exchange of GDP in favour of GTP, and GTPase Activating Protein (GAP) that induces the hydrolysis of GDP that turns off KRAS signalling. Cancer-associated RAS genes display missense mutations that encode single amino acid substitutions primarily at one of three mutational hot spots: glycine-12 (G12), glycine-13 (G13), or glutamine-61 (Q61). These mutations render RAS persistently GTP-bound and constitutively active regardless extracellular stimuli. Persistent activation of RAS results in the continuing stimulation of downstream signalling partners, which results in many of the phenotypic hallmarks of cancer including increased proliferation, the suppression of apoptosis, altered metabolism, alteration of the tumour microenvironment, evasion of the immune response, and metastasis [24].

3.1 KRAS signalling in pancreas

Oncogenic KRAS signalling in PDAC is highly complex and is thought to involve three major pathways: Raf/MEK/ERK, PI3K/Pdk1/Akt and the Ral GTPases pathway (Figure 5, [25]).

1. The Raf-MEK-ERK pathway (Figure 5, red dotted) comprises the major part of the mitogen-activated protein kinase (MAPK) pathway system, and the A-, B- and C-Raf kinases are on the top of this cascade. Once KRAS is active, Rafs are recruited to the membrane when they get phosphorylated. Activated RAF phosphorylates kinases MEK1 and MEK2, which in turn activate the serine–threonine kinases ERK1 and ERK2. Interestingly, despite $KRAS^{G12D}$ is a shared mutation both in PDAC and non-small cell lung cancer, C-Raf is required for tumour development only for the latter, whereas it displays only little effect on pancreatic cancer [26], [27]. In mice, pancreas-specific expression of the $B\text{-}Raf^{V600E}$ oncogene leads to the rapid formation of multifocal PanIN lesions [28].

2. The PI3K/PTEN/AKT pathway (Figure 5, green dotted) is a second well-characterized RAS effector pathway in pancreatic cancer. Among membrane lipids, phosphoinositides are negatively charged constituents involved in intracellular signalling: they're formed by phosphorylation of hydroxyl groups on positions 3', 4', or 5' of the inositol ring of phosphatidyl inositol (PI) by PI 3'-OH kinase (PI3K). PI3Ks are composed of different catalytic subunits that belong to one of three classes (I, II and III). In PDAC, class I PI3Ks gets active upon GTP-KRAS stimulus; active PI3K stimulates the production of PIP3 (phosphatidylinositol 4,5-triphosphate) from PIP2 (phosphatidylinositol 4,5-biphosphate), which serves as recruitment platform for both AKT and the phosphoinositide-dependent kinase 1 (PDK1). AKT then gets activated via phosphorylation [25]. Phospho-AKT downstream signalling includes MTOR and RAC pathways. On the contrary, PTEN hydrolyses PIP3 into PIP2 by 3'-dephosphorylation [29]. Mutations in PI3K/PTEN/AKT pathway are so powerful that oncogenic class I $PI3KA^{H1047R}$ drives ADM, PanIN formation and adenocarcinoma in a PDAC mouse model even in the absence of oncogenic RAS; furthermore, these tumours displayed activated AKT and GSK3B at a level indistinguishable from oncogenic KRAS-driven tumours [25].

3. Ral GTPases (Figure 5, blue dotted) represent a third family of Ras effector molecules. Like other small GTPases, Ral cycles between the GDP-bound inactive state and GTP-bound active state in cells; likewise, they rely on RalGEFs to exchange GDP with GTP and RalGAPs to hydrolyse GTP into GDP. RalA and RalB are the two proteins involved in this branch [30]. Importance of this pathway in pancreatic cancer has been elucidated by Lim, Counter and colleagues: in a panel of pancreatic cancer cell lines and patient-derived tumours, RalA was found crucial for tumour initiation whereas RalB is more involved in tumour metastasis. Interestingly, RalA-RalB branch pathway seemed to be more activated in pancreatic tumour tissue than other Ras effector pathways [31], [32].

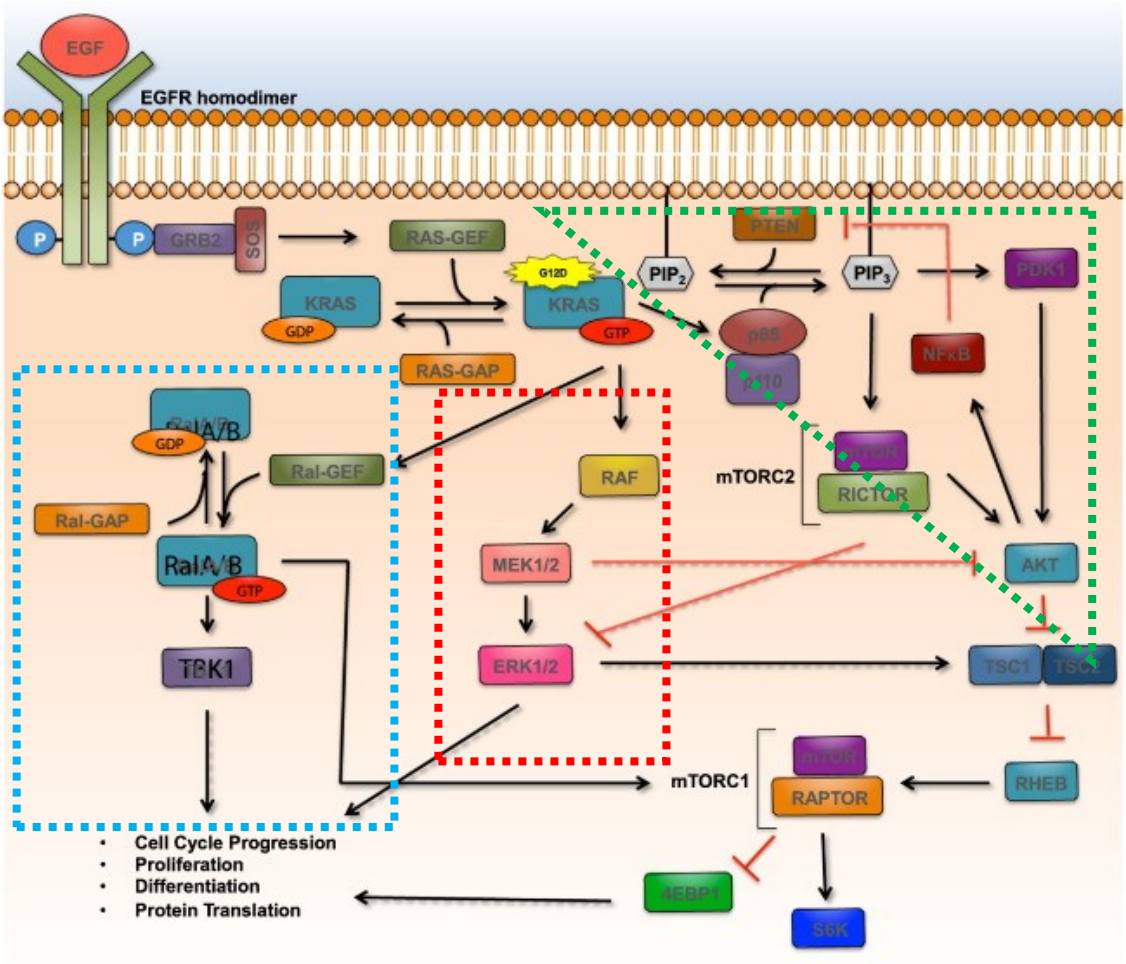

Figure 5. Overview of KRAS signalling cascade in pancreatic cancer (Mann K.M. et al., 2016)

It has been observed that many *RAS*-driven tumours strongly depend on the continued expression of oncogenic *KRAS* [33]. Indeed, recent studies support the notion that *KRAS* reprograms the metabolism in cancer cells in order to produce the biomass necessary to feed a

high proliferation rate [34], [35]. The dependence of the metabolism on specific oncogenes has led to the concept of “oncogene addiction”, according to which cancer cells although depending on a number of genetic aberrations, often develop a dependency on a particular oncogene [36], [37]. Recent data showed that oncogenic KRAS increases the glucose, glutamine and fatty acids uptake as well as their consumption in order to sustain the biosynthesis and to maintain the cellular redox homeostasis [38]. $KRAS^{G12D}$ directs part of the glycolytic flux into the hexosamine/glycosylation pathways and the pentose phosphate pathways (PPP) to produce ribose for nucleotide synthesis and reducing power (NADPH) [34]. Furthermore, *KRAS* mutant pancreatic cancer cells display quite a high consumption of glutamine and serine. As $KRAS^{G12D}$ inhibits the enzyme glutamate dehydrogenase GLUD1, which by converting glutamate into alfa-ketoglutarate channels glutamate into the Krebs cycle, Gln in the mitochondria is deaminated oxidatively into glutamate which is then transaminated with oxaloacetate into aspartate by GOT2. Asp is transported in the cytoplasm where it is reconverted to oxaloacetate, by the aspartate transaminase GOT1, then into malate and pyruvate by the malic enzyme $NADP^+$ - dependent. This unusual metabolic cycle induced by $KRAS^{G12D}$ increases the level of NADPH and

thus the cell redox potential [35] (Figure 6, right hand side [38]). In addition to glutamine, PDAC cells consumes a lot of serine. This is not surprising as serine is the amino acid that supplies one-carbon group to folic-acid pool, the vitamin necessary for the synthesis of the purine and pyrimidine nucleotides [39].

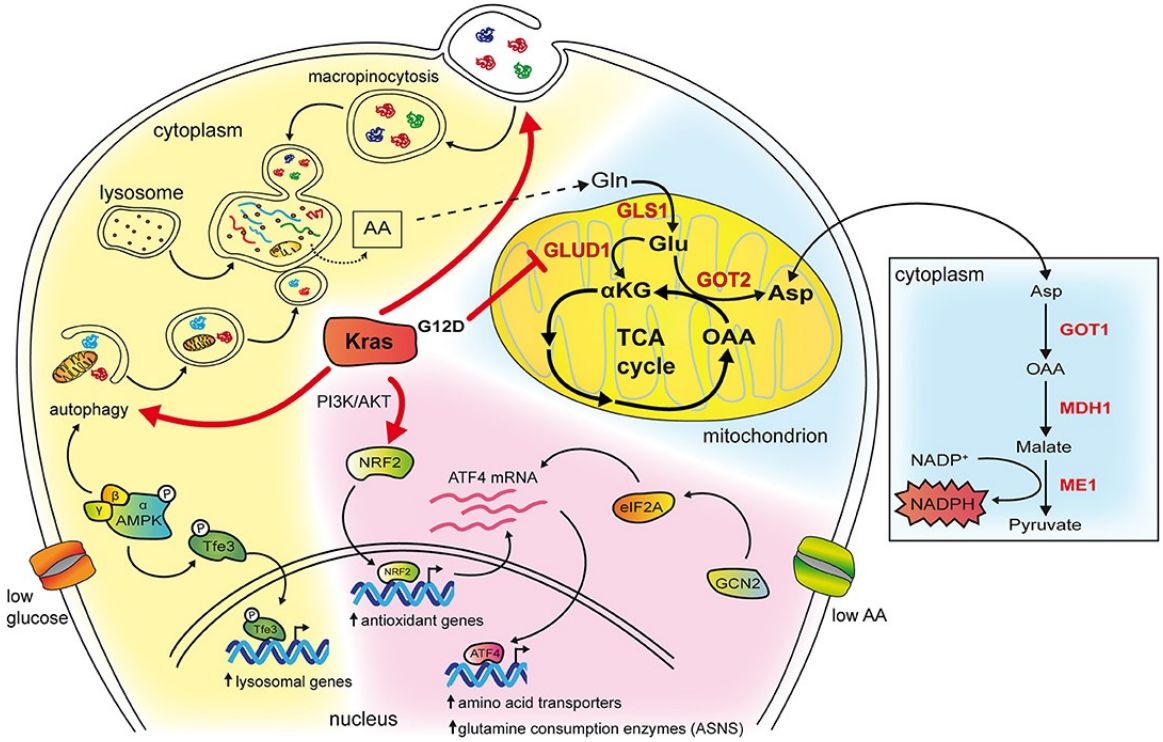

Figure 6. Some of the amino acid metabolism reprogramming to which KRAS^{G12D} is responsible. Pink-colored background is for pathway revealed in non small lung cell cancer (NSCLC), yellow-colored is for common pathways between PDAC and NSCLC. Mutant KRAS enhances both macropinocytosis and autophagy to provide an amino acid pool to sustain tumour growth. Among aa, glutamine is consumed through an alternative pathway: KRAS^{G12D} indeed inhibits glutamate dehydrogenase (GLUD1), preventing Gln to enter TCA cycle, and enhances glutamic-oxaloacetic transaminase (GOT2) that converts Gln into Asp. This latter gets further catabolized by cytosolic enzymes into pyruvate which, in turn, produce NADPH that boosts Reactive Oxygen Species (ROS) production (Pupo et al., 2019)

3.2 Targeting KRAS

As PDAC cells are addicted to oncogenic *KRAS*, this critical oncogene or its product, i.e. the KRAS protein, are regarded as suitable targets for the rationale design of anticancer drugs. In fact, genetically engineered mouse models showed that the initiation of PDAC is caused by oncogenic KRAS [34]. So far attempts to develop small-molecule inhibitors specific for the KRAS protein did

not give the expected results because the surface of the RAS protein lacks of a suitable hydrophobic pocket to host the inhibitor [40]. Alternative strategies on which many researchers focused their efforts are based on the development of inhibitors targeting the association of the KRAS protein to the plasma membrane, the downstream *KRAS* signaling and specific *KRAS*-dependent metabolic pathways [41]. Despite more than two decades of research, no anti-*RAS* drugs have yet reached the clinic, suggesting that KRAS is quite "undruggable". This notwithstanding, oncologists agree about the urgency for finding alternative and innovative strategies to treat *RAS*-driven cancers. Given the negative impact of PDAC in western countries, this represents one of the main challenges of the medical research for the near future.

Recent studies have focused on targeting the metabolic enzymes regulated by KRAS, including those of the glucose and glutamine metabolism and of the lipid homeostasis. It has been recently reported that in lung cancer mutant KRAS upregulates acyl-coenzyme A (CoA) synthetase long-chain family member 3 (ACSL3), which converts fatty acids into acyl-CoA esters to supply β-oxidation [42]. Moreover, mutant $KRAS^{G12D}$ drives a lipogenic gene-expression program to promote *de novo* lipogenesis to produce monounsaturated lipids which are less keen to peroxidation than the polyunsaturated analogues [43]. Synthetic lethal interactions have been widely investigated in cancer therapy, in particular the PARP-inhibitors for cancers deficient in the homologous recombination repair pathway seems one of the most promising [41].

The targeted therapies against KRAS that have been investigated in PDAC cells can be grouped into the following categories:

1. *MEK1/2 inhibitors*. This category includes trials with the purpose of targeting the KRAS MAPK signaling pathway. In the last decade, several trials were assessed to evaluate inhibitors efficacy: three phase 2 trials evaluated MEK inhibitors in combination with gemcitabine in locally advanced and/or metastatic PDAC; two phase 2 studies evaluated the role of dual inhibition of KRAS downstream pathways, selumetinib + erlotinib and selumetinib with MK 2206 (an AKT inhibitor) (reviewed in [44])

2. *Ras Farnesyl transferase inhibitions*. The mevalonate pathway provides all mammalian isoprenoids, a class of metabolites which serves as starting molecules for the synthesis of a conspicuous number of biomolecules i.e. steroids, bile acids, lipoproteins, vitamin D, heme A, ubiquinone, dolichol and isopentenyladenine [45]. Mevalonate is the reduction product of hydroxymethylglutaryl coenzyme A (HMG-CoA), catalyzed by HMG-CoA reductase; mevalonate is then converted into the 5-carbon precursor units isopentenyl pyrophosphate (IPP) and dimethylallyl pyrophosphate (DMAPP). Hereafter, each elongation step adds 5 carbon units: human farnesyl pyrophosphate synthase (hFPPS) produces the C-10 geranyl pyrophosphate (GPP) and then the C-15 isoprenoid farnesyl pyrophosphate (FPP), whereas the immediate downstream human geranylgeranyl pyrophosphate synthase (hGGPPS) enzyme elongates FPP substrate to the C-20 isoprenoid geranylgeranyl pyrophosphate (GGPP). As reported in Chapter 2, KRAS undergoes farnesylation onto the CAAX motif by the action of FTPase, a crucial post-translational modification to anchor KRAS to the inner layer of the cellular membrane. Noteworthily, when FTPase is inhibited, Ras proteins rely on geranylgeranyl phosphate transferase (GGTPase) to get prenylated and exert their function [46]. Several compounds were studied to evaluate their efficacy in PDAC patients, among which R115777 and Tipifarnib showed either low or no amelioration in clinical outcome [47]. Ongoing studies are investigating both geranyl-geranyl transferase and farnesyl transferase.

3. *Targeting the hydrophobic pocket of RAS protein*. Initial attempts to targeting the nucleotide binding domain showed that this strategy is difficult due to the high picomolar affinity of RAS protein towards the nucleotide GDP and GTP, which are present in the intracellular matrix at high micromolar concentrations. GDP-bound KRAS 4B can be stabilized by two ligands: 2-(4,6-dichloro-2-methyl-1H-indol-3yl)ethane-1-amine [48] and N-(2-[(1H-indol-3-yl)methyl]-1H-1,3-benzodiazol-5-yl)pyrrolidine-2-carboxamide [49]. In both case, the interaction prevents the formation of KRAS-GEF complex, and the latter displays greater affinity toward G12D mutated KRAS 4B form. Another promising compound was found by Xie et al. in 2017 [50], named 0375-0604. It binds with moderate affinity to the Switch I – Switch II region of mutant G12D, G12C and Q61H KRAS 4B selectively inhibiting proliferation of non-small lung cancer cells without any effect on

normal cells. This inhibition results in G2/M cell cycle arrest and reduced activation levels of AKT, CRAF and ERK pathways.

4. *Targeting either the promoter or the 5'-UTR/3'-UTR regions of kras gene*.

4.1 In the past years, our laboratory provided a number of different approaches to target KRAS expression in PDAC. Focusing on short non-coding micro RNAs, miR216b resulted atypically downregulated in pancreatic tumours, thus provided a good platform to develop a miR-based strategy to inhibit KRAS expression, hence PDAC viability [51]. Double-stranded miR-26b mimics, with unlocked nucleic acid (UNA) modifications in the guide strand, specifically suppress the KRAS gene in PDAC cells. Also UNA-modified single strand miRNAs turned out to be strongly active. The strategy was further validated when Panc-1 and Mia PaCa2 cells were treated with designed lipid-modified miR-216 delivers with palmityl-oleyl-phosphatidylcholine liposomes. Clonogenic assays showed that these siRNAs caused a marked decrease of cell growth [51].

4.2 KRAS 5'-UTR was found to adopt a non canonical nucleic acid structure, known as G-quadruplex (see "G-Quadruplex, a non canonical DNA/RNA structure" section). Stabilization of this structure is a key element to prevent KRAS translation [52], [53]. Small anthrafurandione (ATFD) and anthrathiophenedione (ATPD) molecules tested in our lab strongly induce apoptosis and reduce the metabolic activity and colony formation of Panc-1 cells [54]. Recently, another common G4 ligand has been used both *in vitro* and *in vivo* to evaluate its effect on PDAC cells: porphyrin TMpyP4. Our lab improved its permeability to cells by increasing its degree of lipophilicity with the attachment of a C14 or C18 alkyl chain [55]. These alkylated porphyrins bind efficiently to the KRAS and NRAS transcripts at the G4 structures located in 5'-UTR causing the breakdown upon photoirradiation of mRNA. This resulted in a strong reduction of Panc-1 metabolic activity; moreover, C14-porphyrin reduces cell growth of a Panc-1 xenograft and induce apoptosis [55].

4.3 In the late 1980s, Perucho and Jordano found that the promoter of human KRAS gene reveals a G-rich nuclease-hypersensitive element (NHE), upstream of the transcription start site /TSS), which is essential for transcription [56], [57]. In 2006, our laboratory demonstrated for the first time that NHEs can adopt under physiological conditions a stable G4 structure that serves as a recruitment platform for different nuclear proteins [58]. In the light of these findings, the design of oligonucleotides mimicking KRAS quadruplexes (G4 decoys) should sequester these proteins and block transcription. Experiments carried out in our laboratory showed that the G4 decoys inhibit KRAS expression, cell growth and colony formation in pancreatic cancer cells [59].

4 G-Quadruplex, a non canonical DNA/RNA structure

1953 was the year zero for DNA. James Watson and Francis Crick discovered DNA common structure is a double helix, known as B-DNA [60]. The two DNA strands run antiparallelly and are kept together by hydrogen bonds between base pairs (A with T, G with C). Moreover, B-DNA is made of two grooves named major and minor grooves. Duplex DNA can adopt two further conformations: A-DNA (a thicker right-handed duplex) and Z-DNA (left-handed, with a pronounced zig-zag pattern in the phosphodiester backbone). In addition to the canonical structure (Fig. 2A), DNA can form non-canonical DNA structures such as triplex, tetraplex of guanines (G-quadruplex), i-motifs and junction structures, including a cruciform (four-way junction) consisting of two hairpin and a three-way junction (Figure 7) [61].

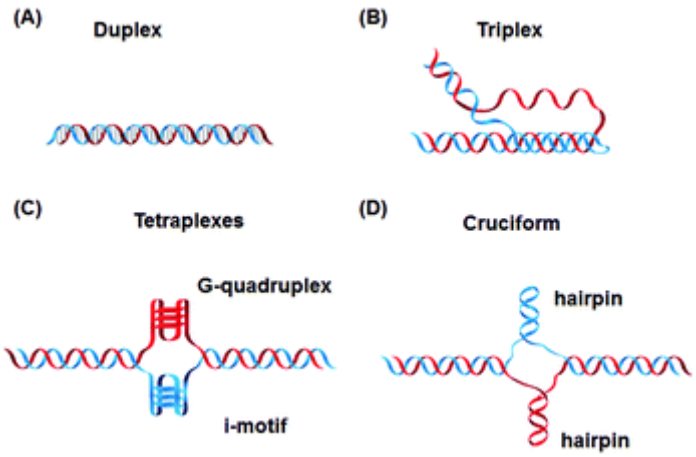

Figure 7. Structure of both canonical and non-canonical DNA structures (Tateishi-Karimata and Sushimoto, 2020)

In 1910 Bang reported that a concentrated solution of GMP (25 mg/ml) at pH 5 becomes viscous and forms a gel, suggesting the formation of a high-order structure [62]. About a half century later, Gellert et al. reported that guanylic acid has the ability to form tetrameric structures by self-association [63]. In the 80's, two groups reported conserved DNA sequences of telomeres are able to fold into a so-called G-quadruplexes (G4) structures *in vitro*, providing the first example ever of a DNA trait to adopt such structure [64], [65].

G- quadruplexes are non canonical DNA structure that take place into both DNA and RNA G-rich strands. They're made of two or more G tetrads that stack on top of each other, in which single guanines derive from one G rich tract, known as G-run. In each tetrad, guanines are kept together by Hoogsteen-like hydrogen bonds between neighbouring bases: N1-H····O6 and N2-H····N7. In the centre, a monovalent cation stabilizes this structure, i.e. K^+ (the major monovalent cation in

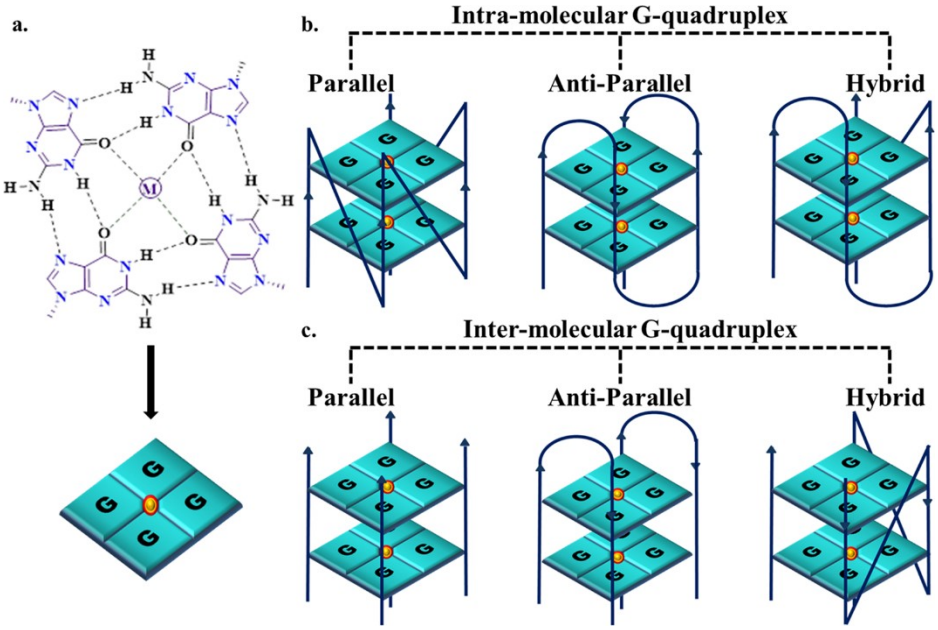

Figure 8 Structure of G quadruplex; a) A G tetrad seen from above, in which 4 guanines are kept together by Hoogsteen bonds and coordinated by a monovalent cation (M) in the center; b;c) Different topologies adopted by G quadruplex (Majee et al., 2020)

the cells), Na^+ or NH_4^+, but also bivalent cations like Mg_2^+ or Ca_2^+ (Figure 8a, [66]).

G4s structures display a variety of topologies that can arise from the intra- or inter-molecular folding of G-rich strands (Figure 8b;c, [66]): in the first case G-runs come from the same strand, whereas inter-molecular folding occur upon dimerization or tetramerization of separate filaments. The number of G stacks in the quadruplex, as well as the length and the composition of loops which take no part to the tetrad formation affect thermal stability of G quadruplex. Strands orientation is the criterium according to which G4 can be classified into: parallel, antiparallel or hybrid. Orientation is strictly correlated with the *anti* or *syn* conformational state of the glycosidic bond between guanine and sugar [67]: the *anti* conformation characterizes a parallel folding, while antiparallel G4s are found to adopt both *syn* and *anti* orientations [68].

4.1 G4 presence in genomes

Given the rising interest toward G4s and their role in biology, many bioinformatic tools have been developed to find putative G4 sequences in genomes [69], [70]. Potential G4 forming sequences can be described as follows:

$$G_m - X_n - G_m - X_o - G_m - X_p - G_m$$

Where "m" is the number of G bases in each G run, usually involved in the tetrad formation; X_n, X_o, and X_p can be any combination of residues, including G, that take part in the loops [67]. For instance, a $G_3 - X_{1-7} - G_3 - X_{1-7} - G_3 - X_{1-7} - G_3$ consensus sequence input on the human genome revealed that it contains over 300,000 sequences that have the potential to form G-quadruplexes [71]. G4s distribution is non random: they are mainly abundant onto promoters, telomeres, ribosomal DNA, untranslated region (UTR) of mRNA, micro- and mini-satellite repeats, borders between introns and exons and immunoglobulin heavy chain switch regions [72], [73].

Presence of putative G4 sequences (pG4s) has been described also in plants , bacteria and human DNA and RNA viruses [15]. Moreover, topoisomerase I in *S. cerevisiae* yeast was found to have crucial role in suppressing a number of genome rearrangements related to G4 formation upon transcription [74].

G4s were found to affect transcription and translation level in cells. Evolutionally speaking, G4s were kept in regulatory regions of genes, especially promoters and close to the transcription start site [71]. A great step beyond has been made by the production of a G4-specific antibody (BG4) [75]: based on that, it was reported existence of G4 within cells and its formation to rely on cell cycle [75]; furthermore, HeLa cells tested with BG4 provided evidence that G4s are present both in telomeric regions and elsewhere in the chromosomes [76]. Employing G4-forming condition and combining features of the polymerase stop assay with Illumina next-generation sequencing, almost 700,000 G4 structures were revealed, especially within many oncogenes such as *BRCA1, BRCA2, MAP3K8, MYC, TERT, AKT1, FGFR3, BCL2L1, CUL7, FOXA1, TUSC2* and *HOXB13* [77]. Starting from the previous approach, Balasubramanian and co-workers implemented this technique using the BG4 specific antibody as a probe to perform a G4-specific ChIP-seq. The number of G4 structures (~10,000 G4 ChIP–seq peaks) is substantially lower than was predicted by computation or observed by G4–seq. Interestingly, G4 enrichment in cancer genes i.e. *MYC*,

PTEN and *KRAS* was found in immortalized HaCaT cell line compared to physiological NHEKs cells, suggesting a link between G4 occurrence and transcriptionally active chromatin state. Overall, this can be explained in two ways: either a possible suppressive role played by heterocromatin in the formation of G-quadruplexes or higher sensibility displayed by G4 ChIP-seq than BG4 immunostaining [78].

4.2 G4s as therapeutic target

Given its biological relevance in cancer development, G4s have stimulated researchers mind to design molecules able to bind and stabilize them so to prevent unfolding, thus oncogene expression. Drug design basically follows two G4 features: it's made of a large π-surface and it carries a negative charge. In the light of this, candidate drug should have both a positive charge and a large π-surface as well [79]. Some of these molecules are reported in Figure 9 [80]. A549 lung cancer cells stop proliferating, thus undergoing cell death, upon high-dose treatment with porphyrin TMPyP4 or its derivative TPyP4-Pt [81]. Upon irradiation with either visible or near infrared light, porphyrin molecules display their effect releasing Reactive Oxygen Species (ROS); as discussed in next section, ROS release is a promising approach to induce tumour cell death because they can cause extensive DNA damage overcoming antioxidant response triggered by cancer cells. Interestingly, G4 ligands and NHEJ regulatory factors DNA-PK, PARP1 or WRN, display synergistic effect [82] in a synthetic lethality-like fashion (explained in "PARP1 and cancer" section). Indeed, HeLa and U2OS cancer cell lines exposed to the WRN inhibitor NSC-19630 display higher sensitivity toward G4 ligand telomestatin [83]. Similarly, treatment of HT29 human colon cancer xenografts with a combination of the G4 ligand RHPS4 and the PARP1 inhibitor GPI results in a 50% reduction in tumour weight and an increase in the survival rate of mice by 45%, which is higher than that obtained by treatment with either RHPS4 or GPI alone [84].

In PDAC, MM41, a tetra-substituted naphthalene diimide derivative, was found to sensibly decrease MIA PaCa-2 pancreatic cancer growth *in vivo* [85]. Starting from MM41, Marchetti, Neidle and colleagues designed another naphthalene diimide G4-binding compound (2,7-bis(3-morpholinopropyl)-4-((2-(pyrrolidin-1-yl)ethyl)amino)benzo[lmn][3,8]phenanthroline-1,3,6,8(2H,7H)-tetraone, called CM03) [86]. CM03 was found to down-regulate key pathways to maintain PDAC phenotype, including hippo signalling, axon guidance, and endocytosis. CM03

shows potent antiproliferative activity *in vitro*, as well as *in vivo* antitumoural action in mouse xenograft model of PDAC [86].

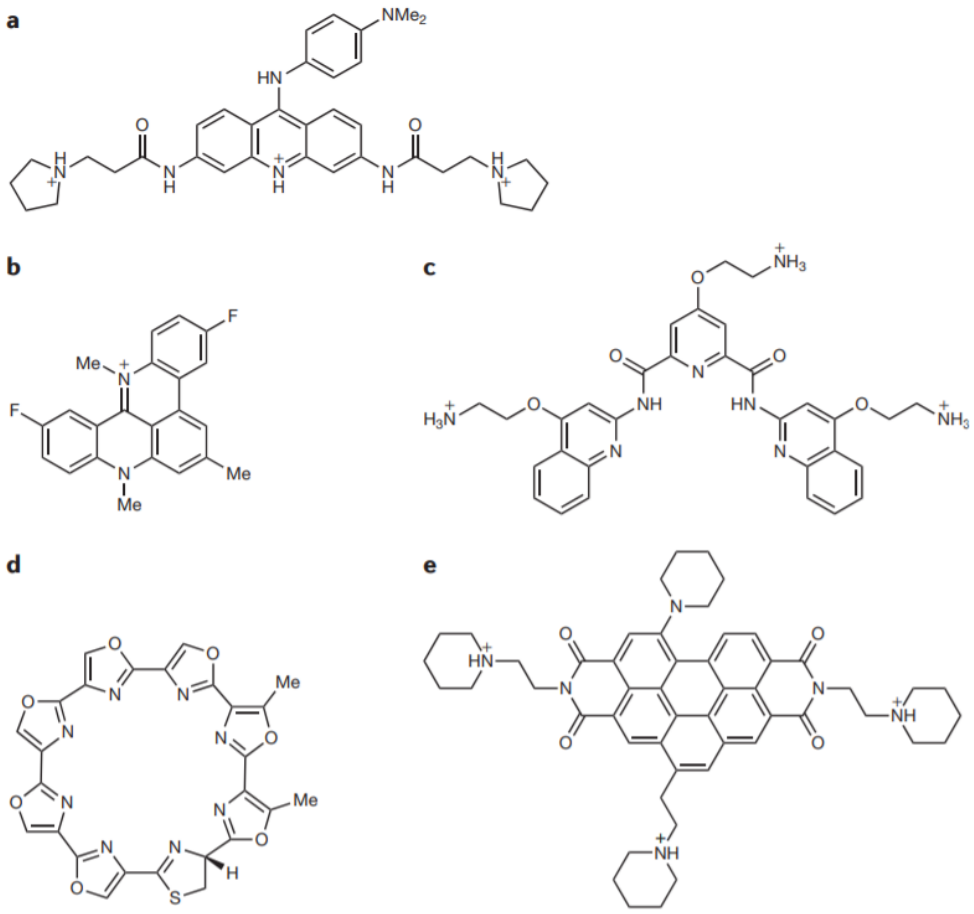

Figure 9. Some of the G4 targeted molecule used for anticancer therapies. a. A 3, 6, 9-trisubstituted acridine ligand, BRACO-19; b. 3,11-Difluoro-6,8,13-trimethyl-8H-quino[4,3,2-kl]acridinium methosulfate (RHPS4). C. An N, N'-bis(quinolinyl)pyridine-2,6-dicarboxamide derivative, pyridostatin. d. Telomestatin. e. A tetra substituted perylene derivative, EMICORON91. (Neidle S., 2017)

Our laboratory focused on alternative G4 ligands in the last years. Anthrafurandione **2a** and its anthrathiophenedione analogue **2b** (Figure 10, left, [54]) were found to bind and stabilize KRAS 5'-UTR preventing translation, thus remarkably reducing viability of Panc-1 and BX PC3 cell lines as reported by detection of apoptotic caspase 3/7 and annexin/propidium iodide staining and reduced metabolic activity, as well as colony formation. More recently, tetra-meso(N-methyl-4-pyridyl) porphyrin (TMPyP4), a G4-binding validated compound, was derivatized with alkyl group of different length (Figure 10, right, [55]): this modification resulted not only in increased KRAS G4 5'-UTR affinity, but also in a more efficient cellular uptake and cytoplasmatic localization in

PDAC cells. Once photoactivated, these compounds generate ROS that break down RNA structure, with consequent apoptosis induction.

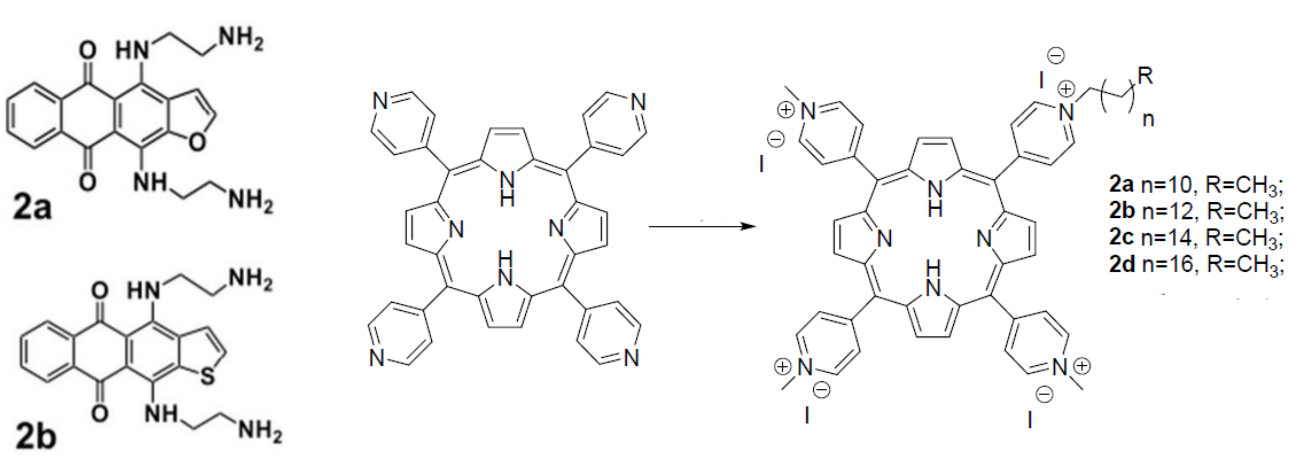

Figure 10. Left: structure of Anthrafurandione 2a and its anthrathiophenedione analogue 2b (adapted from Miglietta et al., 2017). Right: structure of 5-(4-N-alkylpyridyl)-10,15,20-tri(4-N-methylpyridyl)- 21H,23H-porphyrine (P4) and its alkyl-derivatized analogues (adapted from Ferino et al., 2020)

5 Oxidation

Aerobic organisms rely on oxygen for all biological process in their life. Adenosine triphosphate (ATP), the energy-vector in cells, is made by oxidative phosphorylation in which nutrients-derived electrons are directed by mitochondrial enzymes to reduce O_2 into H_2O: this chain of reactions allows to create a proton gradient used to drive ATP formation. Conversion of O_2 into H_2O is not a quantitative reaction: when only one electron is transferred to molecular oxygen, it gives birth to an anion radical: the superoxide anion ($O_2{\cdot}^-$) [87], [88], one of the member of Reactive Oxygen Species (ROS). ROS can be also deliberately produced by specific enzymes in a strictly controlled manner, i.e. mitochondrial NADPH oxidases. They produce ROS by transferring electrons from NADPH via FAD and across two non equivalent hemes to molecular oxygen, the electron acceptor [89]. Superoxide anion can also be additionally produced by two enzymes: xanthine oxidase and cyclooxygenases. The first is a form of xanthine oxidoreductase that oxidizes GMP-derived hypoxanthine and AMP-derived xanthine into uric acid; this enzyme plays an important role in the catabolism of purines in some species, including humans [90]. Cyclooxygenase-1 and cyclooxygenase-2 (COX-1 and COX-2) instead are involved in the transformation of arachidonic acid (a polyunsaturated fatty acid) into prostaglandin H2, a substrate for cytosolic synthases that produce pro-inflammatory mediators [91]. $O_2{\cdot}^-$ can react with nitric oxide from NOS synthases activity with formation of peroxynitrite ($ONOO^-$), which plays a role as cytotoxic effector molecule

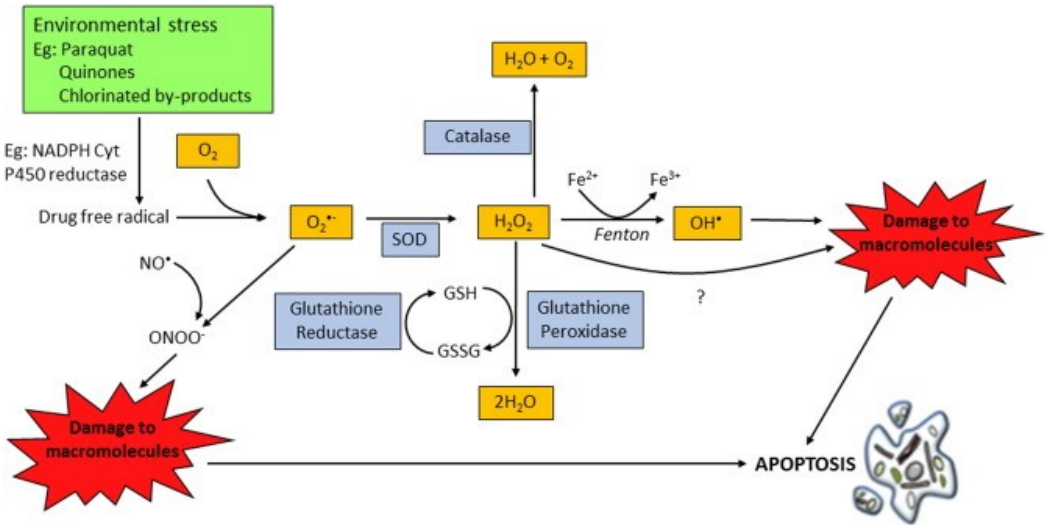

Figure 11. Extrinsic (i.e. environmental stress) and intrinsic (i.e. mitochondrial electron transport) factors contribute to free radicals generations. First ROS produces is superoxide ($O_2^{\bullet-}$), which either reacts with nitric oxide ($NO^{\bullet}$) to produce peroxynitrite ($ONOO^-$), or undergoes dismutation to generate hydrogen peroxide (H_2O_2), in a reaction catalyzed by superoxide dismutase (SOD). H2O2 can either be tackled by antioxidant systems such as catalase and GSH/glutathione peroxidase, or can generate hydroxyl radical ($OH^{\bullet}$) by the iron-catalyzed Fenton reaction. Extensive ROS and RNS damage to macromolecules can lead cells to trigger apoptosis pathways (Redza-Dutordoir and Averill-Bates, 2016)

against invading organisms such as bacteria and unicellular parasites that could be phagocytized by macrophages or neutrophils [92]. As depicted in Figure 11, superoxide anion may undergo dismutation to generate hydrogen peroxide (H_2O_2), a reaction catalysed by superoxide dismutase (SOD). In the presence of Fe^{2+}, H_2O_2 can be converted into hydroxyl radical ($^{\bullet}OH$) able to cause severe damage to DNA and lipids. The presence of Fe^{2+} has been reported to be common in mitochondrial environment, as aconitase holds a $[4Fe\text{-}4S]^{2+}$ cluster highly susceptible to oxidation: Kennedy et al. suggested the $[4Fe\text{-}4S]^{2+}$ aconitase is oxidized by superoxide, generating the inactive $[3Fe\text{-}4S]^{1+}$ aconitase. In this reaction, the likely products are Fe^{2+} and hydrogen peroxide. Consequently, the inactivation of m-aconitase by superoxide may increase the formation of $^{\bullet}OH$ through the Fenton reaction [93].

Excess of ROS is tackled by two antioxidant system: enzymatic and non-enzymatic. The first one is made of a battery of enzymes including superoxide dismutase (SOD), catalase (CAT), glutathione peroxidase (GPx), and glutathione reductase (GR), whereas the non enzymatic one comprises scavenging free radicals molecules, i.e. glutathione, flavonoids, vitamin A, C and E [94], [95].

5.1 ROS and cancer

At low to modest doses, ROS are considered to be essential for the regulation of normal physiological functions involved in development such as cell cycle progression and proliferation, differentiation, migration and cell death [96]. In contrast, tumour cells produce elevated level of ROS to sustain their growth, resulting in enhanced cell proliferation, increased cellular growth, cell survival and in the development of cancer through the regulation of mitogen activated-protein kinase (MAPK)/extracellular-regulated kinase 1/2 (ERK1/2), phosphoinositide-3-kinase (PI3K)/Akt and protein kinase D (PKD) signalling pathways, negative regulation of phosphatases, PTEN and protein tyrosine phosphatase 1B (PTP1B), regulation of nuclear factor kB (NF-kB) activating pathways, as well as mutations in transcription factors and tumour suppressor genes including Nrf2 and p53 [97].

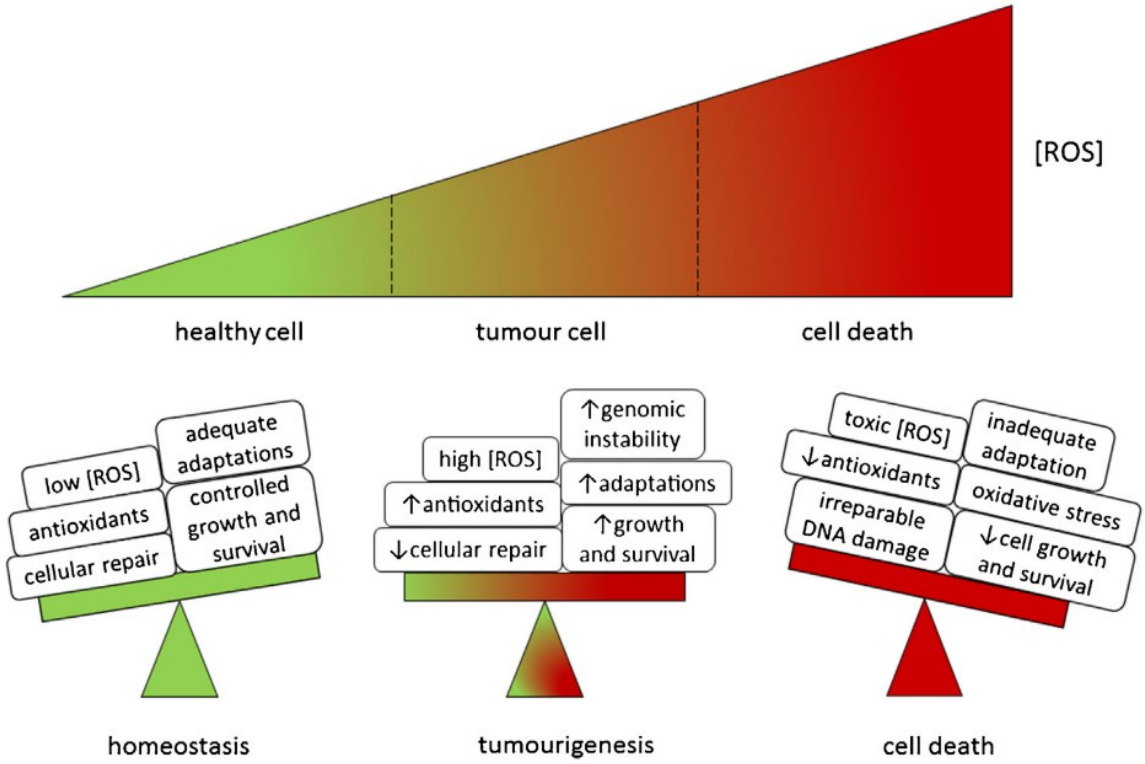

Figure 12. ROS balance is crucial for cell fate. Homeostasis is characterized by balanced generation of ROS, sufficient antioxidant activity and uncompromised cellular repair pathways. On the contrary, tumour cells rely on enhanced metabolic activity that lead to higher ROS production and, consequently, genomic instability. To counterbalance augmented oxidative stress, tumour cells increase antioxidant response while keeping pro-tumorigenic signalling. If ROS level rises furtherly, tumour cells show insufficient adaptation and undergo cell death (Moloney and Cotter, 2018)

As reported in Figure 12, tumorigenesis is kept by a delicate ROS balance between homeostasis and death [97]. Overproduction of ROS in tumour cells must be kept under control or these can undergo cell death. ROS adaptation in cancer cells is driven by enhancing their antioxidative defence to lower ROS levels and by inducing autophagy to reduce the oxidative damage to biomolecules and organelles [98]. ROS-driven boosting of oncogene expression is the same responsible of the antioxidant defence enhancement: i.e. activation of endogenous KRAS (G12D), B-Raf (V619E) and MYC (ERT2) led to lowering of intracellular ROS due to the increased transcription of Nrf2 and elevation of the basal Nrf2 antioxidant program [99]; moreover, thioredoxin and glutathione pathways seem to synergize to drive cancer progression [100]. Nuclear factor erythroid2-related factor 2 (Nrf2) is a potent transcription activator belonging to the Cap'n'Collar (CNC) transcription factor family; along with Kelch-like ECH-associated protein 1 (KEAP1), they constitute the main defence mechanism against cell redox balance alterations. Under normal conditions, Nrf2 is constitutively kept inactive by CUL3-KEAP1 E3 ubiquitin ligase complex and subjected to degradation by proteasomes [101]. Upon oxidation, Nrf2 is freed from

CUL3-KEAP1 control and migrates into the nucleus to switch on antioxidant response element (ARE) or electrophile response element (EpRE) genes, including: peroxiredoxin (PRDX), superoxide dismutase (SOD), catalase, glutathione reductase, thioredoxin, thioredoxin reductase and glutathione peroxidase [102]. As stated earlier, Nrf2 overexpression promotes tumorigenesis preventing ROS level to rise beyond the toxic level threshold. As reviewed by de la Vega et al., Nrf2 plays both direct and indirect roles in each of the cancer hallmarks: sustained proliferative signalling, insensitivity to antigrowth signals, resistance to apoptosis, limitless replicative power, sustained angiogenesis, tissue invasion and metastasis, metabolic reprogramming, tumour-promoting inflammation, avoiding immune destruction, genomic instability, altered redox balance and proteotoxic stress [103].

In PDAC, $KRAS^{G12D}$ activates Nrf2 via MAPK pathways; in turn, Nrf2 switches on a series of anti-oxidant genes and also mediates an unusual metabolic pathway of glutamine to generate NADPH (see Figure 6). An interesting interplay between ROS, KRAS and Nrf2 in pancreatic cancer cells has been recently provided by our lab [104]. Treatment with a ROS-producer molecule stimulates KRAS expression in PDAC cell lines which, in turn, upregulates Nrf2 expression. KRAS-induced Nrf2 lowers ROS level, which results in the upregulation of pro-survival Snail and the downregulation of pro-apoptotic RKIP. Interestingly, PDACs rarely display somatic mutations in either the KEAP1 or Nrf2 genes; hence, the Nrf2-mediated antioxidant program in PDAC is exclusively activated by oncogenic KRAS [105].

In case of toxic level of ROS, both intrinsic and extrinsic apoptosis pathways are triggered, leading to cell death by intrinsic apoptotic signalling in the mitochondria or extrinsic apoptotic signalling by death receptor pathways [97]. Oxidative stress can cause from mild to severe damage to biomolecules such as membranes, lipids, proteins, lipoproteins, and DNA. In physiological conditions cysteine residues that exist as anion thiolates (Cys-S-) are more susceptible to oxidation if compared to the protonated thiol form Cys-SH. Oxidation of this protein residues results into the abundancy of the sulfenic form (SO-), which causes allosteric modification in protein conformation altering its function. In the case of DNA, the most common product of oxidation is 8-oxo-7,8-dihydroguanine (8-OG).

5.2 8-oxo-7,8-dihydroguanine

8-OG is generated through the introduction of an oxo group on the carbon 8 (C8) and the addition of a hydrogen atom to the nitrogen at position 7 (N7) of deoxy-guanine [106]. Guanine results the most susceptible base to oxidation, resulting the most electron rich among the bases [107]. It is estimated that up to 100,000 8-OG lesions can be formed daily in DNA per cell [108]. The 8-OG lesion is particularly threatening, given its ability to camouflage as a T base when in the *syn* conformation, resulting in a stable 8-OG(*syn*): A(*anti*) base pair (Figure 13, [109]). Hence, replicative DNA polymerases incorporate C and A opposite 8-OG; thus, the repair system for this lesion must convert both 8-OG:C and 8-OG:A mispairs into a G:C pair. If 8-OG is excised from 8-OG:A and the gap is filled subsequently with DNA polymerase, a G→T transversion results.

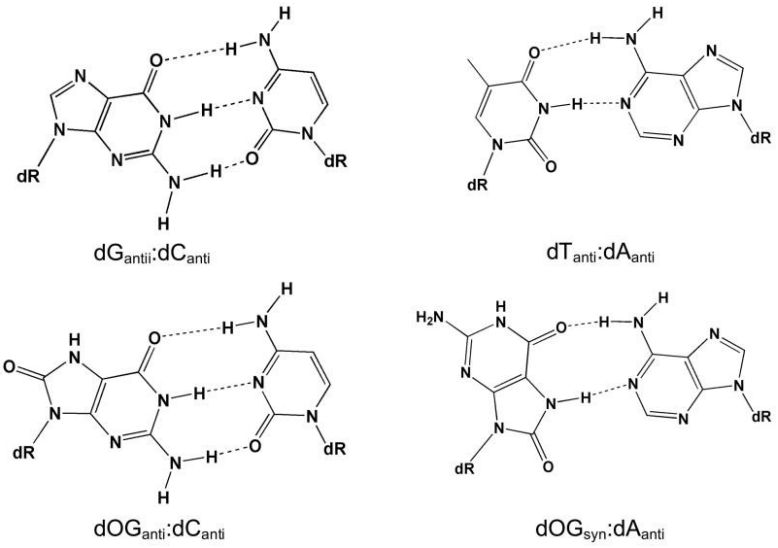

Figure 13. Top: canonical G:C and A:T pairing. Bottom: 8-oxoguanine is able to pair either with C when in anti conformation (leading to template and polymerase distortions), or with A in syn conformation (generating G:C → T:A transversion) (David et al., 2007)

Organisms have evolved mechanisms to escape from oxidative damage. First description was in *E. coli* with the "GO-system", yet evidences indicated this system is shared among other prokaryotes and eukaryotes. Prokaryotes system is made of three enzymes: MutT, MutY, MutM; their corresponding part in humans are MTH1, OGG1 and MUTYH. Repair of 8-OG is achieved by base excision repair (BER), starting with 8-OG removal when base paired with C by the action of 8-oxoguanine glycosylase 1 (OGG1) in mammals; in contrast, when OG is incorrectly base paired with A, MutY DNA glycosylase (MUTYH) removes the A allowing a second chance for a polymerase

to insert C opposite OG for further action by OGG1. Following removal of 8-OG by OGG1, an abasic site (AP) is formed that is a substrate for apurinic/apyrimidinic endoDNase I (APE1) to cleave the 5'-phosphodiester linkage yielding a nick in the DNA. The repair process is completed by polymerase β (POLB) that removes the sugar fragment at the nick site followed by inserting the correct G nucleotide, and finally ligase (LIG) seals the nick to return the DNA back to its native state [110].

5.3 8-OG and G-quadruplex

When 8-OG occurs in a G4-folded structure, it can affect both its physical and chemical features. When guanine gets oxidized, the N7 hydrogen bond acceptor on G is lost in turn of an O8-carbonyl with significative consequences on G4 stability (Figure 14, [111]).

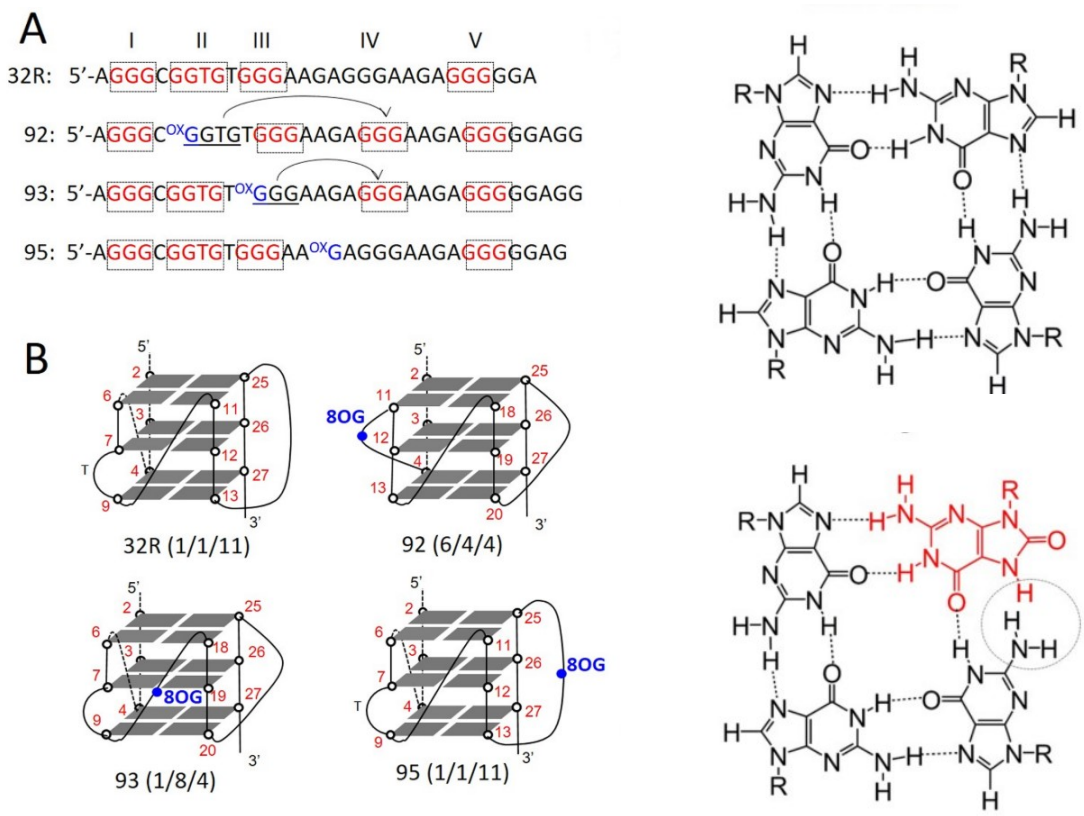

Figure 14. Effect of 8-OG location in G4 formation of KRAS promoter. A. WT G4 proximal sequence of KRAS promoter (32R) and three different oxidized forms (92, 93 and 94) lodging 8-OG in different positions. G-runs involved in tetrad formations are highlighted in red. Arrows indicate alternative G-run replacing the one where 8-OG is present. B. Different topology of G4 proximal sequence of KRAS promoter according to 8-OG location. Right hand side: when 8-OG (red labelled) occurs within a G tetrad, one hydrogen bond is missing, thus inducing G4 destabilization (Ferino et al., 2018)

Analysis on VEGF by Burrows' group [112] and KRAS promoter by our lab [111] provided evidence that, in case of oxidation within a G-run involved in tetrad formation, a fifth G-run takes its place to keep the stability of the fold. Furthermore, the new topology assumed by the G4 sequence in the KRAS promoter displays a decreased melting point as result of a reduced stability [111]. Such plasticity was also reported for human telomeres when a G4-core G was replaced by either guanidinohydantoin or inosine [113]. Common in these cases is the presence of a fifth G-run that, according to Burrows and Fleming hypothesis, may serve as a "spare tire" in case 8-OG falls in a G-run crucial for the quadruplex formation [88].

Noteworthily, presence 8-OG in the G4 can affect protein recruitment: in oxidized G4, pulled-down proteins amount (including MAZ, hnRNP A1 and PARP1) is higher than this recovered from the wt bait. PARP1 was indeed the object of our investigation.

6 PARP1 and PARylation

Poly(ADP-ribosyl)ation (PARylation) is a post translational modification firstly described half a century ago. In the early 1960s, Collier, Honjno and collegues found that toxicity of diphtheria toxin relied on NAD^+ to inhibit mammalian protein synthesis [114]–[116]. First description of a DNA-dependent poly-ADP-ribose producing reaction starting from NAD^+ was made by Mandel and co-workers [117]. The poly(ADP-ribose) polymerase (PARP) family of proteins is responsible for catalysing this reaction; this includes 17 members encoded by different genes and displaying a conserved catalytic domain homologous to the diphtheria toxin ART fold responsible for the PARylation (this explains why PARPs are also known as ART diphtheria toxin-like (ARTD) enzymes [118]). PARylation in the covalent attach of ADP-ribose unit on glutamate, aspartate, arginine, lysine and serine residues either on PARP itself (auto-PARylation) or other target proteins (PARylation) [119].

PARPs and their homologous are present in almost every domain of life, from bacteria [120], archaea [121] to eukaryotes, with the exception of yeasts [122]. PARP enzymes can be structurally and functionally divided into five subclasses: DNA-dependent PARPs, TankyRases, CCCH PARPs, PARPs with macro-domain and unclassified PARPs [123]. Moreover, PARPs can be divided into three groups according to their catalytical activity: PARPs capable of PARylation with His-Tyr-Glu (H-Y-E) triad (“ART signature”) in their active site, PARPs capable only of mono ADP-ribosylation activity (MARylation) and PARPs inactive protein (they lack NAD^+ binding site) [119].

PARP1 is thought to account for more than 90% of the PARylation activity upon DNA damage [124]. PARP1 PARylation consists in a SN1-like reaction mechanism [125] that can be summarized into three steps: (i) the attachment of the first ADP-ribose monomer to the acceptor protein (initiation); (ii) the formation of a (2’-1’’) ribose-ribose glycosidic bond (elongation) and (iii) the formation of a (2’’- 1’’’) ribose-ribose bond between ADP-ribose units (branching) (Figure 15) [126].

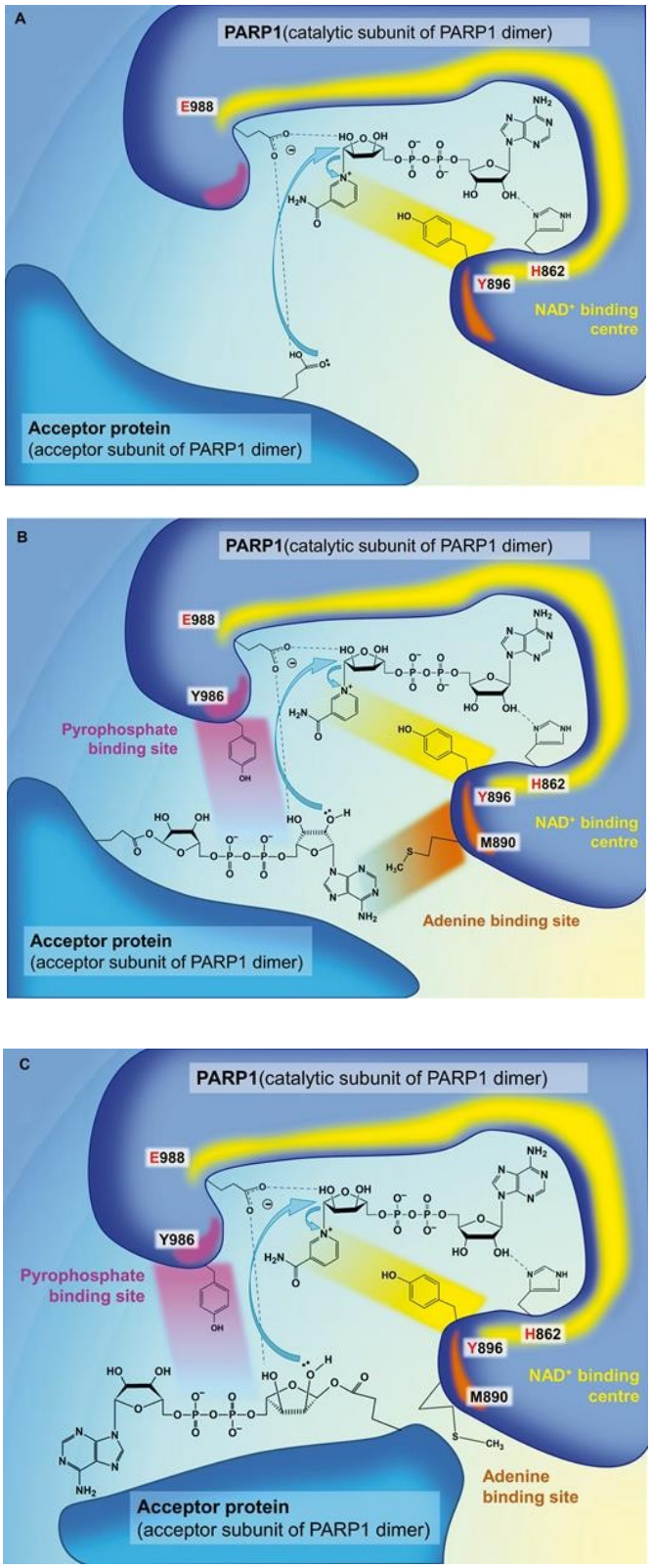

Figure 15. PARP1 reaction mechanism. A) Initiation step. B) Elongation step. C) Branching step. Key amino acids H-Y-E forming the catalytic core are highlighted in red. M890 and Y986 residues were also found crucial for reaction (Alemasova and Lavrik, 2019).

PAR turnover is very fast and de-PARylation is carried out by a number of glycohydrolases including PAR glycohydrolase (PARG), terminal ADP-ribose protein glycohydrolase 1 (TARG1), ADP-ribosylhydrolase 3 (ARH3), MacroD1 and MacroD2, and Nudix-Type Motif 9 and 16 (NUDT9, NUDT16) [119]. PARG is the main enzyme involved in PAR catabolism: it exhibits both exo- and endo-glycosidase activities responsible of glycosidic bond cleavage between ADP-ribose units [127]. As summarized by Tanuma and co-workers in a recent review, PARP and PARG inhibition leads to different cell damage: whereas PARP blockade induces necroptosis, PARG inhibition provokes extensive DNA damage triggering apoptosis [128].

PARP1 structure has been extensively studied by Pascal group. The modular structure consists of six domains (Figure 16, [129]).

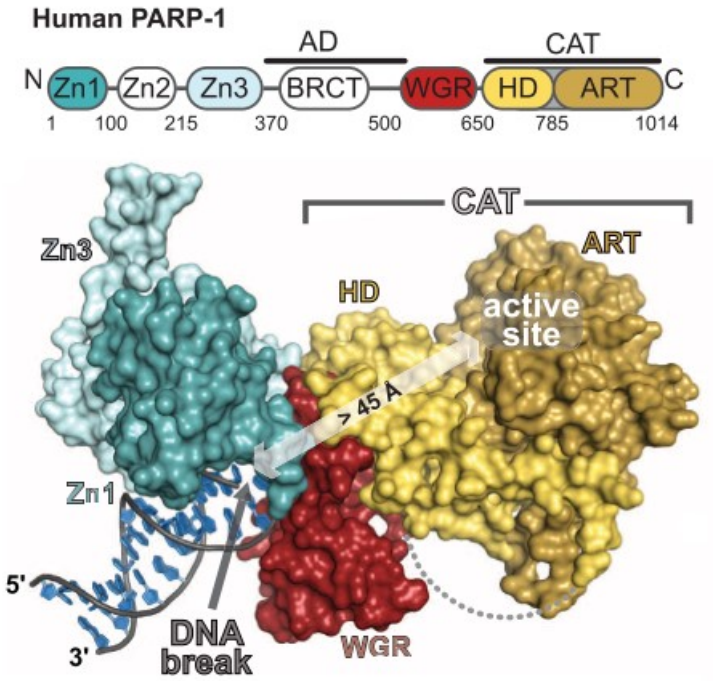

Figure 16 PARP1 structure. Top : modular architecture of PARP1. Zn1, Zn2, Zn3 = zinc-binding domains; AD = auto-modification domain ; BRCT = BRCA C-terminus domain; CAT = catalytic domain, with the two subdomain that is made of: helical subdomain (HD) and the catalytic ART core. B) Representation of PARP1 wrapped around DNA (Langelier et al., 2012)

At the N-terminus we find two homologous zinc-finger domains, Zn1 and Zn2, belonging to PARP-like zinc finger family: these zinc fingers are the sentinel for DNA breaks and, whenever they detect one, they contact a continuous segment of the DNA backbone (“the backbone grip”) and the nucleobases that were exposed at the DNA end (“the base-stacking loop”) [130]. A third zinc

finger has been discovered in 2008 [131], whose structure and roles have been elucidated three years later: Zn3 domain harbours a zinc ribbon structure completely unrelated from Zn1 and Zn2 domains and it's involved in the catalytic turnover of the DNA-dependent PAR synthesis reaction, in activated PARP1 assembly upon DNA damage and in compacting chromatin structure [132]. The auto-modification domain is located in the centre of the enzyme and it contains a BRCA1 C-terminus domain (BRCT) involved in protein-protein interaction [129], [133]. WGR domain is made of three residues (Tryptophane-Glycine-Arginine) whose function is linked to recognition of DNA strand breaks in a structure-specific and sequence-independent manner [130]. W residue in particular is essential for initiating DNA-dependent release of DNA from PARP1 [134]. Finally, the catalytic domain consists of a helix domain (HD) and the catalytic core known as ADP-ribosyltransferase domain (ART) at the far end of the C terminus. ART domain contains a donor site where ADP-donor is positioned for transferase reaction and comprises: a nicotinamide-binding pocket (included is the catalytic triad made of His-Tyr-Glu, known as "ART signature"), a phosphate binding site and an adenine-ribose-binding site [126]. ART domain also includes an acceptor site that binds either the PARylation target during initiation or the distal ADP-ribose monomer of the growing PAR chain ('acceptor') during elongation/branching stages [126]. Helical domain (HD) was found to display an inhibitory action toward PARP1 activity: when PARP1 is bound to DNA damaged site, HD get displaced from nicotinamide binding pocket in the ART domain, allowing NAD^+ to enter the catalytic site [135].

In a free-state, these domains are connected by flexible linkers like 'beads on a string' [136]; upon DNA damage recognition, PARP1 undergoes a conformational change in favour of its catalytically active state. It remains unclear whether PARP1 auto-modification occurs either intra- or inter-molecularly [126].

6.1 PARP1 role in cells

PARP1 role has been highlighted in a wide number of biological functions. Growing evidences in the last years suggested PARP1 plays a crucial role in almost every DNA damage pathway, including: single strand break repair (SSBR) and base excision repair (BER), nucleotide excision repair (NER) [17,18], classical non-homologous end-joining (cNHEJ), alternative non-homologous end-joining (aNHEJ), microhomology-mediated end-joining (MMEJ), homologous recombination

(HR), DNA mismatch repair (MMR) and maintenance of replication fork stability (reviewed in [137]). In regard of BER, single-strand break left by OGG1-APE1 action can be resolved by either short- or long-patch repair: some of these factors (i.e. XRCC1, DNA polymerase (DNAP) β, DNA ligase III, proliferating cell nuclear antigen (PCNA), aprataxin, and condensin I) are known PARylation targets by PARP1 [138]. OGG1 was found to interact physically with PARP1. Evans and co-workers found that OGG1 binding to PARP1 is enhanced by DNA damage and OGG1 binds to auto(ADP-ribosyl)ated PARP1; this first step is crucial for the formation of a PAR-mediated multiprotein complex for the following steps of SSB pathway. Furthermore, lack of OGG1 enhances cells sensitivity toward both PARP inhibitors and oxidizing agents [139]. DNA repair is also facilitated by PARP1 ability to remodel chromatin structure: PARylation of histones results in chromatin relaxation, thus allowing DNA repair machinery and chromatin remodelers to access damage site [140]. New studies have seen PARP1 involved also in RNA metabolism i.e. splicing [141], polyadenylation [142] and nuclear export [143]. An interesting paper by Brody et al. revealed an interplay between PARP1, PARG and the RNA binding protein HuR. The group established that resistance of pancreatic ductal adenocarcinoma cells toward PARP1 inhibitors is driven by HuR-induced overexpression of PARG: PARP1 PARylation of HuR promotes its nuclear export toward cytosol, whereas it binds to and stabilizes PARG mRNA, thereby increasing PARG expression and modulating PARP1-chromatin dynamics. HuR inhibition results in PARG inhibition, that in turn leads to enhancing chromatin-trapped PARP1 and accumulation of damaged DNA and apoptosis [144].

PARP1, as well as PARPs enzymes, play major role in inflammatory pathways. Upon inflammation, PARP1 is acetylated by two CREB-binding protein (CBP) and p300: PARP1-CBP-p300 complex interacts with NF-κB, thus activating it. NF-κB results in transcription of proinflammatory cytokines, chemokines, transcription factors, and other inflammatory mediators [145].

6.2 PARP1 and cancer

PARP enzymes were proved to take part into six of the eight “cancer hallmarks”: metastasis, never-ending proliferation, angiogenesis, cell death resistance, independence from growth

suppression, proliferative signalling, deregulation of cellular energetics, and immune escaping [146]. Since 1980s, great effort was put to develop PARP1 inhibitors. As reviewed in [147], three generations of PARP1 inhibitors have been developed: the first is “nicotinamide analogue” family, according to the observation that nicotinamide, the by-product of NAD^+ cleavage by PARP1, is able to inhibit reaction; the second generation included quinazoline analogues (structurally related to nicotinamide) which provided a major effectiveness and target specificity; finally, the last generation collects all the molecules currently running trial tests, among which we cite: Rucaparib, Olaparib, Veliparib, Niraparib, Talazoparib. PARP1 inhibition leads to cell death in two fashions: the blockade of Base Excision Repair (in the context of synthetic lethality) and the trapping of PARP1-DNA complex [148]. In the last years, numerous trials have been started to validate PARP1 inhibitors to tackle cancer progression [149].

In regard of pancreatic cancer, synthetic lethality approach seems to be very promising, since 10-to-20% of pancreatic tumours display mutations in homologous recombination genes [148]. According to this model, when Base Excision Repair (BER) is impaired, there’s the conversion of a single strand nick into a double strand break (DSB). If the tumour cell has an underlying defect in HR, (commonly those harbouring BRCA1/2 mutations), it will be unable to repair the DSBs and will die [148].

6.3 PARP1 vs oncogene G4s

PARP1 activity at enhancers and promoters occurs mainly by functional interactions with other transcriptional factors, as well as nuclear receptors; surprisingly, PARP1 can act either as positive or negative regulator of gene transcription; moreover, its enzymatic activity is not always required to display transcriptional activity [150]. To date, few examples of G4-driven oncogene expression by PARP1 have been provided.

6.3.1 PARP1 vs *CKIT* G4

CKIT belongs to the tyrosine-kinase receptor class-III family (RTK) that acts as cell-surface receptors. *CKIT* deregulation results in tumourigenesis in very different ways such as gain of function, loss of function, overexpression, and point mutations [151]. Only few reports address a relationship between PARP1 and CKIT1: in BRCA1-mutated ovarian cancer cell lines, Olaparib-driven PARP1 inhibition results in overexpression of CKIT1 [152]; also, CKIT1 mutation was associated with resistance to Olaparib in acute myeloid leukaemia patients [153].

A brilliant work made by *Ladame and co-workers* explored the interaction between PARP1 and *CKIT* 1 G4 structure, revealing a protein:DNA stoichiometry of 2:1. Once bound to G4, PARP1 undergoes *in vitro* auto-PARylation, in the presence of NAD^+ [154]. Starting from this striking evidence, *Dai et al.* developed a method to detect the amount of PARP1 tethering onto the G4 [155]: briefly, a modified CKIT 1 is covalently assembled on a gold electrode in presence of mercaptohexanol (MCH), a compound known to create uniform monolayer and induce G4 formation [156]. Once PARP1 binds to CKIT 1, it undergoes auto-PARylation, a negatively charged post-translational modification easily detected by positively charged signal molecules, i.e. hexaammineruthenium(III) chloride (RuHex), that can be adsorbed onto the electrode surface, causing an intense electrochemical response. The amplitude of the electrochemical signal is directly proportional to PAR extension, therefore to PARP1 molecules bound to the G4.

6.3.2 PARP1 vs *CMYC* G4

CMYC belongs to the superfamily of basic helix-loop-helix DNA-binding proteins and is involved in the control of several normal cellular functions. It's one of the most frequent mutation among human cancers; alterations in its physiological level result in the occurrence of the mostly common cancer hallmarks i.e. cell proliferation enhancement, glycolysis and mitochondrial biogenesis stimulation and shift in the glutamine metabolism [157]. The interplay between PARP1 and *CMYC* has been already proved in a couple of papers: pharmacological inhibition of *MYC* expression induces PARP inhibitors sensitivity in triple-negative breast cancer cell line MB 231 [158] and doxycycline induced expression of *MYC* renders glioblastoma stem-like cell lines less susceptible to PARP inhibition [159]. In cervical cancer cell lines, PARP1 inhibition was found

to lower *CMYC* expression via β-catenin signalling pathway [160]. Maione and colleagues found out that PARP1 is associated to *CMYC* promoter; this induces PARylation that keeps *CMYC* promoter chromatin to an active state through histone modifications [161].

Pal et al. found PARP1 to be a positive modulator of this gene by binding both *in vitro* and *in vivo* to the G4 structure present in the human *CMYC* gene promoter; once bound, PARP1 catalyzes conversion from G4 to canonical B-DNA, allowing gene expression [162]. Results are supported by previous reports in which the presence of G4 within CMYC promoter negatively correlates with gene expression [163]–[165]

6.3.3 PARP1 vs telomeres G4

Telomeres are the end of chromosomes. They comprise tandem repeats of 6 nucleotides (5' – TTAGGG – 3')$_n$ with a 3' overhang provided by nucleolytic degradation [166] and play a plethora of roles such as: keeping genomic stability, preventing chromosome fusions, protecting chromosomes ends from DNA repair pathways that might recognize them as DSBs and silencing nearby genes (a phenomenon known as telomere position effect (TPE) [167]). The 3' overhang folds into higher-order chromatin structure and telomere-associated proteins in a huge complex called shelterin [168], [169]. Due to the end replication problem, telomeres progressively shorten after each cell cycle [166] leading to cell death or senescence, yet two mechanisms for telomere maintenance have been discovered in previous studies: transcriptional activation of a telomere reverse transcriptase called telomerase and the activation of alternative lengthening of telomeres (ALT), which is telomerase-independent and works via HR pathway [170]. Aberrant telomeres length has been reported to be shared among lot of tumours; i.e. telomeres shortening has been described for cervical and endometrial cancers whereas glioma and sarcoma display the longest chromosome ends [171]. Involvement of PARP family in telomeres behaviours have been reported: tankyrase 1, a PARP1-like enzyme, modulates telomerase inhibition in human cancer cells and can be seen as a potential telomere-directed anticancer target [172]; in colorectal cancer cell lines, PARP1 inhibition prevents the escaping a telomere-driven crisis after a certain number of cell divisions through induction of telomere intra-chromosomal fusions [173]; PARP1 deficient mice exhibited telomere shortening and increased end-to-end chromosome fusions [174]; finally, normal cells deficient for PARP-2 display a spontaneously increased frequency of

chromosome and chromatid breaks, suggested by a lack of 5' - TTAGGG - 3' repeats at their ends [175].

Presence of G4 has been reported in human telomeres [176], [177], providing also a platform for protein recruitment [178]–[181]. Cells treated with G4-interactive compound RHPS4 display an increased recruitment of PARP1 upon damaged telomeres; moreover, both RNA interfering and GPI-mediated PARP1 inhibition enhances the antitumoural activity of RHPS4-based therapy [84].

6.3.4 PARP1 vs *KRAS* G4

In human *KRAS* promoter, a polypurine site in a nuclease hypersensitive element (NHE) was found to fold into quadruplex by our lab [58]. PARP1 inhibition was reported to affect KRAS mutant cell lines viability and ameliorate clinical outcome in patients harbouring KRAS mutant tumours [182]–[184].

The closer NHE sequence to the transcription start site (called 32R) was found to be recognized by PARP1 [185], [186]. Moreover, either PARP1 silencing or enzymatic inhibition led to a reduction of murine KRAS level [186]. In accordance to further reports [187]–[189], it is widely believed that PARP1 is positively correlated with genes expression.

To date, there's still no report in human cells that proves *KRAS* G4 promoter activity is regulated by PARP1. This work provides such evidence for the first time, assessing a ROS-PARP1-KRAS axis that has never been shown so far.

7 Aim of the work

In this PhD program, I focused my research work on the role of KRAS in pancreatic ductal adenocarcinoma cells (PDAC cells) from a biochemist point of view. Despite the increasing amount of data so far collected, pancreatic cancer remains one of the deadliest malignancies with a very poor prognosis that poorly respond to conventional chemotherapies. It is now clear that mutations in codons 12, 13 and 61 of the *KRAS* proto-oncogene are able to initiate and maintain pancreatic cancer. Previous work in our lab investigated how KRAS expression is regulated, as this oncogene is responsible for the initiation of pancreatic cancer. Firstly, *KRAS* promoter was found to contain a G-rich sequence that affects gene expression. Within this DNA stretch, three G4 motifs - hereafter called G4-near, G4-middle and G4-far, according to their distance to the transcription start site - can adopt each a G-quadruplex conformation under physiological conditions. As these unusual conformations are formed within a promoter sequence critical for transcription, our laboratory has investigated if the G4 structures play any role in the process governing transcription. Although the implications of G4 DNA in transcription is still matter of debate, the work of our laboratory strongly support the hypothesis that the G4s serve as a recruitment platform for nuclear proteins. By means of pulldown and mass spectrometry experiments we discovered that the *KRAS* G4 nearest to TSS is recognized by MAZ, hnRNP A1, Ku70 and PARP1: transcription factors essential for the transcription of the gene. Considering that cancer cells produce higher level of reactive oxygen species (ROS) than normal cells, we asked if ROS can have any impact in the transcription of *KRAS*. This because guanine, having the lowest redox potential among the nucleobases, has a great tendency to oxidize to 8-oxoguanine (8OG). Indeed, we demonstrated by ChIP and qPCR that the levels of 8OG in PDAC cells is higher than in non-cancer cells and that the level 8OG in the promoter containing the G4 motifs is higher than in other genomic sequences. From this observation we asked what is the impact of PARP1 on KRAS expression under enhanced oxidative stress typical of PDAC cells. We specifically focused on PARP1 (Poly ADP-Ribose Polymerase 1) as it is involved in DNA damage recognition and repair, including base excision repair (BER) accounting for removal of oxidized bases, including 8OG. Together with other members of PARP superfamily, PARP1 is responsible of both mono(ADP-ribosylation) as well as poly(ADP-ribosylation): NAD^+-dependent post-translational modifications that consist in the attachment of ADP-ribose moieties to proteins and DNA. The structure of PARP1 can be divided into a N-terminus, responsible of DNA recognition (among which DNA and RNA non canonical structure,

i.e. G-quadruplexes), and a C-terminus accounting for enzymatic activity. Previous work from our laboratory reported that G4-near is recognized by several proteins including PARP1, essential for transcription. It was also found that the oxidation of G4-near results in an increase of the recruitment to the promoter of the transcription factors. The data suggested that 8OG behaves as an epigenetic mark for activating the transcription platform. The pivotal role played by PARP1 in the KRAS promoter was evidenced by the fact that its silencing by shRNA reduced dramatically KRAS expression, clearly indicating that PARP1 behaves as an activator of this oncogene.

On the basis of these observations, the main objective of my PhD project was to investigate the role of PARP1 on the *KRAS* promoter, in particular under conditions of enhanced oxidative stress, as occurs in cancer cells. First, to demonstrate that 8OG is more abundant in the KRAS promoter G4 motifs than in non-G4 sequences, I performed pull-down/ChIP experiments using a biotinylated molecule (b-6438) capable to bind to G4 DNA as a bait. Sheared chromatin from Panc-1 cells was incubated with b-6438 and pulled down with streptavidin-coated magnetic beads. The recovered chromatin enriched with G4-containing fragments was immuno-precipitated with an antibody specific for 8OG, and analyzed by qPCR with primers specific for the promoter G4 and control regions. The results showed that the *KRAS* promoter region harboring the G4 motifs contained, compared to control regions, 3-fold more 8OG than non-G4 regions. These data further support the notion that ROS increase the level of 8OG more in the promoter region harboring the G4 motifs than in G-rich control regions unable to form G4. Then, the work focused on the binding between PARP1 and G4-near/G4-middle sequences following two approaches: electrophoretic mobility-shift assays and fluorescence experiments taking advantage of the fact that the intrinsic fluorescence of PARP1 is quenched when it binds to G4. The data suggested the formation of two DNA-protein complexes of stoichiometry 1:1 and 1:2. Then by performing pull-down experiments with synthetic oligonucleotides mimicking the G4s formed by G4-near and G4 middle, I found that G4-near behaves as a platform for the formation of a multiprotein complex with PARP1, MAZ and hnRNP A1, located upstream of TSS. PARP1 plays a critical role in the KRAS promoter as when it is silenced by siRNA or its enzymatic activity is inhibited by small molecules, the expression of KRAS is strongly inhibited. Then I addressed the issue regarding how PARP1 stimulates KRAS expression. I discovered that PARP1, upon binding to the *KRAS* G4, undergoes auto-PARylation. All these data allowed me to propose a regulatory mechanism of KRAS expression according to which, an increase of oxidative stress, stimulates the recruitment of PARP1 to the KRAS promoter. The protein then binds to G4 and undergoes auto-PARylation. This post translational

modification confers negative charge to PARP1, that works as an antenna for the recruitment of cationic proteins such as MAZ and hnRNP A1. The formation of a multiprotein complex drives the unfolding of G4 and the reconstitution of canonical duplex DNA, the excision of 8OG by OGG1 and the activation of transcription. The data of this work has been published in International Journal of Molecular Sciences [190].

Another aspect that I have investigated regards the G4 structures formed by G4-near, located immediately upstream of TSS. A recent NMR study that our laboratory has performed in collaboration with a French group from Bordeaux, revealed that G4-near folds in a G4 that exists in equilibrium between two conformers. I therefore asked if both conformers are able to bind to PARP1 and the other nuclear factors. To address this issue we carried out EMSA, fluorescence titrations and pulldown experiment with oligonucleotide baits mimicking the two conformers. The results showed that both conformers are recognized by the transcription factors. As one of the two conformers has a unique structure, it may represent an attractive target for anticancer small molecules.

8 Results and discussion

- Cinque G, Ferino A, Pedersen EB, Xodo LE. Role of Poly [ADP-ribose] Polymerase 1 in Activating the Kirstenras (KRAS) Gene in Response to Oxidative Stress. Int J Mol Sci. 2020 Aug 28;21(17):6237. doi: 10.3390/ijms21176237. PMID: 32872305; PMCID: PMC7504130.

- Cinque G, Salgado G, Xodo LE. Critical G-rich motif in KRAS promoter folds in two structurally different G4 conformers recognized by transcription factors

Article

Role of Poly [ADP-ribose] Polymerase 1 in Activating the *Kirsten ras* (*KRAS*) Gene in Response to Oxidative Stress

Giorgio Cinque [1], Annalisa Ferino [1], Erik B. Pedersen [2] and Luigi E. Xodo [1,*]

[1] Department of Medicine, Laboratory of Biochemistry, P.le Kolbe 4, 33100 Udine, Italy; cinque.giorgio@spes.uniud.it (G.C.), annalisa.ferino@uniud.it (A.F.)

[2] Nucleic Acid Center, Institute of Physics and Chemistry, University of Southern Denmark, DK-5230 Odense, Denmark; erik@sdu.dk

* Correspondence: luigi.xodo@uniud.it; Tel.: +39-0432494395

Received: 4 August 2020; Accepted: 23 August 2020; Published: 28 August 2020

Abstract: In pancreatic Panc-1 cancer cells, an increase of oxidative stress enhances the level of 7,8-dihydro-8-oxoguanine (8OG) more in the *KRAS* promoter region containing G4 motifs than in non-G4 motif G-rich genomic regions. We found that H_2O_2 stimulates the recruitment to the *KRAS* promoter of poly [ADP-ribose] polymerase 1 (PARP-1), which efficiently binds to local G4 structures. Upon binding to G4 DNA, PARP-1 undergoes auto PARylation and thus becomes negatively charged. In our view this should favor the recruitment to the *KRAS* promoter of MAZ and hnRNP A1, as these two nuclear factors, because of their isoelectric points >7, are cationic in nature under physiological conditions. This is indeed supported by pulldown assays which showed that PARP-1, MAZ, and hnRNP A1 form a multiprotein complex with an oligonucleotide mimicking the *KRAS* G4 structure. Our data suggest that an increase of oxidative stress in Panc-1 cells activates a ROS-G4-PARP-1 axis that stimulates the transcription of *KRAS*. This mechanism is confirmed by the finding that when PARP-1 is silenced by siRNA or auto PARylation is inhibited by Veliparib, the expression of *KRAS* is downregulated. When Panc-1 cells are treated with H_2O_2 instead, a strong up-regulation of *KRAS* transcription is observed.

Keywords: G4 DNA; *KRAS*; oxidative stress; 8-oxoguanine; PARP-1; transcription factors; transcription regulation

1. Introduction

Pancreatic ductal adenocarcinoma (PDAC) is one of the most lethal human cancers with a median survival of about 6–8 months after diagnosis [1]. This poor prognosis is ascribable to its high aggressive nature and its resistance to conventional chemotherapies. Recent studies have demonstrated that point mutations in the *KRAS* proto-oncogene are the initial step of the PDAC carcinogenesis [2]. In the mutated form, the oncogene reprograms the metabolism of PDAC by increasing the glycolytic flux, the glutamine and serine metabolism, in order to generate biomass and reducing power necessary for tumour growth [3–5]. The dependence of the metabolic pathways on specific oncogenes led to the concept of "oncogene addiction", according to which cancer cells although depending on a number of genetic aberrations often develop a dependency on a particular oncogene [6,7]. As PDAC cells are addicted to mutant *KRAS*, this oncogene has become the focus of intense investigation [8]. In our laboratory we discovered that the *KRAS* promoter contains upstream of the transcription start site (TSS) a G-rich region adopting a G-quadruplex (or G4) structure recognized by several transcription factors [9–11]. The presence in the *KRAS* promoter of this unusual DNA conformation has been confirmed by ChIP-seq analysis carried out on transcriptionally active chromatin [12]. Although some hypotheses on the role of G4 DNA in gene regulation have been suggested, the data so far obtained are insufficient to propose a general

mechanism for transcription regulation by G4 DNA [13,14]. In 2012 we discovered that PARP-1 binds to the *KRAS* G4 region located upstream of TSS [11]. While PARP-1 was originally described as a protein involved in DNA repair [15], several studies suggest that it has also a role in transcription regulation [16–18]. It has been reported that PARP-1 behaves as a modulator of chromatin, a regulator for DNA-binding transcription factors and DNA methylation [19]. Human PARP-1 is a 113 kDa protein composed by an amino-terminal DNA binding domain comprising two zinc-finger motifs, a B domain containing a nuclear localization signal and a caspase-3 cleavage site, a central auto-modification domain allowing protein–protein interactions and a C-terminal domain harboring a highly conserved sequence that forms the catalytic site [20,21]. PARP-1 binds and cleaves NAD^+ to nicotinamide and ADP-ribose (ADPR), and it couples one or more ADPR units to acceptor proteins, including itself. These may become mono(ADP-ribosyl)ated or poly(ADP-ribosyl)ated: A modification called PARylation [20,21]. Most PARP-1 functions are localized in the nucleus, where the protein is involved in DNA repair, chromatin structure, transcription, translation and oxidative stress [15,19,21]. In the present work we focus on the role of PARP-1 in transcription regulation of *KRAS* in PDAC cells. We report that PARP-1 is associated to a G4-motif region of the *KRAS* promoter, in particular when the cellular levels of oxidative stress and 8-oxoguanine (8OG) are increased. We also found that PARP-1, upon binding to the *KRAS* promoter G4 structures, undergoes auto PARylation. This seems to induce the recruitment of the transcription factors hnRNP A1 and MAZ and the formation of the transcription pre-initiation complex. Previous studies from our and other laboratories showed that MAZ and hnRNP A1 bind to the promoter G4 region of *KRAS* and activate transcription [22–27]. In summary, in this study we have identified a ROS-G4-PARP-1 axis that controls the expression of *KRAS* under conditions of enhanced oxidative stress.

2. Results and Discussion

2.1. G4 Formation in the KRAS Promoter and Guanine Oxidation

The promoter of the human *KRAS* proto-oncogene contains, between −270 and −118 (3′→5′, non-coding strand) from the transcription start site (TSS), three G4 motifs hereafter called G4 32R (also called G4 near), G4 mid and G4 far (Figure 1) [9,28,29]. Previous studies have demonstrated that G4 32R and G4 mid form stable G4 structures under physiological conditions, whereas G4 far forms a G4 which is too weak for determining a thermal stability [28]. In Figure 1 we report typical CD spectra of G4 32R and G4 mid in 100 mM KCl, at 25 and 95 °C. Both exhibit a strong ellipticity at ~265 nm, in agreement with the formation of parallel G4 structures which have T_M's of 62 and 78 °C, respectively. DMS footprinting experiments showed that G4 32R forms a parallel tri-stacked G4 with a 1/1/12 topology, characterized by two 1-nt loops, a 12-nt loop and a T-bulge in one strand (Supplementary Information S3) [11]. A recent NMR study confirmed this structure, but showed that it is in equilibrium with a conformer containing a 11-nt loop, a folded-back guanine and 3-nt cap at the 3′-end [30]. By contrast, G4 mid comprising seven G-runs of at least three guanines can fold in different ways. In 100 mM KCl, G4 mid can fold into a quad-stacked G4 involving G-runs 1, 2, 5, and 6, as proposed in ref. [28]. It embeds, however, two contiguous G4 motifs, each of which is potentially able to form a tri-stacked G4. We called them G4 mid1 and G4 mid2 (Supplementary Information S4 and Table 1). The CD of G4 mid1 suggests that this sequence folds into a parallel G4. Instead, the CD of G4 mid2, showing a strong ellipticity at 260 nm and a shoulder at 295 nm, indicates that the sequence might adopt a mixed parallel/antiparallel G4. These G4 structures show T_M's in 100 mM KCl of 59 °C (G4 mid1) and 67 °C (G4 mid2) (Figure 2A, Supplementary Information S5). The presence in vivo of folded G4 structures in the *KRAS* promoter has been confirmed by a ChiP-seq analysis carried out on transcriptionally active chromatin [12].

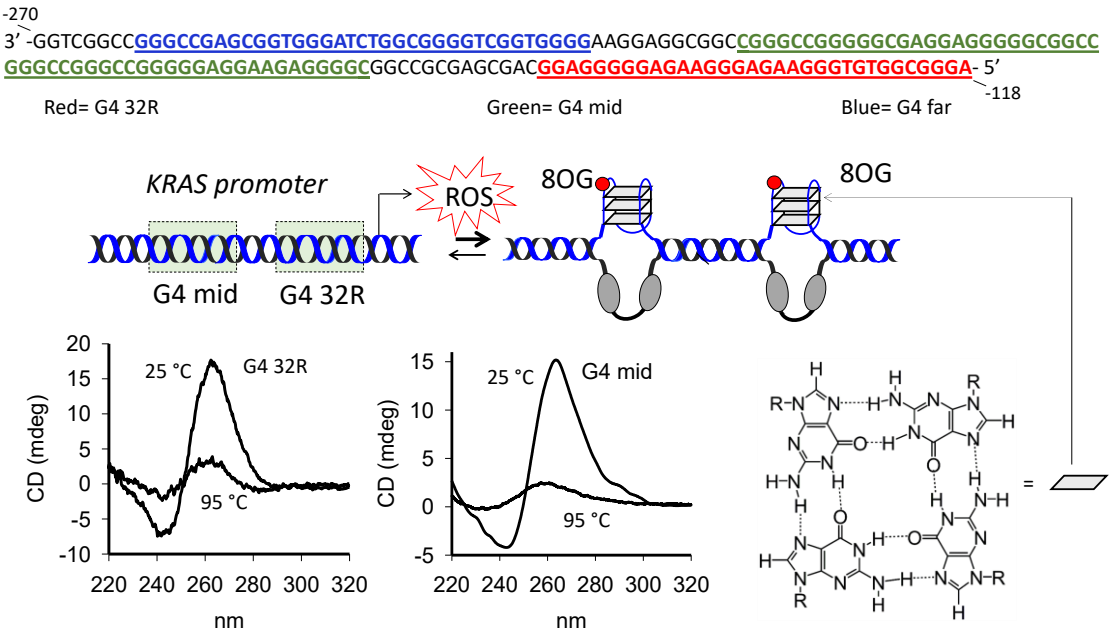

Figure 1. *KRAS* G4-motif sequences located upstream of the transcription start site (TSS). The G4 motifs are located in the non-coding strand between -118 and -270 from TSS: G4 32R (sequence in red, -118/-149); G4-mid (sequence in green, -163/-217; G4-far (sequence in blue, -229-264). G4 32R and G4 mid form G4 structures with a well-defined melting profile. The CD of these sequences (at 25 and 95 °C) suggest the formation of parallel G4 structures. The structure of a G-tetrad, where each guanine forms 4 hydrogen bonds with neighboring guanines, is shown.

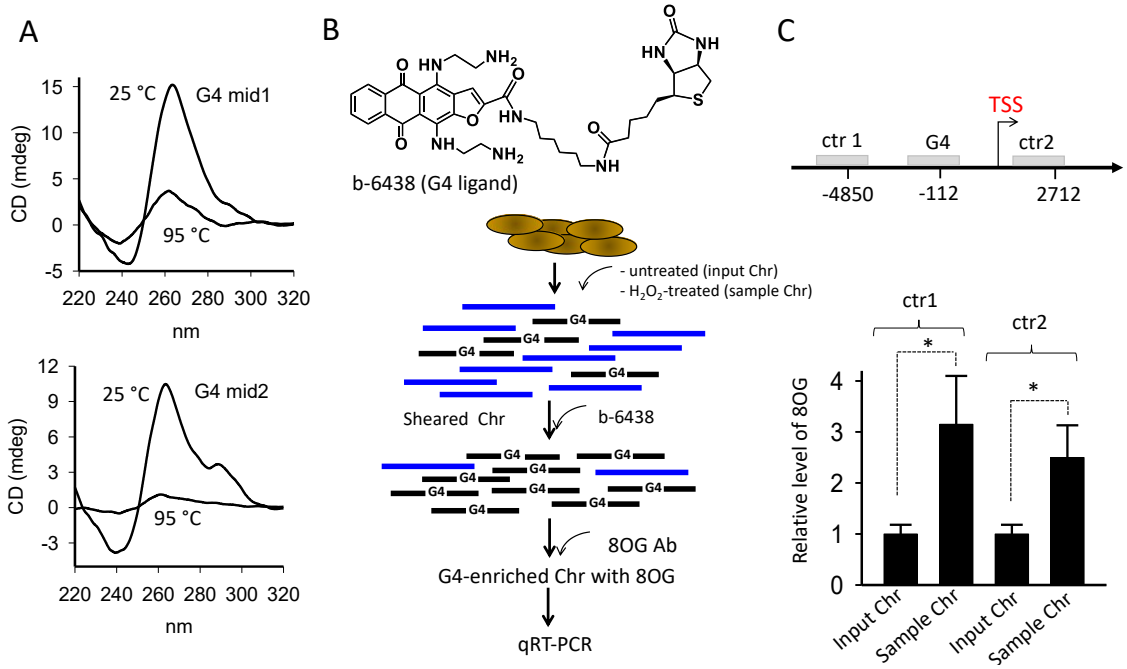

Figure 2. (**A**) CD spectra at 25 and 95 °C for the G4 mid1 and G4 mid2 sequences; (**B**) structure of biotinylated G4 ligand b-6438, which shows much more affinity for G4 DNA than duplex DNA, used in chromatin pull-down experiments. Pull down-ChIP experimental scheme. Chromatin fragments with G4 are depicted in black, fragments without G4 in blue; (**C**) the results of the pull down-ChIP experiment show that 8OG and the G4 motif co-localize in the region of the *KRAS* promoter containing G4 32R compared to control regions ctr1 and ctr2, located more than 4500 and 2500 bp away from TSS, respectively. Error bars from three experiments, Student *t*-test, (*) = $p < 0.05$;

Table 1. DNA sequences used in this work

Oligonucleotide	5′ → 3′	8OG
G4 32R	AGGGCGGTGTGGGAAGAGGGAAGAGGGGGAGG	
92	AGGGC**G**GTGTGGGAAGAGGGAAGAGGGGGAGG (1) (3)	1
96	AGGGCGGTGTGGGAA**G**AG**G**GAAGAGGGGGAGG (1) (3)	2
G4 mid	CGGGGAGAAGGAGGGGGCCGGGCCGGGCCGGCGGGGG AGGAGCGGGGGCCGGGC	
G4 mid1	CGGGGAGAAGGAGGGGGCCGGGCCGGGC	
G4 mid2	CGGGCCGGCGGGGGAGGAGCGGGGGCCGGGC	
b-32R	b-TTTTAGGGCGGTGTGGGAAGAGGGAAGAGGGGGAGG (2)	
b-**92**	b-TTTTAGGGC**G**GTGTGGGAAGAGGGAAGAGGGGGAGG (1) (2) (3)	1
b-**96**	b-TTTTAGGGCGGTGTGGGAA**G**AG**G**GAAGAGGGGGAGG (1) (2) (3)	2
b-mid	b-TTTTCGGGGAGAAGGAGGGGGCCGGGCCGGGCCGGCG--GGGGAGGAGCGGGGGCCGGGC (2)	
b-mid1	b-TTTTCGGGGAGAAGGAGGGGGCCGGGCCGGGC (2)	
b-mid2	b-TTTTCGGGCCGGCGGGGGAGGAGCGGGGGCCGGG (2)	
b-mid^{OX}	b-TTTTCGGGGAGAAGGAGGGGGCC**G**GGCC**G**GGCCGGCG--GGGGAGGAGCGGGGGCCGGGC (1) (2)	2
b-mid1^{OX}	b-TTTTCGGGGAGAA**G**GAGGGGGCCGGGCCGGGC (1) (2)	1
b-mid2^{OX}	b-TTTTCGGGCC**G**GCGGGGGA**G**GAGCGGGGGCCGGGC (1) (2)	2
Cy5.5-32R	Cy5.5-AGGGCGGTGTGGGAAGAGGGAAGAGGGGGAGG	
Cy5.5-mid1	Cy5.5-CGGGGAGAAGGAGGGGGCCGGGCCGGGC	
Cy5.5-mid2	Cy5.5-CGGGCCGGCGGGGGAGGAGCGGGGGCCGGGC	
Cy5.5-mid	Cy5.5-CGGGGAGAAGGAGGGGGCCGGGCCGGGCCGGCG GGGGAGGAGCGGGGGCCGGGC	
32Y	CCTCCCCCTCTTCCCTCTTCCCACACCGCCCT	
G4 mid Y	GCCCGGCCCCCGCTCCTCCCCCGCCGGCCCGGCCCGGCC CCCTCCTTCTCCCCG	
Oligo dT	TTTTTTTTTTTTTTT	
ODN1	Cy5.5-CATCAGAAGGCTAGCAATCA	
ODN2	Cy5.5-AATAGTAATTGCTTAGCCTG	
ODN3	Cy5.5-CCTAATGCTGCTAAACTCCC	

(1) Underlined G = 7,8-dihydro-8-oxoguanine (8OG); (2) b = biotin; (3) 92 and 96 = G4 32R analogues containing 8OG.

It has been found that guanine, in particular in G-rich sequences, is susceptible to oxidation to 7,8-dihydro-8-oxoguanine (8OG), due to its low redox potential [31,32]. Indeed, the amount of 8OG in the genome of aerobic organisms is considered a biomarker for oxidative stress [33]. We previously have observed that pancreatic cancer cells (Panc-1, BxPC3, and MiaPaCa-2), due to their higher metabolic rate, show a higher basal level of 8OG than non-cancer HEK 293 cells [34]. We also discovered by ChIP experiments that when Panc-1 cells are treated with H_2O_2, 8OG is about 5-fold more abundant in the *KRAS* promoter region containing the G4-motifs than in G-rich non-G4 regions located at least 3000 bp away from TSS [35]. These data suggest that guanines in the G4-motifs are more exposed to oxidation than other guanines. Saito et al. [36] reported that contiguous guanines are characterized by a higher rate of oxidation than isolated guanines and that the 5′-G in a G-run shows the lowest ionization potential. To provide further support that 8OG is more abundant in G4 than non-G4 motifs, we performed a pull-down/ChIP experiment as outlined in Figure 2B. We synthesized a G4-bait,

namely b-6438, by linking biotin to an anthrathiophenedione molecule binding to G4 much more than to duplex DNA [37].

We previously demonstrated that this molecule efficiently pulls down G4 strands from nucleic-acid mixtures [37]. Sheared chromatin obtained from untreated (input Chr) and H_2O_2-treated (sample Chr) Panc-1 cells were incubated with b-6438 and pulled down with streptavidin-coated magnetic beads. The recovered chromatin enriched with G4-containing fragments obtained from the input Chr and sample Chr were immuno-precipitated with an antibody specific for 8OG, and analyzed by qPCR with primers specific for the promoter G4 region and control ctr1 and ctr2 regions located in the *KRAS* gene (Figure 2B,C) [35]. The results showed that in sample Chr the *KRAS* promoter region harboring the G4 motifs contains, compared to ctr1 or ctr2, 3-fold more 8OG than in input Chr. These data further support the notion that ROS increase the level of 8OG more in the promoter region harboring the G4 motifs than in G-rich control regions unable to form G4. This is in keeping with an 8OG-Seq analysis showing that in the mouse genome, 8OG is 2-fold more abundant in gene promoters than in genic and intergenic regions [38,39]. In a previous work we asked if 8OG affects the topology and stability of the G4 formed by G4 32R [35]. In brief, we found that when the oxidative lesion lies in a loop (as in sequence **96**, Table 1), both the topology (1/1/12) and the stability (~62 °C) of the resulting G4 did not appreciably change. By contrast, when 8OG lies in the G-tetrad core (as in sequence **92**, Table 1), the damaged G-run is replaced by the additional G-run present in G4 32R, through an alternative folding. This is due to the fact that 8OG destabilizes G-tetrad [35] (Supplementary Information S6). The topology of G4 changed from 1/1/12 into 4/4/6 and the T_M decreases by ~10 °C [35]. These data show that the impact of 8OG on G4 depends on the position of the oxidized base within the G4 motif [40,41]. The effect of 8OG in G4 mid1 and G4 mid2 is similar to that observed with G4 32R. If we assume that G4 mid1 and G4 mid2 form, as observed for G4 32R, a G4 structure containing a 1-nt loop and a bulge in one strand, 8OG in G4 mid1^{OX} and G4 mid2^{OX} are expected to fall in the G4 core, destabilizing the structure. Indeed, we found that the T_M's of G4 mid1^{OX} and G4 mid2^{OX} are respectively 3 and 4 °C lower than the wild-type analogues (Table 1, Supplementary Information S5).

2.2. Under Oxidative Stress, PARP-1 Is Recruited to the KRAS Promoter where It Binds to G4 32R and G4 mid1 and G4 mid2

In the past years, evidence that G4 32R is involved in transcription regulation [9,10] has been provided. G4 32R is located few helical turns upstream of TSS and is recognized by several transcription factors including PARP-1, Ku70, MAZ, and hnRNP A1 [11]. PARP-1 plays two important roles on transcription: It promotes the decondensation of chromatin [42] and it acts as a component of the transcription pre-initiation complex [43]. Due to its critical role in transcription, we focused here on PARP-1. By electrophoresis mobility-shift assays (EMSA), we explored the capacity of recombinant PARP-1 to bind to the G4s formed by G4 32R and G4 mid1, G4 mid2 (the entire G4 mid sequence showed little binding, not shown) (Figure 3A). The results obtained by incubating the oligonucleotides 5′-labelled with Cy5.5 (50 nM), mimicking the *KRAS* G4s, with increasing amounts of PARP-1 (protein:G4 ratios = 0, 2.2, 4.4, 8.6, 17.2, 34.4), are reported in Figure 3B. The interaction between PARP-1 and the G4s is rather strong, as a 4.4-fold excess of PARP-1 over G4 is sufficient to show a retarded band in the gel. In contrast, the three unstructured oligonucleotides (at PARP-1/ODN of 34.4) did not show any affinity for PARP-1 (negative control). It can be seen that protein:G4 ratios < 4 favor the formation of a 1:1 complex, whereas protein:G4 ratios > 4 favor the formation of a 2:1 complex (2 PARP-1 per G4). We reported in a plot for each G4, the fraction of bound G4 as a function the PARP-1 concentration (Figure 3C). As the curves showed a sigmoidal shape, they have been best-fitted to the Hill equation. We obtained the following K_D's values: 0.2 ± 0.03 μM for G4 32R; 0.36 ± 0.02 μM for G4 mid1; 0.37 ± 0.02 μM for G4 mid2. The three best-fits gave a cooperativity Hill coefficient of n ~ 3. In a previous study, the K_D's between PARP-1 and CKIT-1 or *Htelo* G4s, determined by surface plasmon resonance (SPR), were found to be 65 nM for CKIT-1 and 5.8 μM for *Htelo* [44].

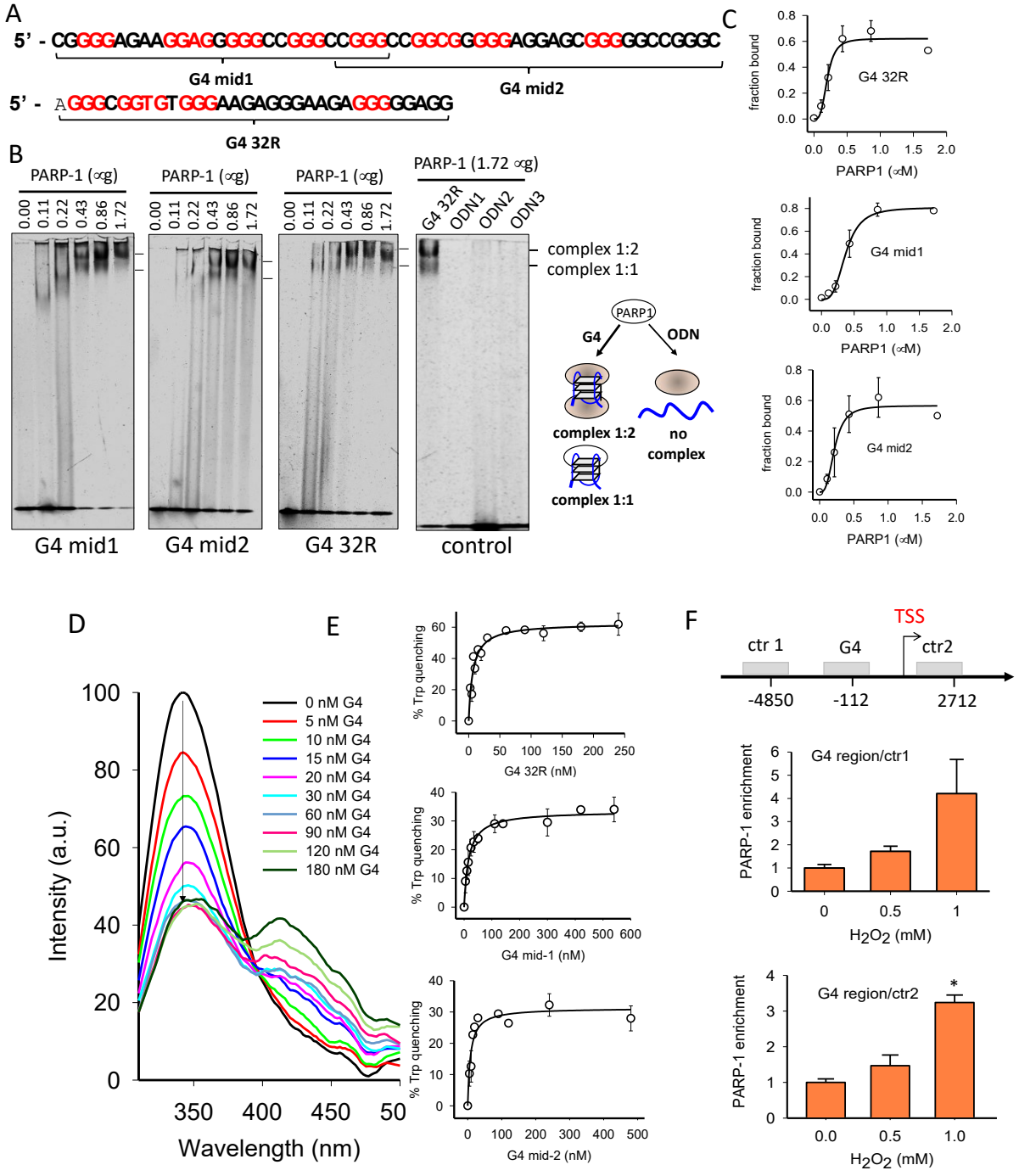

Figure 3. (**A**) Sequences of G4 32R, G4 mid1 and G4 mid2; (**B**) EMSA showing the binding of recombinant PARP-1 to Cy5.5-labelled G4-mid1, G4 mid2, G4 32R and control oligonucleotides ODN1, ODN2 and ODN3 (50 nM), with increasing amounts of PARP-1. Reaction was carried out in 20 mM Tris–HCl pH 8, 30 mM KCl, 1.5 mM $MgCl_2$, 1 mM DTT, 8% glycerol, 1% Phosphatase Inhibitor Cocktail I (Sigma, Milan, Italy), 5 mM NaF, 1 mM Na_3VO_4, 2.5 ng/mL poly [dI-dC], 50 mM ZnAc for 30 min at RT. 50 nM Cy5.5-labelled G4 was incubated with 0, 0.11, 0.22, 0.43, 0.86, and 1.72 μM PARP-1; (**C**) Plots reporting the fraction of G4 bound to PARP-1 as a function of the PARP-1 concentration. The data have been best-fitted to the Hill equation. Error bars are from two experiments; (**D**) Typical fluorescence titration of PARP-1 with G4 32R. The titration was carried out in a 500 μL quartz cuvette containing a solution of PARP-1 (60 nM) in 50 mM Na-cacodylate, pH 7.4, 100 mM KCl, 50 μM ZnAc, 1 mM DTT. G4 32R was added to the PARP-1 solution and the readings were performed 5 min after incubation. The fluorescence spectra were recorded at 20 °C between 310 and 500 nm, excitation at 295 nm. Titrations were carried out also with G4 mid1 and G4 mid2; (**E**) Plots reporting the % Trp quenching induced by increasing amounts of G4 32R, G4 mid1, and G4 mid2. Error bars are from two experiments; (**F**) ChIP showing the

recruitment of PARP-1 to the G4 promoter region compared to non-G4 control ctr1 and ctr2 regions, following H_2O_2 treatment of Panc-1 cells. Error bars are from three experiments, (*) = $p < 0.05$.

As PARP-1 contains multiple Trp residues in its DNA-binding domain [44], we followed the binding of PARP-1 to G4 DNA by measuring the quenching of the Trp fluorescence upon addition of G4 to a PARP-1 solution. In Figure 3D we report a typical titration obtained by adding increasing amounts of G4 32R to a PARP-1 solution (60 nM). G4 32R quenched the fluorescence by ~50%, whereas G4 mid1 and G4 mid2 by ~30%. The percentage of quenching (measured at 345 nm) as a function of increasing amounts of G4 gave the curves shown in Figure 3E. From these plots we determined the stoichiometry of the interaction by the "tangent" method. The results pointed to a stoichiometry of two PARP-1 molecules per G4, in keeping with the results obtained with the CKIT G4 [44] and the EMSA shown in panel 3B.

Next, we explored by ChIP if PARP-1 is recruited to the G4-region of the *KRAS* promoter when the cells are treated with H_2O_2, i.e. after an increase of oxidative stress (Figure 3F). Panc-1 cells were treated with two doses of H_2O_2, 0.5 and 1.0 mM, the chromatin was extracted, sheared and used for a ChIP assay with an antibody specific for PARP-1. Input Chr (from untreated cells) and recovered Chr (from H_2O_2 treated cells), immuno-precipitated with antiPARP-1 Ab, were analyzed by qPCR with primers for the *KRAS* promoter G4 region and primers for the ctr1 and ctr2 regions. The data obtained showed that the occupancy of the G4 region by PARP-1 compared to control ctr1 and ctr2 regions increased up to 4-fold as a function of H_2O_2, i.e. in a dose-response manner (Figure 3F).

We have previously reported that MAZ and hnRNP A1 too are recruited to the KRAS promoter G4 region rich in 8OG, in response to a H_2O_2 treatment [35]. Indeed, we found by a ChIP-reChiP experiment that MAZ and hnRNP A1 localize in the promoter region of *KRAS*, where the 8OG level is higher than in the control region [35]. Moreover, by EMSA we found that MAZ and hnRNP A1 bind to both G4 32R [22,23] and G4 mid sequences (Supplementary Information S7, S8).

2.3. G4 32R Forms A Multi-Protein Complex with PARP-1, MAZ and hnRNP A1

The nuclear factors recruited to the critical *KRAS* G4-region, located upstream of TSS, following a treatment with H_2O_2, are likely to form the transcription pre-initiation complex. To support this notion, we performed biotin-streptavidin pull-down assays with a Panc-1 nuclear extract and as DNA baits biotinylated G4 32R and G4 mid, in the wild-type or oxidized form (Figure 4B–D). The G4 baits mimicking G4 32R are wild-type b-32R and its oxidized forms b-**92** and b-**96** (Table 1). We prepared DNA baits also for G4 mid: b-mid, b-mid1 and b-mid2 and oxidized analogues b-mid^{OX}, b-mid1^{OX} and b-mid2^{OX} carrying one or two 8OGs (Table 1). Each G4 bait was incubated with 80 μg of nuclear extract from Panc-1 cells. The proteins bound to the G4 bait were pulled down with streptavidin-coated magnetic beads, eluted with Laemmli buffer and analyzed by immunoblotting with antibodies specific for MAZ, hnRNP A1 and PARP-1. It can be seen that the G4 baits mimicking G4 32R (b-32R, b-**92** and b-**96**), independently from their oxidation state, pulled down all three transcription factors. This suggests that G4 32R forms a multiprotein complex, which is presumably the transcription pre-initiation complex. The eluates from the beads incubated with the nuclear extract in the absence of G4 bait, contained a small amount of proteins due to unspecific interactions between the magnetic beads coated with streptavidin and the proteins (lane "beads"). By contrast, the eluates from the beads bound to b-32R, b-**92**, and b-**96** contained a higher amount of the target proteins, due to their specific binding to the G4 structures. The nuclear factors recognize G4 32R also in the duplex conformation (obtained by hybridizing the biotinylated G4s with the complementary strand). Figure 4B shows that MAZ and PARP-1 bind to both wild-type and oxidized G4 32R in duplex conformation.

In agreement with previous studies [22], we found that whereas hnRNP A1 binds only slightly to the wild-type duplex, it binds clearly to the oxidized duplexes.

We also performed pull-down experiments with wild-type and oxidized b-mid, b-mid1 and b-mid2 as G4 baits (Table 1) (Figure 4C). These show that the 53-mer oligonucleotide b-mid, forming a putative quad-stacked G4 with a T_M = 78 °C, is not bound by the nuclear factors, whereas b-mid1 (T_M = 59 °C) and b-mid2 (67 °C) clearly bind to PARP-1. Instead, the binding of MAZ and hnRNP A1 to G4 mid1 and G4 mid2 is very weak, as the amounts of protein pulled down is comparable to those present in the input. PARP-1 binds to G4 mid1 and G4

mid2 also when they include 8OG. Some binding of MAZ to b-mid^{OX} is observed. Furthermore, and expectedly, we found that G4 mid in duplex conformation interacts with PARP-1 and MAZ but not with hnRNP A1 (Figure 4D). Together, the pull-down assays show that PARP-1, MAZ and hnRNP A1 form with the critical G4 32R sequence of *KRAS*, localized immediately upstream TSS, a transcription pre-initiation complex. G4 mid1 and G4 mid2 seems to have the function of recruiting PARP-1 in the promoter region, thus acting as a platform for the assembly of the pre-initiation complex.

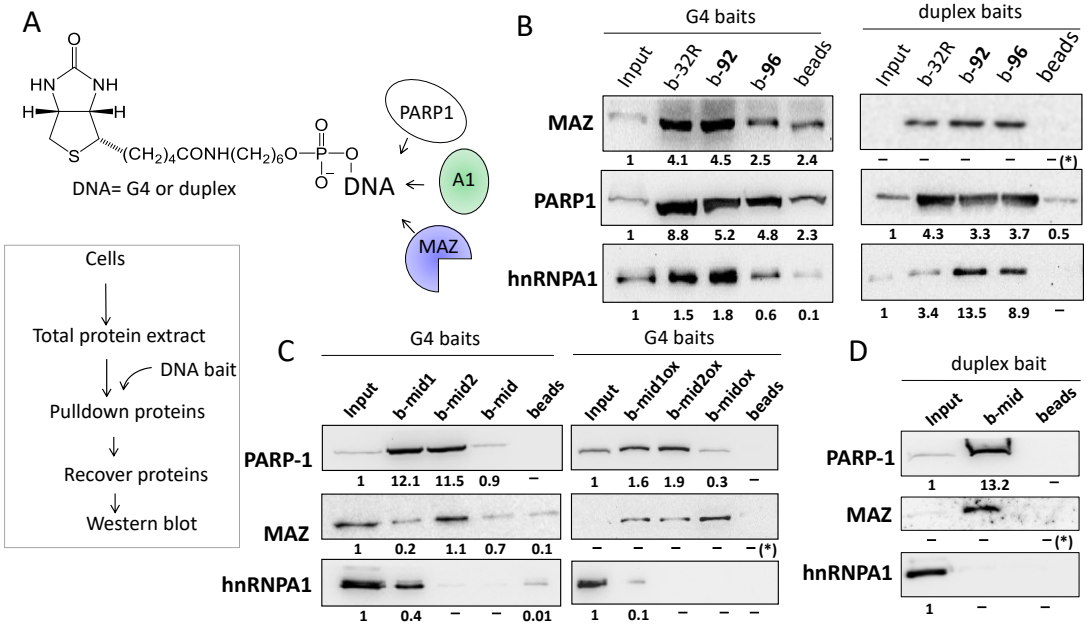

Figure 4. (**A**) Structure of the DNA baits used in the pull-down experiments. The scheme of the pull-down experiments is illustrated; (**B**) Pull-down with wild-type and oxidized G4 32R sequence in the G4 or duplex conformation. b-32R is wild-type G4 32R, while b-**92** bears one 8OG in a G-run, b-**96** bears two 8OG bases in the 12-nt loop (see structure in ref [35]) (Table 1). The biotinylated G4 or duplex baits (80 nM) were incubated with 80 µg of nuclear extract for 30 min at RT. The DNA bait-protein complexes formed were pulled down with streptavidin magnetic beads. The pulled-down proteins were recovered and analyzed by Western blot with anti MAZ, anti PARP-1 and anti hnRNP A1 primary antibodies and a secondary antibody conjugated to horseradish peroxidase; (**C**,**D**) Pull-down with wild-type G4 mid sequences b-mid, b-mid1 and b-mid2 or oxidized b-midox, b-mid1ox and b-mid2ox, in G4 or duplex conformation. The protocol followed is the same as in (**B**). We reported below each Western blot the band/input ratios. The uncertainty of these values from two experiments is about 20 %; (*) = the band/input ratios could not be determined.

2.4. PARP-1 Undergoes Autoparylation upon Binding to the KRAS G4

PARP-1 is a protein that catalyzes poly(ADP-ribosyl)ation (PARylation) of target proteins including itself (auto PARylation). Free PARP-1 consists of 6 independent domains one connected to the other by a flexible linker [45]. It has been reported that when the protein binds to DNA with a lesion through its two zinc-finger domains, it undergoes a structural change that starts the synthesis of ADP-ribose units, by using NAD^+ (the coenzyme derived from nicotinamide, NAM) as a source of ADP-ribose. PARylation is a heterogeneous reaction in terms of length (up to 200 ADP-ribose units) and branching [46–49]. However, PARP-1 can also transfer few ADP-ribose unit or even only one [mono(ADP-ribosyl)ation] [48]. Both properties and function of PARP-1 have been summarized in a recent review [21]. In the PARylation process, DNA behaves as a positive allosteric effector, by upregulating the basal catalytic activity of PARP-1. Considering that PARP-1 associated to the *KRAS* promoter binds to G4 DNA, we wondered if the G4 structures actually behave as activators of PARP-1, as DNA with a nick or an abasic site does. There is one report in the literature addressing this issue: The autoPARylation

of PARP-1 observed when the protein interacts with the ckit-1 and Htelo quadruplexes [44]. To test if the KRAS G4s activate recombinant PARP-1, we performed in vitro autoPARylation assays (Figure 5).

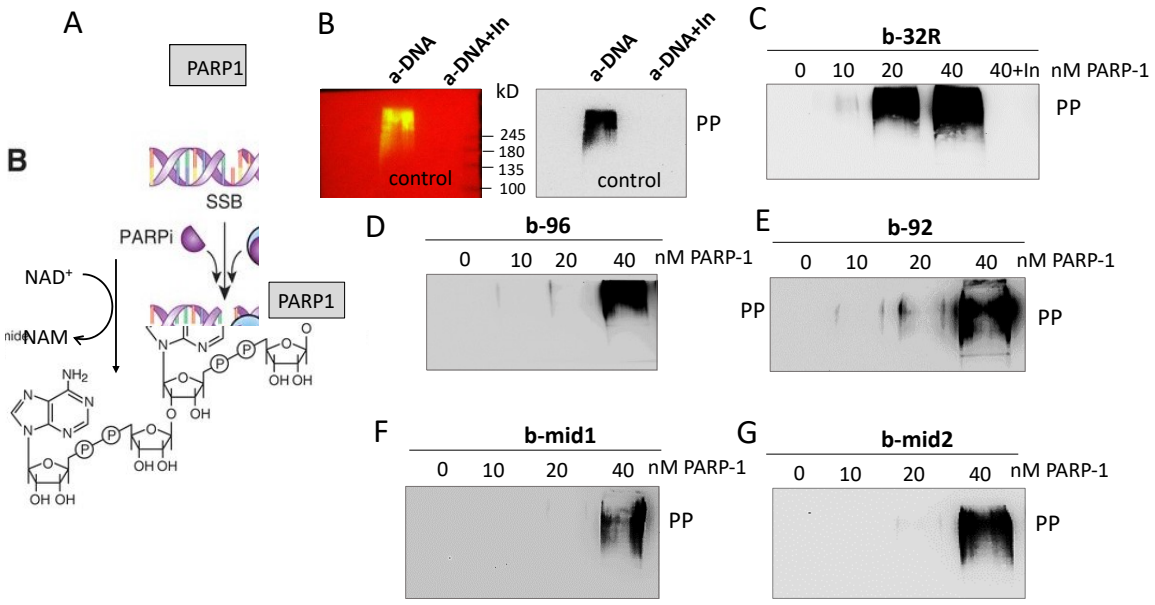

Figure 5. (**A**) The reaction of PARP-1 autoPARylation. NAM = nicotinamide; (**B**) AutoPARylation of recombinant PARP-1 induced by a-DNA (positive control from supplier). When Veliparib, an enzymatic inhibitor of PARP-1 (indicated with In), was added to the reaction mixture no PARylation was observed (negative control). The Western blot was performed with anti poly/mono ADP-ribose Ab and a secondary Ab conjugated to horseradish peroxidase. A membrane replica showing the protein markers (right) is also reported. PP = PARylated PARP-1; (**C–G**) AutoPARylation of recombinant PARP-1 (P) induced by KRAS G4 32R (**C**), **96** (**D**) and **92** (**E**) quadruplexes and G4 mid1 (**F**) and mid2 (**G**) quadruplexes. The mixtures contained 10, 20 and 40 nM of PARP-1 and 10 nM G4.

As positive control we used a PARP-1 activator, a-DNA (a lesioned DNA), supplied with the "PARP-1 Enzyme Activity Assay" kit (Merck Life Science, Milano, Italy). PARP-1 is a 113 kDa protein, whereas its autoPARylated form induced by a-DNA has a molecular weight > 245 kDa, suggesting an extensive auto PARylation synthesis. We then used as DNA activator KRAS G4s, both in the wild-type or oxidized form. The G4 activators (10 nM) were incubated with increasing amounts of PARP-1 (10, 20 and 40 nM) in a buffer containing NAD^+. After incubation, the mixtures were blotted and analyzed with an anti poly/mono ADP-ribose Ab. The results show that the G4 activators promote to a different extent auto PARylation of PARP-1. The strongest activator is wild-type G4 32R; its oxidized variants **92** and **96** are weaker effectors. Indeed, auto PARylation induced by **92** and **96** is observed only in the presence of 40 nM PARP-1, while auto PARylation promoted by 32R is detected at 20 nM PARP-1. As expected, when Veliparib [50] (Supplementary Information S9), an inhibitor of PARP-1, is added to the reaction mixture, the autoPARylation is not observed. G4 mid1 and G4 mid2, wild-type and oxidized, promote autoPARylation of PARP-1 as well, but to a lesser extent than G4 32R. Together, these data demonstrate that both G4 32R and G4 mid1/G4 mid2, in wild-type and oxidized forms, activate PARP-1 auto PARylation. Next, we asked if PARylation is also observed within the cell context. We investigated if the proteins recruited to the KRAS promoter, recognizing the G4 structure of G4 32R, are PARylated. To address this issue, we followed the scheme outlined in Figure 6 Panc-1 cells were treated with H_2O_2 to induce guanine oxidation and stimulate the recruitment of PARP-1, MAZ and hnRNP A1 to the KRAS promoter. The nuclear extracts were treated with biotinylated b-32R, b-**92** and b-**96**. The pulled down samples were analyzed by Western blot with anti poly/mono ADP-ribose Ab. It can be seen that all three G4 baits pulled down PARylated proteins. Compared to untreated cells, the results show that PARylation increases with the cell exposure to H_2O_2. We also report in the figure the membrane replicas showing the molecular weight of the protein markers. The molecular weight of the markers loaded in the gel show that the PARylation involves a

protein of ~115 kDa, suggesting that this is most likely PARP-1. Note that H_2O_2 gave in the input (protein extract untreated with b-G4) PARylated proteins in the range between ~130–250 kDa, while the PARylated protein captured by the G4 baits gave only a sharp band, corresponding to a protein of the size of PARP-1. This suggests that PARP-1 captured by G4 is characterized by a limited auto PARylation, if not a mono (ADP-ribosyl)ation [48].

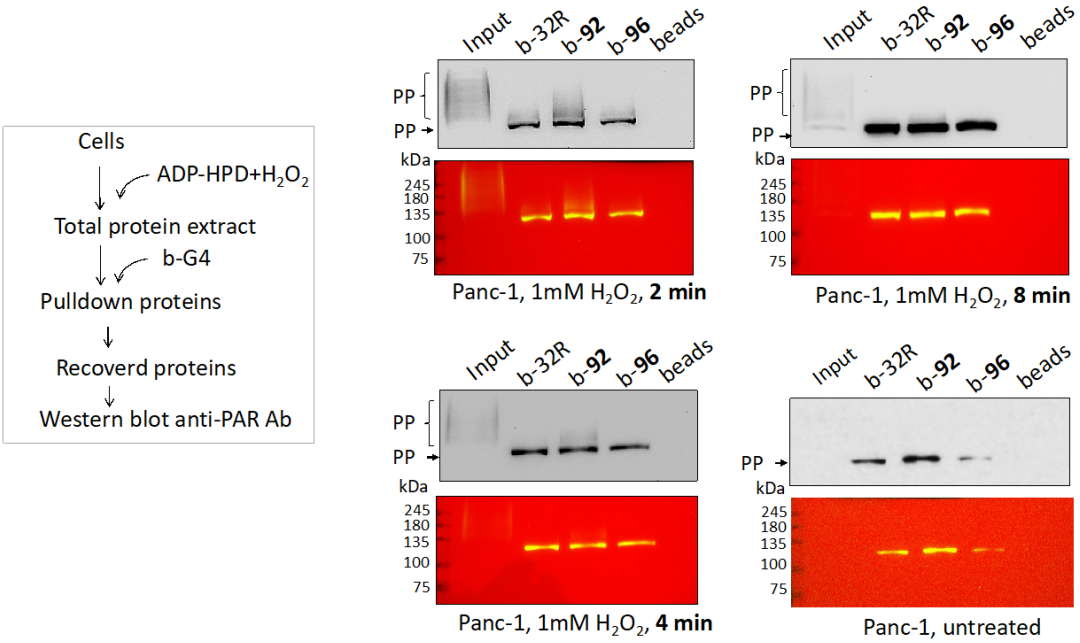

Figure 6. Western blots showing that b-32R and its oxidized variants b-**92** and b-**96**, pulled down PARylated proteins, from Panc-1 cells treated with H_2O_2. Pulled-down PARylated proteins migrate in the gel with a strong band of approximately 120–125 kDa. In contrast, the input, composed by proteins that have not been pulled down with a G4 bait, shows PARylated proteins that have molecular weights > 125 kDa. Membrane replicas showing the protein markers are also reported, PP = PARylated proteins.

2.5. The Transcription Pre-Initiation Complex Formed at G4 32R Contains Parylated PARP-1

The experiment described above showed that there are proteins bound to G4 32R that are PARylated. Although we had an indication that the main PARylated protein could be PARP-1, we wanted to unambiguously confirm it. An insight was obtained by the experiment reported in Figure 7. Nuclear extract from Panc-1 cells untreated or treated with 0.5 or 1.0 mM H_2O_2 was pull-down with anti poly/mono-ADP ribose Ab. The recovered PARylated proteins were separated by SDS-PAGE and blotted on nitrocellulose. Using specific antibodies we tested for the presence of PARP-1, MAZ and hnRNP A1 within the PARylated proteins. Only PARP-1 turned out to be PARylated, while MAZ and hnRNP A1 did not. The PARylation of PARP-1 occurs in a dose-response manner as, compared to untreated cells, auto PARylation increases with the amount of H_2O_2 used. The amount of PARylated PARP-1 in the cells treated with 0.5 and 1.0 mM H_2O_2 is ~4-fold more abundant than in the input (see bar plot). We concluded that upon binding to the *KRAS* G4 motif, PARP-1 undergoes autoPARylation. According to the data reported in this and previous studies, we are convinced that PARP-1 plays a key role in the mechanism controlling the expression of *KRAS* in pancreatic cancer cells. The crucial experimental observation supporting the mechanism proposed in Figure 8A is that an increase of intracellular ROS results in the upregulation of *KRAS* up to 2.5-fold, following H_2O_2 treatment. A similar result was obtained also when Panc-1 cells were phototreated with TMPyP4: A cationic porphyrin producing ROS upon irradiation [34]. As stated before, an increase of ROS enhances the level of 8OG in the G4-region of *KRAS* and stimulates the recruitment of PARP-1, MAZ, and hnRNP A1 to the promoter [35]. Pull-down experiments of chromatin with biotinylated G4 ligand b-6438 followed by a ChIP with anti 8OG Ab showed that 8OG and G4 DNA co-localize in the same promoter region (at ~0.2 kb resolution). If we assume that 8OG is present in the G4 motifs, because

of their high guanine content, the recruitment stimulated by H_2O_2 increases the occupancy of the promoter G4 motifs by the transcription factors. This is indeed in keeping with pull-down and Western blot assays showing that the G4 motifs of the *KRAS* promoter form together with PARP-1, MAZ and hnRNP A1 the transcription pre-initiation complex. It is possible that 8OG behaves as an epigenetic mark for the recruitment to the promoter of the transcription factors [51–53]. We observed that PARP-1 binds to both G4 32R and G4 mid, either in a wild-type or oxidized form. When PARP-1 binds to G4 32R and G4 mid, it undergoes a structural change that makes the protein catalytically active, capable of auto PARylation. The auto PARylation process promoted by G4 has been confirmed in vitro, while cell-based experiments with anti poly/mono-ADP ribose and anti PARP-1 Abs showed that only few ADP-ribose units are present on PARylated PARP-1. The units of ADP-ribose attached on the surface of the protein assign a negative charge to PARP-1, which becomes anionic in nature. By contrast, MAZ and hnRNP A1, having isoelectric points (pI) of 8.1 and 9.2, respectively, are cationic in nature under physiological conditions. Thus, a possible function of PARP-1 bound to the G4 motifs is to recruit, through electrostatic interactions, the two transcription factors (Figure 8B). In this way MAZ and hnRNP A1 spatially accumulate in the promoter region where the transcription pre-initiation complex will be formed. According to this model, *KRAS* transcription is expected to be inhibited if MAZ or hnRNP A1 are suppressed. This has indeed been reported in previous works [22,24,35]. Moreover, given the important role attributed to PARP-1, the suppression or inhibition of its catalytic activity should strongly inhibit *KRAS* expression. This central issue will be addressed in the next and last section.

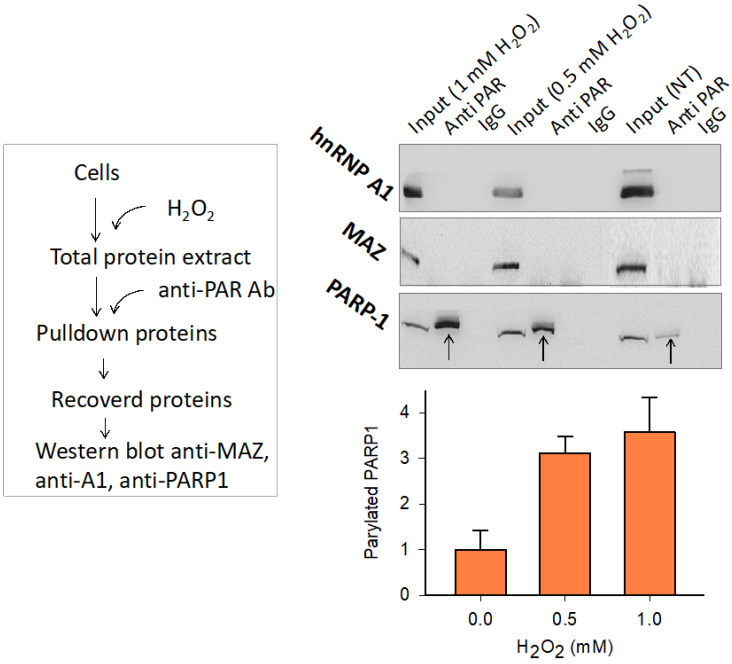

Figure 7. Anti-PAR immunoprecipitation assay. (Left) Experimental scheme; (Right) Western blot showing that among the PARylated proteins present in Panc-1 cells treated with 0.5 and 1 mM H_2O_2, there is only PARP-1 and not MAZ and hnRNP A1. The bar plot reports the ratio PARP-1 (pulled down)/PARP-1 (input) as a function of the H_2O_2 concentration. Error bars are from two experiments.

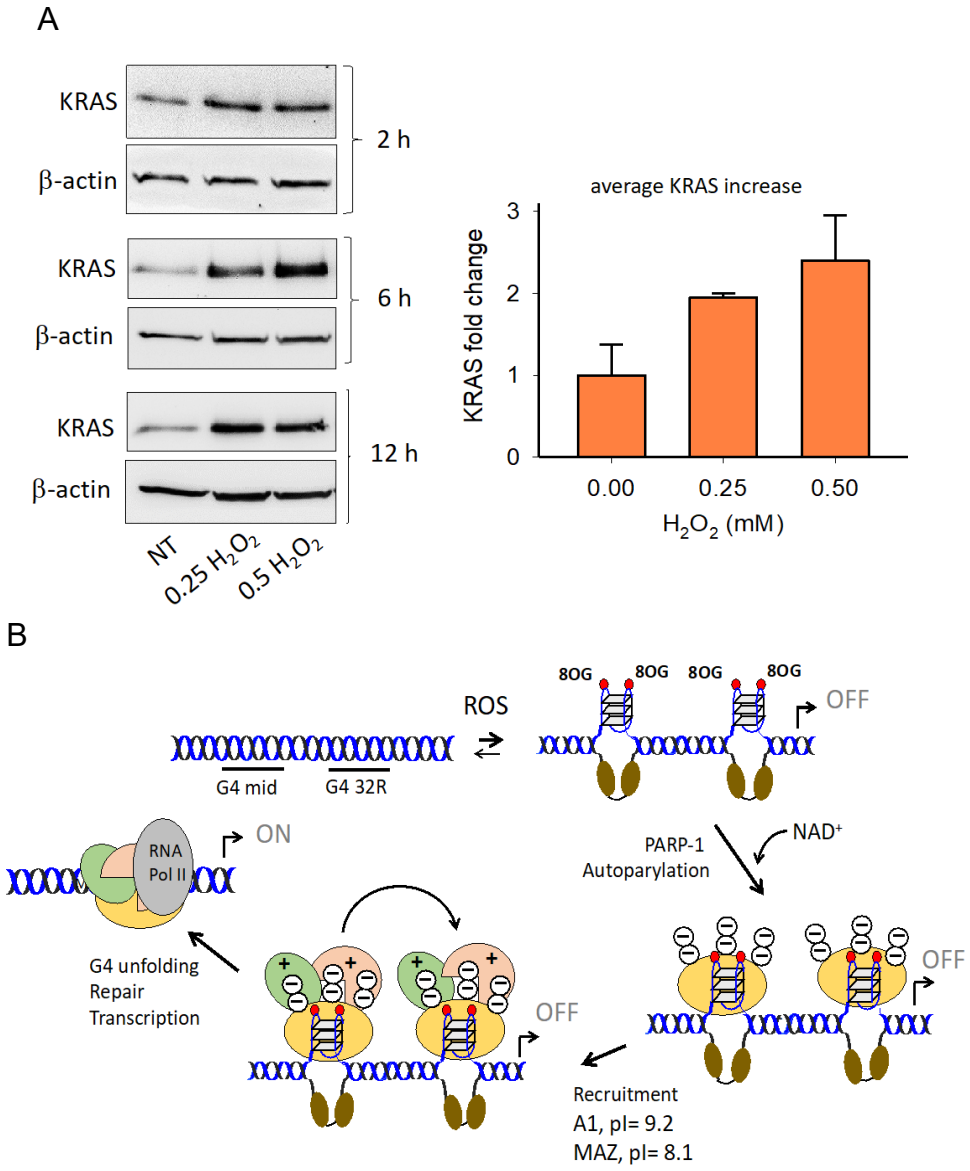

Figure 8. (**A**) Western blots of lysates obtained from Panc-1 cells treated with 0, 0.25, and 0.5 mM H_2O_2 for 2, 6, and 12 h. The cell lysates were obtained to determine the level of expressed KRAS protein respect to β-actin. Band density was assessed with ImageJ Software. The bar plot, reporting the average KRAS/β-actin values from the three treatments, shows that KRAS transcription is stimulated by ROS; (**B**) Proposed mechanism of KRAS activation caused by an increase of oxidative stress. A1 = hnRNP A1, pI = isolectric point.

2.6. PARP-1 and G4 Are Essential for KRAS Expression

Besides regulating transcription through the modification of chromatin structure [17], PARP-1 interacts with the promoter of *KRAS*, thus acting as a classical transcription factor. Previous studies have reported that PARP-1 is associated with RNA Pol II in open chromatin [54]. We therefore asked what the impact of PARP-1 is on the *KRAS* promoter. We treated Panc-1 cells for 24 and 48 h with a PARP-1 specific siRNA and analyzed by Western blot the expression of PARP-1, KRAS and β-actin. After 48 h the siRNAs suppressed PARP-1 to ~30% of the control (siRNA ctr) and indirectly KRAS to ~10% of the control (Figure 9B). Such a result clearly shows that the expression of KRAS dramatically depends on PARP-1. We also asked if G4 DNA might play a central role in the formation of the transcription pre-initiation complex. We therefore transfected Panc-1 cells with a decoy oligonucleotide mimicking the G4 formed by G4 32R and measured by Western blot the level of KRAS protein (Figure 9C). The Western blot shows that 72 h after transfection with 600 nM G4 32R, the expression of the KRAS protein is completely suppressed. This result suggests that the exogenous G4 32R oligonucleotide transfected in the cells sequesters the transcription factors that normally form the transcription pre-initiation complex at the promoter G4 32R sequence. Finally, according to our model, transcription activation involves autoPARylation of PARP-1 bound to G4 32R and G4 mid1/G4 mid2 in order to favor the electrostatic recruitment of cationic MAZ and hnRNP A1 on the promoter. To test if PARP-1 PARylation is an important step in the mechanism activating *KRAS* transcription, we used inhibitors of the poly/mono(ADP-ribosyl)ation catalyzed by PARP-1, Olaparib and Veliparib [50,55]. Panc-1 cells were treated with 30 and 70 μM Olaparib and Veliparib for 48 h and the levels of the KRAS and β-actin proteins were measured by Western blot. The results reported in Figure. 9E,F indicate that Veliparib decreases the expression of KRAS by ~60% compared to the control (untreated cells). This behavior is fully consistent with our hypothesis that the autoPARylation of PARP-1 plays a critical role in activating the expression of the *KRAS* oncogene under oxidative stress.

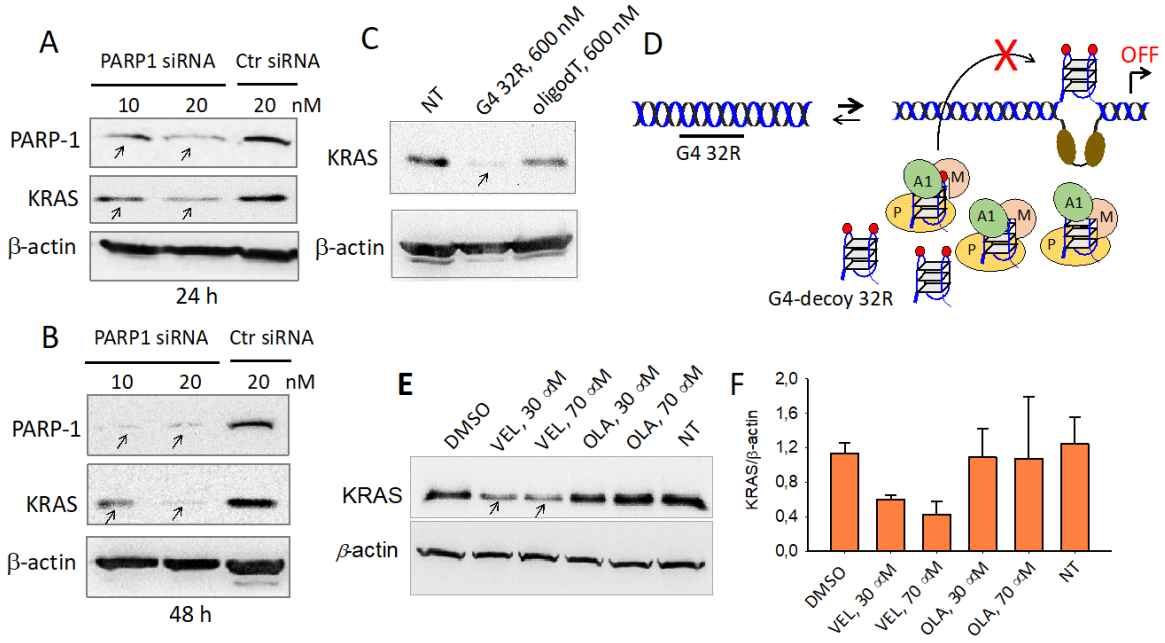

Figure 9. (**A**,**B**) Western blot assays showing that 10 and 20 nM PARP-1 siRNA suppress PARP-1 and *KRAS* as well, in Panc-1 cells, control siRNA-ctr does not. The analysis was carried out 24 and 48 h after siRNA treatment; (**C**) Western blot showing that Panc-1 cells treated with G4 32R inhibits the expression of *KRAS* by acting as a G4 decoy which sequester the transcription factors. As a control an oligo dT was used; (**D**) Mechanism of action of G4 32R acting as a G4 decoy; (**E**,**F**) Western blot experiment. Panc-1 cells treated with 30 and 70 μM Veliparib (VEL) and Olaparib (OLA), small-molecules inhibiting the catalytic activity of PARP-1, result in >50% down-regulation of KRAS protein compared to control (untreated cells). Bands density were assessed with ImageJ Software. The bar plot reports KRAS/β-actin ratios. Error bars are from two independent experiments.

3. Materials and Methods

3.1. Oligonucleotides

The non-modified oligonucleotides used in this study have been purchased from Microsynth-AG, Balgach, Switzerland. 8-oxoG-substituted oligonucleotides were synthesized from 8-oxo-dG CEP from Berry & Associates in 1-μmol scale on solid support by standard procedure, except using concentrated ammonia in the presence of 2-mercaptoethanol (0.25 M) in the deprotection step, as described by Bodepudi et al. [56]. The oligonucleotides were purified by reverse-phase high pressure (or high performance) liquid chromatography on a Water system 600, equipped with a C18 column (XBridge OST C18, 19 × 1000 mm, 5 μm). The composition of the oligonucleotides was verified by Matrix Assisted Laser Desorption Ionization-Time of Flight (MALDI-TOF). Sequences are reported in Table 1.

3.2. Cell Culture

Human pancreatic ductal adenocarcinoma cells (Panc-1), bearing a heterozygous missense G12D mutation in the *KRAS* gene, were maintained in exponential growth in Dulbecco's modified Eagle's medium High Glucose (DMEM-High Glucose) containing 100 U/mL penicillin, 100 mg/mL streptomycin, 20 mM L-glutamine and 10% fetal bovine serum. All reagents were purchased from EuroClone S.p.A.,Pero (Milano), Italy.

3.3. Chromatin Immunoprecipitation and Quantitative PCR

ChIP was carried out by using the ChIP-IT® Express Shearing Kit (Active Motif, Carlsbad, CA, USA). In brief, 8×10^5 Panc-1 cells were seeded in 6-well plates and after 24 h some plates were treated with 1 or 0.5 mM H_2O_2 for 30 min in serum-free DMEM-High Glucose. Then, the cells were washed with phosphate buffered saline (PBS) and fixed for 10 min in serum-free DMEM-High Glucose containing 1 % formaldehyde. After fixing, the cells were washed with cold PBS and Glycine Stop-Fix Solution was added to arrest the fixing reaction. The cells were then washed again with cold PBS, treated with Scraping Solution and centrifuged at 720 g for 10 min at 4 °C. The pellet was re-suspended in ice-cold lysis buffer supplemented with PMSF and PIC (protease inhibitor cocktail) and incubated for 30 min on ice. The cells were transferred to an ice-cold dounce homogenizer for 10 strokes to release the nuclei. The homogenate was centrifuged for 10 min at 2400 g at 4 °C, to pellet the nuclei. The nuclei were re-suspended in Shearing Buffer and the chromatin sheared by sonication (10 × (30 s pulse on/30 s pulse off)) on Bioruptor Plus (Diagenode, Seraing, Belgium) into DNA fragments of about 300–400 bp. The sheared chromatin was centrifuged at maximum speed for 15 min, 4 °C. The chromatin concentration was determined with a spectrophotometer by UV absorption at 260 nm. Ten micrograms of chromatin were treated overnight at 4 °C with 1 μg PARP-1 specific antibody (Santa Cruz Biotechnology, Heidelberg, Germany). In addition to the antibody, the mixtures were added with Protein G Magnetic Beads, ChIP buffer-1 and PIC, following the Active Motif Kit protocol. After overnight incubation at 4 °C, the mixtures were spun and the chromatin bound to the antibody collected with a magnetic bar. The collected beads were washed once with ChIP buffer-1 and twice with ChIP buffer-2. The beads were then re-suspended in Elution Buffer AM2 and let to incubate on shaking for 15 min at room temperature. The beads were treated with Reverse Crosslinking Buffer and the supernatant with the chromatin was collected. 1 μg of chromatin was used as "input" to assess G4 enrichment after incubation with Ab-PARP-1; in addition to the chromatin, the mixtures were added with ChIP Buffer-2 and 10 mM NaCl. Both input and immuno-precipitated chromatins were heated at 95 °C for 15 min, added with Proteinase K and incubated at 37 °C for 1 h. Finally, Proteinase K Stop Solution was added to halt the reaction. The DNA fragments were amplified by qPCR using primers specific for genomic *KRAS* (accession number NG_007524):
G4-plus 5′-GTACGCCCGTCTGAAGAAGA-3′ (nucleotides (nt) 4889–4908, 0.2 μM),
G4-minus 5′-GAGCACACCGATGAGTTCGG-3′ (nt 4958–4977, 0.1 μM),
Ctr1-plus 5′-ACAAAAAGGTGCTGGGTGAGA-3′ (nt 12–32, 0.2 μM),
Ctr1-minus 5′-TCCCCTTCCCGGAGACTTAAT-3′ (nt 248–268, 0.2 μM),

Ctr2-plus 5′-CTCCGACTCTCAGGCTCAAG-3′ (nt 7536–7555, 0.15 μM), Ctr2-minus 5′-CAGCACTTTGGGAGGCTTAG-3′ (nt 7692–7711, 0.15 μM). The *KRAS* G4 region is located upstream TSS in the non-coding strand, ctr1 is about 5 k-bp upstream TSS while ctr2 is in an intron, about 3 k-bp downstream TSS. The % GC contents of the G4, ctr1, and ctr2 regions are 65, 44 and 59 %, respectively. The lower GC content of ctr1 is only apparent because it contains three 29-mer sequences with a GC content of 55, 59, and 60 %. The G4, ctr1, and ctr2 sequences are within chromatin fragments of 300–400 bp; the length of the amplified sequences are 91, 256, and 176 bp, respectively. The qPCR reactions were carried out with a CFX-96 real-time PCR apparatus controlled by Optical System software (version 3.1) (Bio-Rad Laboratories, Segrate (Milano), Italy) on 1 μl of immuno-precipitated chromatin or input, which were mixed to Sybr Green mix following manufacturer instructions (Kapa Sybr Fast QPCR Mix, Kapa Biosystems, MA, USA) and primers. For G4-region amplification cycles were: 3 min at 95 °C, 40 cycles 30 sec at 95 °C and 40 sec at 59 °C. For controls amplification cycles were: 3 min at 95 °C, 40 cycles 10 s at 95 °C and 30 s at 57 °C (ctr1) or 61 °C (ctr2). All reactions have been validated before amplification for each target and couple of primers. The Ct-values (number of cycles required for the fluorescent signal to cross the threshold) given by the instrument (Bio-Rad, CFX96 Real-time PCR detection System) were used to evaluate the difference between sample and input. The adjusted Ct input was obtained by Ct input − log2 (input dilution factor). Then ΔCt = Ct sample − Adjusted Ct input. The % Input for each sample was calculated as follows: % Input = $100 \times 2^{-\Delta Ct}$. The % Input was obtained for the G4 region and also for the non-G4 regions (ctr1 and ctr2). The enrichment in 8-oxoG or MAZ or hnRNP A1 or OGG1 of the G4 region respect to the non-G4 regions was determined by the ratio:

[% Input (G4 region)]/[% Input (non-G4 region)]

3.4. Mobility Shift Assays

Recombinant PARP-1 was purchased by Antibodies-online GmbH, Germany and provided as powder; the lyophilized protein was reconstituted with dH_2O following manufacturer instructions.

Recombinant MAZ and hnRNP A1 proteins were obtained as reported in Supplementary Information S1. Before EMSA, 5′Cy5.5 G4 oligonucleotides (G4 32R, G4 mid1 and G4 mid2) were allowed to form their structure in 50 mM Tris–HCl, pH 7.4, 100 mM KCl, heated at 95 °C for 5 min and incubated overnight at RT. Cy5.5-oligonucleotides (50 nM) were treated for 30 min at 25 °C with different amounts of PARP-1/hnRNP A1/MAZ, ([protein]/[oligonucleotide] ratios reported in the text) in 20 mM Tris–HCl pH 8, 30 mM KCl, 1.5 mM $MgCl_2$, 1 mM DTT, 8% glycerol, 1% Phosphatase Inhibitor Cocktail I (Merck Life Science, Milano, Italy), 5 mM NaF, 1 mM Na_3VO_4, 2.5 ng/mL poly [dI-dC], 50 μM ZnAc. After incubation, the reaction mixtures were loaded in 5% TB (1×) polyacrylamide gel and run at 300 V, 50 mA, 30 W for 2 h at 20 °C. After running, the gel was analyzed with Odyssey CLx Imaging System (Li-COR Biotechnology, Bad Homburg, Germany).

3.5. Nuclear Extract and Biotin-Streptavidin Pull Down Assay

To obtain nuclear extracts, 6 plates of 15 cm diameter of Panc-1 cells at a given confluence were collected and exposed to 0.5 μM ADP-HPD, an inhibitor of PARG enzyme (Merck Life Science, Milano, Italy) for 1 h. Subsequently, the cells were washed with PBS and treated with 1mM H_2O_2 in serum free DMEM-High Glucose for 2, 4, and 8 min. The cells were collected in PBS buffer, centrifuged at 800 g for 10 min at 4 °C. Next, the cells were resuspended in hypotonic buffer (10 mM HEPES-KOH, pH 7.9, 1.5 mM $MgCl_2$, 10 mM KCl, 0.2 mM PMSF, 0.5 mM DTT, 5 mM NaF, 1 mM Na_3VO_4) and kept in ice for 10 min. The swollen cells were homogenized with a Dounce homogenizer and the nuclei, pelleted by centrifugation and resuspended in low-salt buffer (20 mM HEPES-KOH, pH 7.9, 25 % glycerol, 1.5 mM $MgCl_2$, 20 mM KCl, 0.2 mM EDTA, 0.2 mM PMSF, 0.5 mM DTT). Release of nuclear proteins was obtained by the addition of a high-salt buffer (low-salt buffer containing 1.2 M KCl). Protein concentration was measured according to the Bradford method. Biotinylated 32R, **92**, **96**, mid1, mid2, mid, midox mid1ox and mid2ox were folded in 50 mM Tris-HCl, pH 7.4 and 100 mM KCl by heating the solutions at 95 °C for 5 min and successive incubation at RT overnight. The corresponding duplexes were obtained by annealing (5 min at 95 °C and overnight at RT) the G4 oligonucleotides with the complementary strands in 50 mM Tris–HCl pH 7.4, 100 mM NaCl. 80 μg of Panc-1 nuclear extract were incubated for 30 min at

RT with 80 nM biotinylated 32R, **92**, **96**, mid1, mid2, mid, midox, mid1ox and mid2ox in 20 mM Tris–HCl, pH 7.4, 150 mM KCl, 8 % glycerol, 1 mM DTT, 0.1 mM ZnAc, 5 mM NaF, 1 mM Na_3VO_4 and 2.5 ng/μL poly[dI-dC]. Then 80 μg of Streptavidin MagneSphere Paramagnetic Particles (Promega Italia, Milano, Italy) were added and let to incubate for 30 min at RT. The beads were captured with a magnet and washed two times. The proteins were denatured and eluted with Laemmli buffer (4% SDS, 20% glycerol, 10% 2-mercaptoethanol, 0.004% bromophenol blue and 0.125 M Tris–HCl).

3.6. Western Blots

Protein samples were separated in 10–12% SDS-PAGE and blotted onto nitrocellulose membrane at 70 V for 2 h. The nitrocellulose membrane was blocked for 1 h with 5 % fat dried milk in PBS and 0.1 % Tween (Merck Life Science, Milano, Italy) at room temperature. The primary antibodies used were: Anti-MAZ (clone 133.7, IgG mouse, Santa Cruz Biotechnology, Dallas, TX, USA), anti-hnRNP A1 (clone 9H10, IgG mouse, Merck Life Science, Milano, Italy), anti-PARP-1 (polyclonal antibody, IgG rabbit, Cell Signalling Technology, Leiden, The Netherlands), anti-PAR (Poly/Mono-ADP Ribose (E6F6A) Rabbit mAb #83732, Cell Signalling Technology, Leiden, The Netherlands), anti-β-actin [Anti-Actin (Ab-1) Mouse mAb (JLA20)], (Merck Life Science, Milano, Italy), anti-KRAS (Mouse monoclonal Anti-KRAS, clone 3B10 2F2, Merck Life Science, Milano, Italy). The membranes were incubated overnight at 4 °C with the primary antibodies, then washed with 0.1% Tween in PBS and incubated for 1 h with the secondary antibodies conjugated to horseradish peroxidase: Anti-mouse IgG (diluted 1:5000), anti-rabbit IgG (diluted 1:5000) and anti-mouse IgM (diluted 1:5000) (Merck Life Science, Milano, Italy). The signal was developed with Super Signal® West PICO, and FEMTO (Thermo Fisher Scientific, Waltham, MA, USA) and detected with ChemiDOC XRS, Quantity One 4.6.5 software (Bio-Rad Laboratories, Segrate, (Milano), Italy). Bands quantification was performed with the ImageJ software.

3.7. PAR Immunoprecipitation Assay

Panc-1 cells were seeded onto 15 cm diameter plates. At a confluence of 80%, the cells were treated with 1 and 0.5 mM H_2O_2 in serum-free DMEM High Glucose medium for 30 min. Then the nuclear proteins were extracted and quantified as described in the "Nuclear extract and biotin-streptavidin pull down assay". For immunoprecipitation, 1.5 mg of Protein A-Dynabeads (ThermoFisher Scientific-Invitrogen, Waltham, MA, USA) were incubated with 3 μg of PAR antibody (Poly/Mono-ADP Ribose (E6F6A) Rabbit mAb #83732, Cell Signalling Technology, Leiden, The Netherlands) and 3 μg of IgG Rabbit (ThermoFisher Scientific-Invitrogen, Waltham, MA, USA) as negative control in 20 mM Tris-HCl, pH 7.4, 150 mM KCl, 8% glycerol, 1mM DTT and 0.1 mM ZnAc for 15 min at RT. After one wash with the same buffer, 80 μg of nuclear extracts were allowed to react with anti-PAR- and IgG rabbit-derivatized Dynabeads for 30 min at RT. The beads were captured with a magnet and washed twice with the same buffer. The proteins were denatured and eluted with Laemmli buffer (4% SDS, 20% glycerol, 10% 2-mercaptoethanol, 0.004% bromophenol blue and 0.125 M Tris–HCl).

3.8. PARP-1 AutoPARylation and Inhibition Assays

Oligonucleotides 32R, **92**, **96**, mid1, mid2, and mid sequences were allowed to fold into G-quadruplex as reported previously. 0, 10, 20, and 40 nM rPARP-1 (Antibodies-online, Aachen, Germany) was incubated with 10 nM biotinylated sequences in 50 mM Tris-HCl, pH 7,4, 50 mM KCl, 2 mM $MgCl_2$, 1 mM DTT, 50 μM ZnAc and 150 μM NAD^+ in 15 μL final volume for each reaction. Samples include both positive (PARP-1 incubated with activating-DNA from "PARP-1 Enzyme Activity Assay", Merck Life Science, Milano, Italy) and negative control (PARP-1 incubated with 400 μM Veliparib inhibitor, purchased from Selleckchem, Munich, Germany). Incubation was carried out for 30 min at RT and stopped with the addition of Laemmli buffer (4% SDS, 20 % glycerol, 10% 2-mercaptoethanol, 0.004% bromophenol blue and 0.125 M Tris–HCl).

3.9. Inhibition of KRAS by G4 Decoys, siRNA and Veliparib

To evaluate KRAS expression by Western blot, 5×10^5 cells/well were seeded onto a 6-well plate and transfected with 600 nM 32R or 600 nM oligodT (control) by jetPEI™. The cells were collected 72 h after transfection in Laemmli Buffer (4% SDS, 20% glycerol, 0.125 M Tris–HCl, pH 7.4) and lysed by Bioruptor Plus (Diagenode, Seraing, Belgium) (30 sec on/30 sec off) repeated 20 times. The proteins in the lysates were determined by Markwell assay [57].

To evaluate the expression level of KRAS following siRNA or PARP-1 inhibitor treatments, we seeded Panc-1 cells (4×10^5 cells/well) onto 6-well plate. After 24 h cells were exposed to either PARP-1 siRNA (Santa-Cruz Biotechnology, Heidelberg, Germany) (10 or 20 nM, 24 and 48 h) or Veliparib/Olaparib (30 or 70 μM, 48 h) (Selleckchem, Munich, Germany) diluted in DMSO. SiRNA were delivered with INTERFERin siRNA transfection reagent (Polyplus Transfection, Illkirch, France). After treatment, the cells were washed with PBS and collected in Laemmli Buffer (4% SDS, 20% glycerol, 0,125 M Tris–HCl). Cell lysates were obtained as described above.

3.10. Panc-1 Nuclear Extract

Untreated or treated Panc-1 cells (8×10^5) (treated with the various molecules used in this study) were seeded onto a 6-well plate. The following day, the cells were treated with 0, 0.25, and 0.5 mM H_2O_2 in serum-free DMEM High Glucose for 2, 6, and 12 h. The medium was then removed, the cells washed with PBS and collected in Laemmli Buffer (4% SDS, 20% glycerol, 0.125 M Tris–HCl, pH 7.4). The cells were lysed on Bioruptor Plus (Diagenode, Seraing, Belgium), by adopting as lysis protocol, 30 sec on/30 sec off, repeated 20 times. The lysates were quantified with Markwell assay [57].

3.11. UV-Melting and CD

UV-melting was performed by using Jasco V-750 UV-visible spectrophotometer equipped with a Peltier temperature control system (ETCS-761) (Jasco Europe, Cremella, Italy). The spectra were analyzed with Spectra Manager (Jasco Europe, Cremella, Italy). The oligonucleotides (5 μM) were annealed in 50 mM Na-cacodylate, pH 7.4 and 100 mM KCl, (5 min at 95 °C, overnight at RT). The melting curves were recorded at 295 nm in a 0.5 cm path length quartz cuvette, heating (25–95 °C) at a rate of 0.5 °C/min.

Circular Dichroism (CD) spectra were obtained on a JASCO J-600 spectropolarimeter, equipped with a thermostated cell holder, with 5 μM oligonucleotide solutions in 50 mM Na-cacodylate, pH 7.4, 100 mM KCl. The spectra were recorded in 0.5 cm quartz cuvette at 25 and 95 °C and reported as ellipticity (mdeg) versus wavelength (nm). Each spectrum was smoothed and subtracted to the baseline.

3.12. Fluorescence Experiments

32R, mid1 and mid2 were allowed to fold into quadruplex in 50 mM Na-cacodylate, pH 7.4, 100 mM KCl, (5 min at 95 °C, overnight at RT). The Trp fluorescence was titrated by adding to a 60 nM of recombinant PARP-1 solution (500 μL) in 50 mM Na-cacodylate, pH 7.4, 100 mM KCl, 50 μM ZnAc, 1 mM DTT, increasing amounts of G4 (see plots). A solution (without PARP-1) was used as blank. The aliquots of G4 were directly added to the PARP-1 solution and reading was performed 5′ after the incubation between PARP-1 and G4s. The fluorescence was measured on a Cary Eclipse Fluorescence Spectrophotometer (Agilent Technologies Italia, Cernusco sul Naviglio, Italy), equipped with a thermostated cell holder. The spectra were recorded at 20 °C between 310 and 500 nm, excitation at 295 nm. Each spectrum was smoothed and subtracted to the baseline.

3.13. Biotinylated-Anthrathiophenedione Pull-Down Assay

The pull down of chromatin fragments containing G4 structures with a G4-specific ligand b-6438 is described in Supplementary Information S2.

4. Conclusion

In this work we have examined the role of PARP-1 in the activation of the transcription of KRAS in pancreatic cancer cells. The function of this oncogene is essential in PDAC, as it reprograms the glucose and glutamine metabolism with the aim of fueling an increased anabolic demand, typical of rapidly dividing cells [4,5]. Since cancer cells are characterized by a high metabolic rate, they produce higher levels of ROS than normal cells do. So, we asked what the impact of an enhanced level of ROS is in maintaining the transformed phenotype of PDAC. The starting points of our study are: (i) ROS increase the level of 8OG in the genome, in particular in the G4 motifs composed by contiguous runs of guanines; (ii) ROS stimulate the expression of *KRAS*, the oncogene to which PDAC cells are addicted [8]. Burrows and co-workers reported that the oxidation of guanine to 8OG in the VEGF G4 motif located upstream of Rluc reporter gene increases gene expression by 4-fold [51)]. If this may be considered as a general behavior and if it is applicable to the *KRAS* gene too, our work describes a possible mechanism through which 8OG in *KRAS* promoter upregulates gene expression. We have hypothesized that an increase of intracellular ROS, due to endogenous (metabolism) or exogenous (oxidants) sources, may oxidize guanine into 8OG in the G4-motif of the *KRAS* promoter located upstream of TSS. The oxidized G-rich sequence provides a platform for the assembly of the transcriptional machinery [35,52,58]. We already have found that the upregulation of KRAS occurring in the presence of oxidative stress stimulates the expression of Nrf2 [34]: The master regulator of cellular redox which activates the detoxification program by bringing down the ROS level for optimal cell proliferation [59,60]. We present experimental evidence that the activation of KRAS occurs through a mechanism involving the enrichment in 8OG of the promoter region with the G4 motifs recognized by transcription factors PARP-1, MAZ, and hnRNP A1. The enrichment of 8OG in the KAS G4 32R region produces an increase in the same region of the occupancy by PARP-1, MAZ, and hnRNP A1. This is in agreement with two facts: (i) Recombinant PARP-1 binds in vitro to G4 32R and G4 mid1/G4 mid2 sequences, (ii) biotinylated G4 32R in the G4 conformation pulls down a multi-protein complex containing the three transcription factors. The binding of PARP-1 to the KRAS promoter activates the catalytic property of this protein, which by utilizing NAD^+ undergoes a limited auto PARylation. This process changes the net charge of the protein, that becomes anionic. It also favours the recruitment to the promoter of cationic transcription factors necessary for KRAS transcription, like MAZ and hnRNP A1. Several reports have indeed assigned to PARP-1 a role in the assembly of regulatory complexes at the promoter of the genes [17,61]. In keeping with our results Chowdhury and co-worker found that zinc-finger transcription factors, such as PARP-1 and MAZ, are closely associated to the G4 motifs in the promoter of the human genes [62]. In conclusion, our study shows that the increase of KRAS transcription observed in the presence of enhanced levels of oxidative stress is mediated by PARP-1.

Supplementary Materials: Supplementary materials can be found at http://www.mdpi.com/1422-0067/21/17/ 6237/s1. Supplementary S1: Recombinant proteins MAZ and hnRNP A1. Supplementary S2: Pull-down assay with b-6438. Supplementary S3: Structure of the G4 formed by sequence 32R (G4-near). Supplementary S4: Putative structures formed G4 mid1 and G4 mid2. Supplementary S5: Melting curves of G4 mid, G4 mid^{ox}, G4 mid1, G4 mid1^{ox}, G4 mid2, G4 mid2^{ox}. Supplementary S6: Structure of a G-tetrad with one G replaced by 8OG. Supplementary S7: EMSA showing the binding of hnRNP A1 to the G4 mid sequences. Supplementary S8: EMSA showing the binding of MAZ to the G4 mid sequences. Supplementary S9: Structures of PARP-1 inhibitors Veliparib and Olaparib.

1. **Author Contributions:** Conceptualization and supervision L.E.X.; investigation, G.C. and A.F.; writing—original draft preparation, L.E.X. and G.C.; DNA synthesis, E.B.P.; funding acquisition, L.E.X. All authors have read and agreed to the published version of the manuscript.

Funding: This research was funded by AIRC (Associazione italiana per la ricerca sul cancro), IG 2017, Project code 19898.

Conflicts of Interest: The authors declare no conflict of interest.

Abbreviations

KRAS	*Kirsten ras* gene
MAZ	MYC associated zinc finger protein
hnRNP A1	Heterogeneous nuclear ribonucleoprotein A1
PARP-1	Poly[ADP-ribose] polymerase 1
PDAC	Pancreatic ductal adenocarcinoma
8OG	8-Oxoguanine
TSS	Transcription start site
ChIP	Chromatin immunoprecipitation
PARylation	Poly(ADP-ribosyl)ation

References

1. Vincent, A.; Herman, J.; Schulick, R.; Hruban, R.H.; Goggins, M. Pancreatic cancer. *Lancet* **2011**, *378*, 607–620.
2. Collins, M.A.; Bednar, F.; Zhang, Y.; Brisset, J.C.; Galbán, S.; Galbán, C.J.; Rakshit, S.; Flannagan, K.S.; Adsay, N.V.; Pasca Di Magliano, M. Oncogenic Kras is required for both the initiation and maintenance of pancreatic cancer in mice. *J. Clin. Investig.* **2012**, *122*, 639–653.
3. Ying, H.; Kimmelman, A.C.; Lyssiotis, C.A.; Hua, S.; Chu, G.C.; Fletcher-Sananikone, E.; Locasale, J.W.; Son, J.; Zhang, H.; Coloff, J.L.; et al. Oncogenic kras maintains pancreatic tumours through regulation of anabolic glucose metabolism. *Cell* **2012**, *149*, 656–670.
4. Diehl, F.F.; Lewis, C.A.; Fiske, B.P.; Vander Heiden, M.G. Cellular redox state constrains serine synthesis and nucleotide production to impact cell proliferation. *Nat. Metab.* **2019**, *1*, 861–867.
5. Son, J.; Lyssiotis, C.A.; Ying, H.; Wang, X.; Hua, S.; Ligorio, M.; Perera, R.M.; Ferrone, C.R.; Mullarky, E.; Shyh-Chang, N.; et al. Glutamine supports pancreatic cancer growth through a KRAS-regulated metabolic pathway. *Nature* **2013**, *496*, 101–105.
6. Weinstein, I.B.; Joe, A.K. Mechanisms of Disease: Oncogene addiction—A rationale for molecular targeting in cancer therapy. *Nat. Clin. Pract. Oncol.* **2006**, *3*, 448–457.
7. Pagliarini, R.; Shao, W.; Sellers, W.R. Oncogene addiction: Pathways of therapeutic response, resistance, and road maps toward a cure. *EMBO Rep.* **2015**, *16*, 280–296.
8. McCormick, F. KRAS as a therapeutic target. *Clin. Cancer Res.* **2015**; *21*, 1797–1801.
9. Cogoi, S.; Xodo, L.E. G4 DNA in ras genes and its potential in cancer therapy. *Biochim. Biophys. Acta* **2016**, *1859*, 663–674.
10. Cogoi, S.; Xodo, L.E. G-quadruplex formation within the promoter of the KRAS proto-oncogene and its effect on transcription. *Nucleic Acids Res.* **2006**, *34*, 2536–2549.
11. Cogoi, S.; Paramasivam, M.; Spolaore, B.; Xodo, L.E. Structural polymorphism within a regulatory element of the human KRAS promoter: Formation of G4-DNA recognized by nuclear proteins. *Nucleic Acids Res.* **2008**, *36*, 3765–3780.
12. Hänsel-Hertsch, R.; Beraldi, D.; Lensing, S.V.; Marsico, G.; Zyner, K.; Parry, A.; Di Antonio, M.; Pike, J.; Kimura, H.; Narita, M.; et al. G-quadruplex structures mark human regulatory chromatin. *Nat. Genet.* **2016**, *48*, 1267–1272.
13. Rhodes, D.; Lipps, H.J. Survey and summary G-quadruplexes and their regulatory roles in biology. *Nucleic Acids Res.* **2015**, *43*, 8627–8637.
14. Spiegel, J.; Adhikari, S.; Balasubramanian, S. The Structure and Function of DNA G-Quadruplexes. *Trends Chem.* **2020**, *2*, 123–136.
15. D'Amours, D.; Desnoyers, S.; D'Silva, I.; Poirier, G.G. Poly(ADP-ribosyl)ation reactions in the regulation of nuclear functions. *Biochem. J.* **1999**, *342*, 249–268.
16. Ji, Y.; Tulin, A.V. The roles of PARP-1 in gene control and cell differentiation *Curr. Opin. Genet. Dev.* **2010**, *20*, 512–518.
17. Kraus, W.L. Transcriptional control by PARP-1: Chromatin modulation, enhancer-binding, coregulation, and insulation. *Curr. Opin. Cell Biol.* **2008**, *20*, 294–302.
18. Krishnakumar, R.; Kraus, W.L. The PARP side of the nucleus: Molecular actions, physiological outcomes, and clinical targets. *Mol. Cell* **2010**, *39*, 8–24.
19. Kraus, W.L.; Hottiger, M.O. PARP-1 and gene regulation: Progress and puzzles. *Mol. Asp. Med.* **2013**, *34*, 1109–1123.
20. Schreiber, V.; Dantzer, F.; Amé, J.C.; De Murcia, G. Poly(ADP-ribose): Novel functions for an old molecule. *Nat. Rev. Mol. Cell Biol.* **2006**, *7*, 517–528.

21. Alemasova, E.E.; Lavrik, O.I. Poly(ADP-ribosyl)ation by PARP-1: Reaction mechanism and regulatory proteins. *Nucleic Acids Res.* **2019**, *47*, 3811–3827.
22. Paramasivam, M.; Membrino, A.; Cogoi, S.; Fukuda, H.; Nakagama, H.; Xodo, L.E. Protein hnRNP A1 and its derivative Up1 unfold quadruplex DNA in the human KRAS promoter: Implications for transcription. *Nucleic Acids Res.* **2009**, *37*, 2841–2853.
23. Cogoi, S.; Zorzet, S.; Rapozzi, V.; Géci, I.; Pedersen, E.B.; Xodo, L.E. MAZ-binding G4-decoy with locked nucleic acid and twisted intercalating nucleic acid modifications suppresses KRAS in pancreatic cancer cells and delays tumour growth in mice. *Nucleic Acids Res.* **2013**, *41*, 4049–4064.
24. Chu, P.C.; Yang, M.C.; Kulp, S.K.; Salunke, S.B.; Himmel, L.E.; Fang, C.S.; Jadhav, A.M.; Shan, Y.S.; Lee, C.T.; Lai, M.D.; et al. Regulation of oncogenic KRAS signaling via a novel KRAS-integrin-linked kinase-hnRNP A1 regulatory loop in human pancreatic cancer cells. *Oncogene* **2016**, *35*, 3897–3908.
25. Zhu, X.; Luo, W.; Liang, W.; Tang, F.; Bei, C.; Ren, Y.; Qin, L.; Tan, C.; Zhang, Y.; Tan, S. Overexpression and clinical significance of MYC-associated zinc finger protein in pancreatic carcinoma. *Onco Targets Ther.* **2016**, *9*, 7493–7501.
26. Cogoi, S.; Shchekotikhin, A.E.; Xodo, L.E. HRAS is silenced by two neighboring G-quadruplexes and activated by MAZ, a zinc-finger transcription factor with DNA unfolding property. *Nucleic Acids Res.* **2014**, *42*, 8379–8388.
27. Cogoi, S.; Rapozzi, V.; Cauci, S.; Xodo, L.E. Critical role of hnRNP A1 in activating KRAS transcription in pancreatic cancer cells: A molecular mechanism involving G4 DNA. *Biochim. Biophys. Acta Gen. Subj.* **2017**, *1861*, 1389–1398.
28. Morgan, R.K.; Batra, H.; Gaerig, V.C.; Hockings, J.; Brooks, T.A. Identification and characterization of a new G-quadruplex forming region within the kRAS promoter as a transcriptional regulator. *Biochim. Biophys. Acta* **2016**, *1859*, 235–245.
29. Kaiser, C.E.; Van Ert, N.A.; Agrawal, P.; Chawla, R.; Yang, D.; Hurley, L.H. Insight into the Complexity of the i-Motif and G-Quadruplex DNA Structures Formed in the KRAS Promoter and Subsequent Drug-Induced Gene Repression. *J. Am. Chem. Soc.* **2017**, *139*, 8522–8536.
30. Marquevielle, J.; Robert, C.; Lagrabette, O.; Wahid, M.; Bourdoncle, A.; Xodo, L.E.; Mergny, J.L.; Salgado, G.F. Structure of two G-quadruplexes in equilibrium in the KRAS promoter. *Nucleic Acids Res.* **2020**, gkaa387, doi:10.1093/nar/gkaa387.
31. Cadet, J.; Douki, T.; Ravanat, J.L. Oxidatively generated damage to the guanine moiety of DNA: Mechanistic aspects and formation in cells. *Acc. Chem. Res.* **2008**, *41*, 1075–1083.
32. Kanvah, S.; Joseph, J.; Schuster, G.B.; Barnett, R.N.; Cleveland, C.L.; Landman, U.Z.I. Oxidation of DNA: Damage to nucleobases. *Acc. Chem. Res.* **2010**, *43*, 280–287.
33. Loft, S.; Danielsen, P.H.; Mikkelsen, L.; Risom, L.; Forchhammer, L.; Møller, P. Biomarkers of oxidative damage to DNA and repair. *Biochem. Soc. Trans.* **2008**, *36*, 1071–1076.
34. Ferino, A.; Rapozzi, V.; Xodo, L.E. The ROS-KRAS-Nrf2 axis in the control of the redox homeostasis and the intersection with survival-apoptosis pathways: Implications for photodynamic therapy. *J. Photochem. Photobiol. B* **2020**, *202*, 111672.
35. Cogoi, S.; Ferino, A.; Miglietta, G.; Pedersen, E.B.; Xodo, L.E. The regulatory G4 motif of the Kirsten ras (KRAS) gene is sensitive to guanine oxidation: Implications on transcription. *Nucleic Acids Res.* **2018**, *46*, 661–676.
36. Saito, I.; Takayama, M.; Sugiyama, H.; Nakatani, K.; Tsuchida, A.; Yamamoto, M. Photoinduced DNA Cleavage via Electron Transfer: Demonstration That Guanine Residues Located 5′ to Guanine Are the Most Electron-Donating Sites. *J. Am. Chem. Soc.* **1995**, *117*, 6406–6407.
37. Miglietta, G.; Cogoi, S.; Marinello, J.; Capranico, G.; Tikhomirov, A.S.; Shchekotikhin, A.; Xodo, L.E. RNA G-Quadruplexes in Kirsten Ras (KRAS) Oncogene as Targets for Small Molecules Inhibiting Translation. *J. Med. Chem.* **2017**, *60*, 9448–9461.
38. Ding, Y.; Fleming, A.M.; Burrows, C.J. Sequencing the Mouse Genome for the Oxidatively Modified Base 8-Oxo-7,8-dihydroguanine by OG-Seq. *J. Am. Chem. Soc.* **2017**, *139*, 2569–2572.
39. Clark, D.W.; Phang, T.; Edwards, M.G.; Geraci, M.W.; Gillespie, M.N. Promoter G-quadruplex sequences are targets for base oxidation and strand cleavage during hypoxia-induced transcription. *Free Radic. Biol. Med.* **2012**, *53*, 51–59.
40. Vorlícková, M.; Tomasko, M.; Sagi, A.J.; Bednarova, K.; Sagi, J. 8-Oxoguanine in a quadruplex of the human telomere DNA sequence. *FEBS J.* **2012**, *279*, 29–39.
41. Beckett, J.; Burns, J.; Broxson, C.; Tornaletti, S. Spontaneous DNA lesions modulate DNA structural transitions occurring at nuclease hypersensitive element III1 of the human CMYC proto-oncogene. *Biochemistry* **2012**, *51*, 5257–5268.
42. Thomas, C.J.; Kotova, E.; Andrake, M.; Adolf-Bryfogle, J.; Glaser, R.; Regnard, C.; Tulin, A.V. Kinase-Mediated Changes in Nucleosome Conformation Trigger Chromatin Decondensation via Poly(ADP-Ribosyl)ation. *Mol. Cell* **2014**, *53*, 831–842.
43. Kraus, W.L.; Lis, J.T. PARP goes transcription. *Cell* **2003**, *113*, 677–683.

44. Soldatenkov, V.A.; Vetcher, A.A.; Duka, T.; Ladame, S. First evidence of a functional interaction between DNA quadruplexes and poly(ADP-ribose) polymerase-1. *ACS Chem. Biol.* **2008**, *3*, 214–219.
45. Eustermann, S.; Wu, W.F.; Langelier, M.F.; Yang, J.C.; Easton, L.E.; Riccio, A.A.; Pascal, J.M.; Neuhaus, D. Structural Basis of Detection and Signaling of DNA Single-Strand Breaks by Human PARP-1. *Mol. Cell* **2015**, *60*, 742–754.
46. Eustermann, S.; Videler, H.; Yang, J.C.; Cole, P.T.; Gruszka, D.; Veprintsev, D.; Neuhaus, D. The DNA-binding domain of human PARP-1 interacts with DNA single-strand breaks as a monomer through its second zinc finger. *J. Mol. Biol.* **2011**, *407*, 149–170.
47. Dawicki-McKenna, J.M.; Langelier, M.F.; De Nizio, J.E.; Riccio, A.A.; Cao, C.D.; Karch, K.R.; McCauley, M.; Steffen, J.D.; Black, B.E.; Pascal, J.M. PARP-1 Activation Requires Local Unfolding of an Autoinhibitory Domain. *Mol. Cell* **2015**, *60*, 755–768.
48. Gupte, R.; Liu, Z.; Kraus, W.L. Parps and adp-ribosylation: Recent advances linking molecular functions to biological outcomes. *Genes Dev.* **2017**, *31*, 101–126.
49. Langelier, M.F.; Eisemann, T.; Riccio, A.A.; Pascal, J.M. PARP family enzymes: Regulation and catalysis of the poly(ADP-ribose) posttranslational modification. *Curr. Opin. Struct. Biol.* **2018**, *53*, 187–198.
50. Jain, P.G.; Patel, B.D. Medicinal chemistry approaches of poly ADP-Ribose polymerase 1 (PARP-1) inhibitors as anticancer agents—A recent update. *Eur. J. Med. Chem.* **2019**, *165*, 198–215.
51. Fleming, A.M.; Ding, Y.; Burrows, C.J. Oxidative DNA damage is epigenetic by regulating gene transcription via base excision repair. *Proc. Natl. Acad. Sci. USA* **2017**, *114*, 2604–2609.
52. Ba, X.; Boldogh, I. 8-oxoguanine DNA glycosylase 1: Beyond repair of oxidatively modified base lesion. *Redox Biol.* **2018**, *14*, 669–678.
53. Giorgio, M.; Dellino, G.I.; Gambino, V.; Roda, N.; Pelicci, P.G. On the epigenetic role of guanosine oxidation. *Redox Biol.* **2020**, *29*, 101398.
54. Gibson, B.A.; Zhang, Y.; Jiang, H.; Hussey, K.M.; Shrimp, J.M.; Lin, H.; Schwede, F.; Yu, Y.; Kraus, W.L. Chemical genetic discovery of PARP targets reveals a role for PARP-1 in transcription elongation. *Science* **2016**, *353*, 45–50.
55. Gunderson, C.C.; Moore, K.N. Olaparib: An oral PARP-1 and PARP-2 inhibitor with promising activity in ovarian cancer. *Future Oncol.* **2015**, *11*, 747–757.
56. Bodepudi, V.; Shibutani, S.; Johnson, F. Synthesis of 2′-Deoxy-7,8-dihydro-8-oxoguanosine and 2′-Deoxy-7,8-dihydro-8-oxoadenosine and Their Incorporation into Oligomeric DNA. *Chem. Res. Toxicol.* **1992**, *5*, 608–617.
57. Markwell, M.A.K.; Haas, S.M.; Bieber, L.L.; Tolbert, N.E. A modification of the Lowry procedure to simplify protein determination in membrane and lipoprotein samples. *Anal. Biochem.* **1978**, *87*, 206–210.
58. Fleming, A.M.; Burrows, C.J. Interplay of guanine oxidation and G-quadruplex folding in gene promoters. *J. Am. Chem. Soc.* **2020**, *142*, 1115–1136.
59. Sajadimajd, S.; Khazaei, M. Oxidative Stress and Cancer: The Role of Nrf2. *Curr. Cancer Drug Targets* **2018**, *18*, 538–557.
60. Lee, S.B.; Sellers, B.N.; DeNicola, G.M. The Regulation of NRF2 by Nutrient-Responsive Signaling and Its Role in Anabolic Cancer Metabolism. *Antioxid. Redox Signal.* **2018**, *29*, 1774–1791.
61. Krishnakumar, R.; Kraus, W.L. PARP-1 Regulates Chromatin Structure and Transcription through a KDM5B-Dependent Pathway. *Mol. Cell* **2010**, *39*, 736–749.
62. Kumar, P.; Yadav, V.K.; Baral, A.; Kumar, P.; Saha, D.; Chowdhury, S. Zinc-finger transcription factors are associated with guanine quadruplex motifs in human, chimpanzee, mouse and rat promoters genome-wide. *Nucleic Acids Res.* **2011**, *39*, 8005–8016.

Supplementary Materials

Role of poly [ADP-ribose] polymerase 1

in activating the *Kirsten ras* (*KRAS*) gene in response to oxidative stress

Giorgio Cinque[1], Annalisa Ferino[1], Erik B. Pedersen[2] and Luigi E. Xodo*,[1]

Supplementary S1: Recombinant proteins MAZ and hnRNPA1

Supplementary S2: Pull-down assay with b-6438;

Supplementary S3: Structure of the G4 formed by sequence 32R (G4-near);

Supplementary S4: Putative structures formed G4 mid1 and G4 mid2;

Supplementary S5: Melting curves of G4 mid, G4 mid^{ox}, G4 mid1, G4 mid1^{ox} , G4 mid2, G4-mid2^{ox}

Supplementary S6: Structure of a G-tetrad with one G replaced by 8OG;

Supplementary S7: EMSA showing the binding of hnRNP A1 to the G4 mid sequences;

Supplementary S8: EMSA showing the binding of MAZ to the G4 mid sequences;

Supplementary S9: Structures of PARP-1 inhibitors Veliparib and Olaparib

Supplementary Information S1: Recombinant proteins

Recombinant MAZ and hnRNP A1 proteins tagged to glutathione S-tranferase (GST) were expressed in Escherichia coli DE3/BL21 by using, respectively, plasmid pGEX-hMAZ and pGEX-hnRNPA1. The bacteria were grown at 37 °C in LB broth plus ampicillin 100 μg/mL to an A_{600} of 0.8–1.0 prior to induction with either 1.0 mM (for MAZ) or 0.1 mM (for hnRNP A1) isopropyl 1-thio-β-D-galactopyranoside. Cells carrying pGEX-hMAZ were allowed to grow with 4μM ZnAc overnight at 37°C before harvesting. The cells were centrifuged at 4230 g at 4°C, the supernatant was removed and the cells washed twice with PBS. The pellet was resuspended in a solution of PBS with 1 mM phenylmethylsulfonyl fluoride (PMSF). The bacteria were lysed by sonication (cells containing pGEX-hnRNP A1 were added with 1% Triton X-100 and incubated for 30 min on a shaker at 4 °C) added with 0,1mM PMSF and 0,5mM DTT. The lysate was then centrifuged for 30 min at 4 °C at 34500 g. Glutathione Sepharose 4B resin (GE Healthcare) (50 % slurry in PBS) was added to the supernatant from the previous step and incubated for 1 h at 4 °C on a shaker. The mix was centrifuged for 5 min at 500 g and the pellet was washed 3 times with PBS. The protein was eluted from the resin with 50mM Tris-HCl pH 8, 10mM GSH and stored at -80 °C in the same buffer added with 0,1mM PMSF and 0,5mM DTT.

Supplementary Information S2: Biotinilated-anthrathiophenedione pull-down assay

Panc-1 cells (8×10^5) were seeded onto a 6-well plate and after 48 h some wells were treated with 1 mM H_2O_2 for ½ h in in serum-free DMEM High Glucose. The cells were then washed with phosphate buffered saline (PBS) and fixed for 10 min in serum-free DMEM High Glucose containing 1% formaldehyde. After fixing, the cells were washed with cold PBS and added with Glycine Stop-Fix Solution to arrest the fixing reaction. The cells were washed again with cold PBS, treated with Scraping Solution and centrifuged at 2500 rpm for 10 min at 4°C. The pellet was resuspended in ice-cold lysis buffer supplemented with PMSF, PIC (protease inhibitor cocktail) and incubated for 30 min on ice. The cells were transferred to an ice-cold dounce homogenizer for 20 strokes to release the nuclei. The homogenate was centrifuged for 10 min at 5000 rpm, 4 °C, to pellet the nuclei. The nuclei were resuspended in Shearing Buffer and the chromatin sheared by sonication [10 × (30 s pulse on/30 s pulse off)] on Bioruptor Plus (Diagenode, Seraing, Belgium) into DNA fragments of about 300–400 bp. The sheared chromatin was centrifuged at maximum speed for 15 min, 4◦C. The chromatin concentration was determined with a spectrophotometer by

ultraviolet (UV) absorption (260 nm) and 20 mg were folded in 100 mM KCl, 50 mM Tris-HCl, pH 7.4 (5 min at 95 °C, overnight at RT). The folded chromatin mixed with biotinylated ligand b-6438 (0.8 mM) was incubated at 4 °C for 6h. We incubated the magnetic beads, after saturation with Salmon Sperm DNA (Invitrogen, USA), with chromatin for 30 min at RT. The supernatant was removed and the beads washed three times with 50 mM Tris-HCl, pH 7.4, 50 mM KCl. We then recovered the bound chromatin with a solution 0.8 M NaCl. The following Chromatin Immunoprecipitation experiment was carried out treating the eluted chromatin overnight at 4 °C with 1 mg antibody specific for 8-oxoG (Bioss Antibodies, Woburn, MA, USA), following the Active Motif Kit protocol previously reported in "Chromatin immunoprecipitation and quantitative PCR" section.

Supplementary Information S3: Structure of the G-quadruplex formed by sequence 32R (G4-near) located in the *KRAS* promoter, upstream of TSS. The structure has been determined by DMS-footprinting (ref. 11) and NMR (ref. 30). This 1/1/12 G4 is in equilibrium with a 1/3/11 conformer (ref. 30).

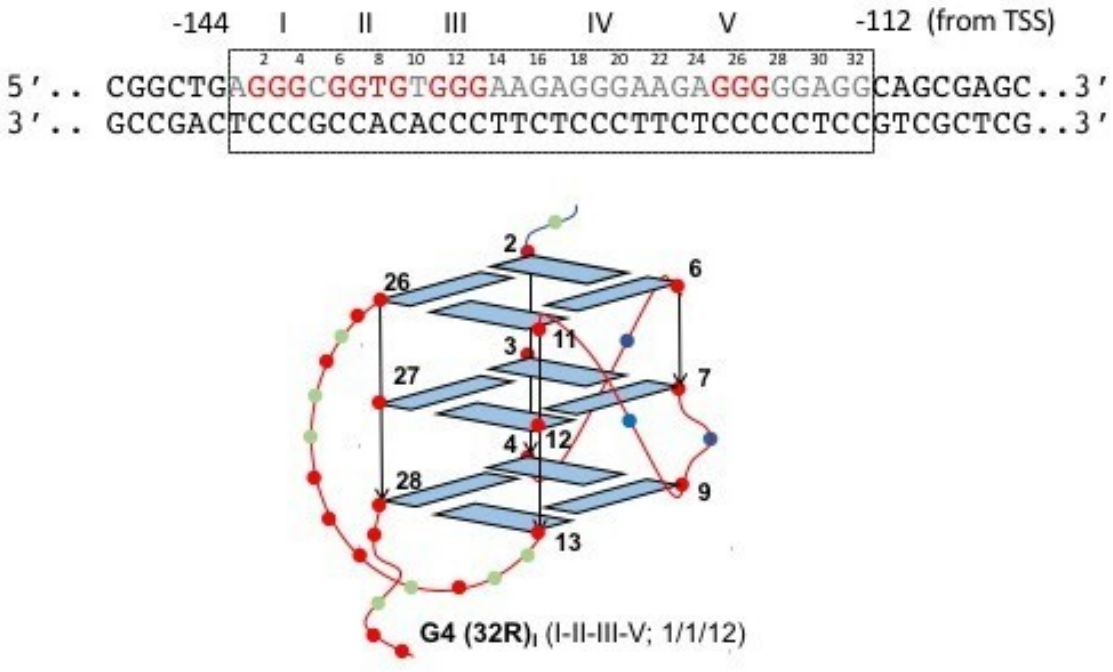

Supplementary Information S4: Putative structures of the G-quadruplexes formed by sequences G4 mid1 (T_M= 59 °C) and G4 mid2 (T_M = 67 °C) located in the *KRAS* promoter, upstream of TSS. For analogy with 32R we propose for both sequences a structure with a bulge and a 1-nt double-

chain reversal loop (loops 4/1/2). This is in keeping with the fact that replacing in G4-mid1 G10 with 8OG, the T_M decreases to 56 °C, because the G-run $G^{OX}GAG$ is replaced by GGG at the 3'end and the G4 assumes a 9/2/2 loop topology. A similar behaviour was observed with 32R (Ref. 27). As with G4 mid1, also G4 mid2 assumes a G4 with a bulge and 1-nt double-chain reversal loop (loops 2/1/6). When G7 and G15 are replaced with 8OG, the T_M goes down to 63 °C, suggesting that G7 is indeed involved in the formation of a G-tetrad.

5′-CGGGGAGAAGGAGGGGCCGGGCCGGGC G4-mid1

3 4 5 10 13 15 17 20 22 25

5′-CGGGCCGGCGGGGAGGAGCGGGGGCCGGGC G4-mid2

2 3 4 7 8 10 12 14 21 23

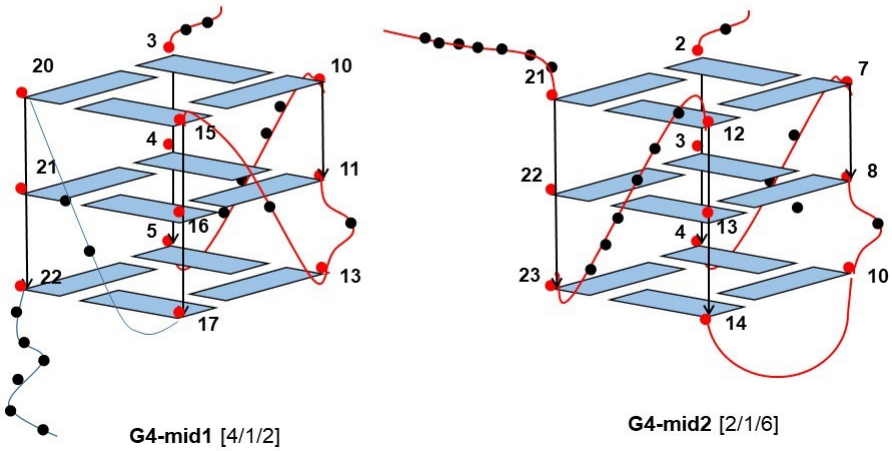

G4-mid1 [4/1/2] **G4-mid2** [2/1/6]

Supplementary Information S5: CD spectra and melting curves of G4 mid, G4 mid1 and G4 mid2 in 50 mM Na-cacodylate, pH 7.4 and 100 mM KCl. The T_M are: 78 °C (G4 mid), 59 (G4 mid1) and 67 (G4 mid2).

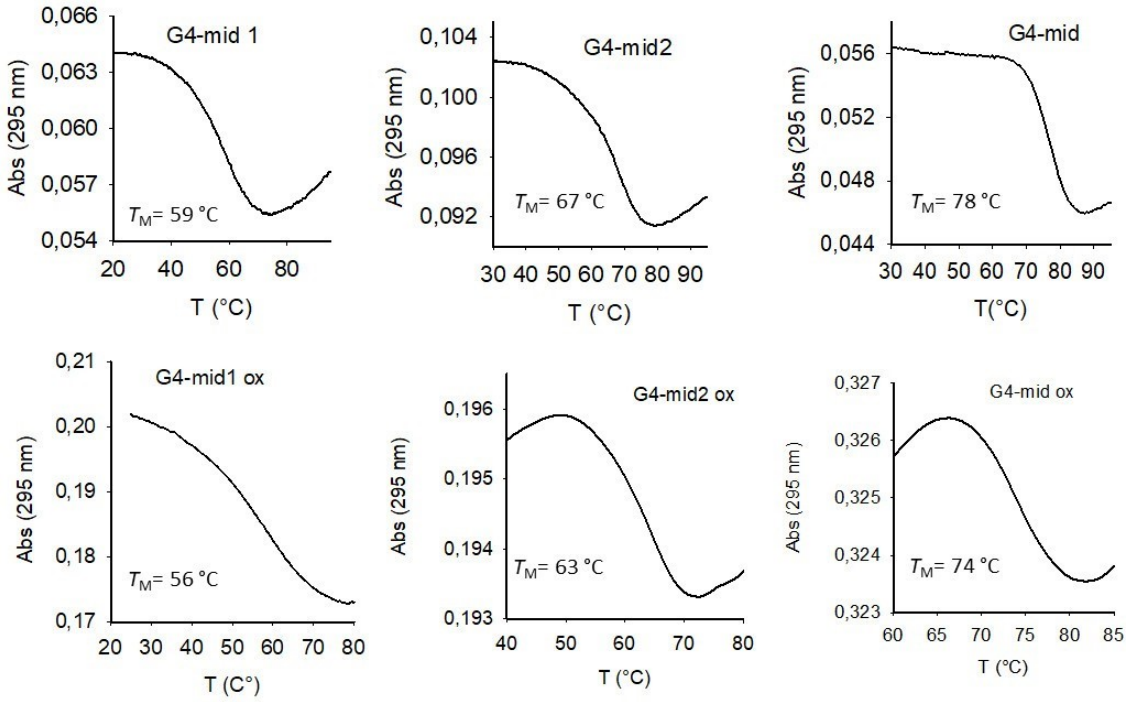

T_M of G-quadruplex structures formed by G4-near and G4-mid wild-type and oxidised (sequences are in Table 1).

32R*	62 °C	G4mid	78 °C	G4mid1	59 °C	G4mid2	67 °C
92*	51 °C	G4 mid^{ox}	74 °C	G4 mid1^{ox}	56 °C	G4 mid2^{ox}	63 °C
96*	61 °C						

*Data from ref. 27

Supplementary Information S6: 8OG destabilizes a G-tetrad: there is the loss of one Hoogsteen hydrogen bond within a G-tetrad and a potential steric hindrance between –NH2 of G and –NH- of 8OG.

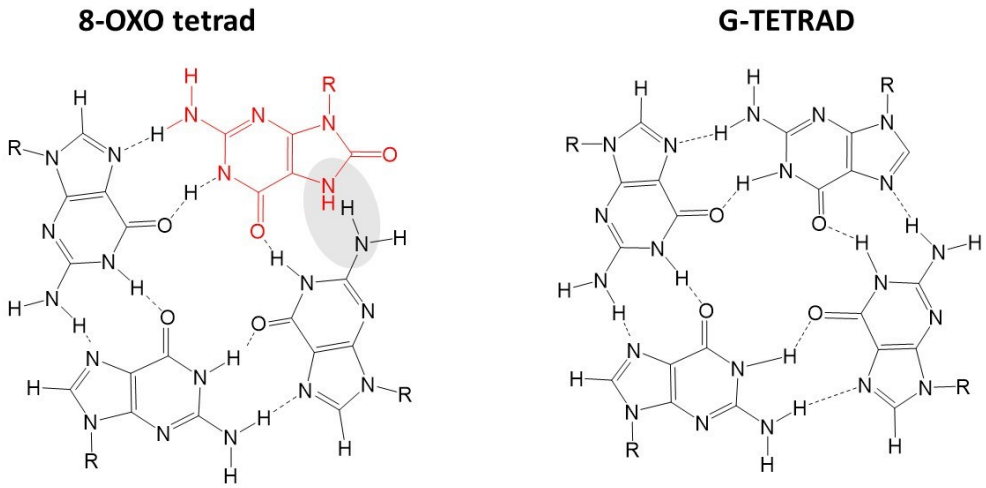

Supplementary Information S7: The results obtained incubating oligonucleotides labelled with Cy5.5 at the 5'end (50 nM), mimicking the *KRAS* G4 mid, G4 mid1 and G4 mid2, with increasing amounts of hnRNP-A1. Reaction was carried out in 20 mM Tris–HCl pH 8, 30 mM KCl, 1.5 mM $MgCl_2$, 1 mM DTT, 8% glycerol, 1% Phosphatase Inhibitor Cocktail I (Merck Life Science, Milano, Italy), 5 mM NaF, 1 mM Na_3VO_4, 2.5 ng/ml poly [dI-dC], 50 μM ZnAc for 30 min at RT. 50nM Cy5.5-labelled G4 was incubated with 0, 0.71, 1.43, 2.85 and 5.7 μM hnRNP A1.

.

5'-CGGGGAGAAGGAGGGGGCCGGGCCGGGCCGGCGGGGGAGAGCGGGGG CCGGGC G4 mid
5'-CGGGGAGAAGGAGGGGCCGGGCCGGGC G4-mid1
5'-CGGGCCGGCGGGGAGGAGCGGGGGCCGGGC G4-mid2

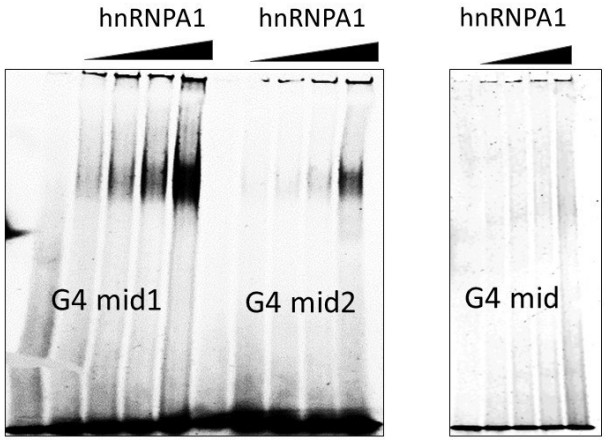

Supplementary Information S8: The results obtained incubating oligonucleotides labelled with Cy5.5 at the 5'end (50 nM), mimicking the *KRAS* G4 mid, G4 mid1 and G4 mid2, with increasing amounts of MAZ. Reaction was carried out in 20 mM Tris–HCl pH 8, 30 mM KCl, 1.5 mM $MgCl_2$, 1 mM DTT, 8% glycerol, 1% Phosphatase Inhibitor Cocktail I (Merck Life Science, Milano, Italy), 5 mM NaF, 1 mM Na_3VO_4, 2.5 ng/ml poly [dI-dC], 50 μM ZnAc for 30 min at RT. 50nM Cy5.5-labelled G4 was incubated with 0, 0.79, 1.57, 3.15 and 6.3 μM MAZ.

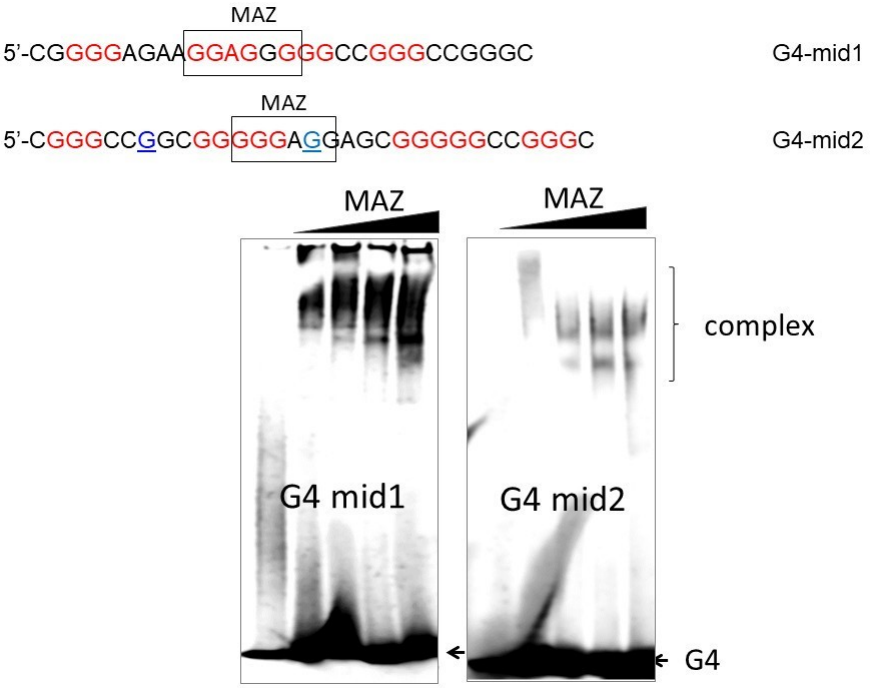

Supplementary Information S9: Structures of Veliparib and Olaparib, two PARP-1 inhibitors

VELIPARIB

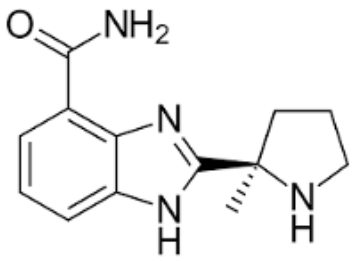

2-[(2*R*)-2-methylpyrrolidin-2-yl]-1*H*-benzimidazole-4-carboxamide

OLAPARIB

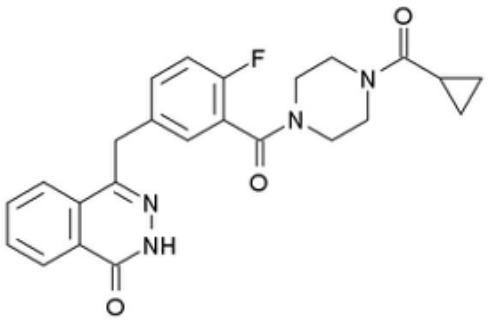

4-[(3-[(4-cyclopropylcarbonyl)piperazin-1-yl]carbonyl) – 4-fluorophenyl]methyl(2H)phthalazin-1-one

Critical G-rich motif in *KRAS* promoter folds in two structurally different G4 conformers recognized by transcription factors

Giorgio Cinque[1], Himanshi Himanshi[1], Gilmar Salgado[2] and Luigi E. Xodo[1,*]

[1] Department of Medicine, Laboratory of Biochemistry, P.le Kolbe 4, 33100 Udine, Italy.

[2] European Institute of Chemistry and Biology (IECB), ARNA laboratory, INSERM U1212 - CNRS UMR 5320, University of Bordeaux, France.

Abstract: We recently reported that PARP1 binds to the *KRAS* promoter at a G4 motif called 32R with regulatory functions. Upon binding to 32R, PARP1 undergoes auto-PARylation acquiring a net negative charge that functions as a platform for the recruitment of transcription factors cationic in nature. Here we demonstrate that the two G4 conformers made by 32R, namely G25T and G9T, are both able to bind to PARP1. In particular, G25T seems to efficiently form a multi-protein complex involving transcription factors essential for the transcription of the *KRAS* oncogene.

Human *Kirsten ras* (*KRAS)* holds two G4 motifs named 32R (between −148/−116 from TSS, also known as G4-near) and G4-middle (−207/−175) forming stable G4 structure. [1-3] The vast majority of the studies reported in literature focused on 32R, as this G-rich motif is a hypersensitive nuclease element playing a key role in transcription.[1] This critical promoter element is recognized by several nuclear factors including PARP1, Ku70, MAZ and hnRNP A1.[4] The first evidence that 32R spontaneously folds into a G4 structure was observed by running primer-extension experiments using as DNA templates two plasmids: one bearing the human G-rich motif, the other the highly homologous murine amalogue.[1,5] The finding that DNA polymerase I paused at the 3'-end of the G-rich motif suggested the formation of a folded G4 structure by both sequences. To determine the guanines of the G-rich motif involved in the formation of the two G4 structures DMS footprinting experiments were carried out.[4,5] In Figure 1 we report a typical cleavage pattern. The nucleotides of 32R have been numbered from 1 to 32, starting from the adenine at the 5'-end. The analysis of the cleavage pattern surprisingly showed that the expected folding involving G-runs I, III, IV and V, each composed by three guanines, was not observed. The footprinting showed that: (i) G-run IV (G18-G19-G20) located in the middle of the sequence is strongly reactive to DMS, suggesting that it does

not contribute to the G-tetrad core; (ii) guanines G6 and G7 are fully protected from DMS, while guanine G9 is only partially protected, indicating that the G-run GGTG takes part to the formation of the G-tetrads, despite being interrupted by a thymidine; (iii) guanines in G-runs I, II, III and V are protected from DMS and form the G-tetrads. As 32R exhibits a CD spectrum with positive and negative ellipticities at 260 and 240 nm respectively, typical of a parallel G4,[6] we proposed for the critical 32R sequence of *KRAS* a tri-stacked parallel G4 structure with two 1-nt and one 11-nt loop (1/1/11 topology) and a T-bulge in one strand.[1,4]

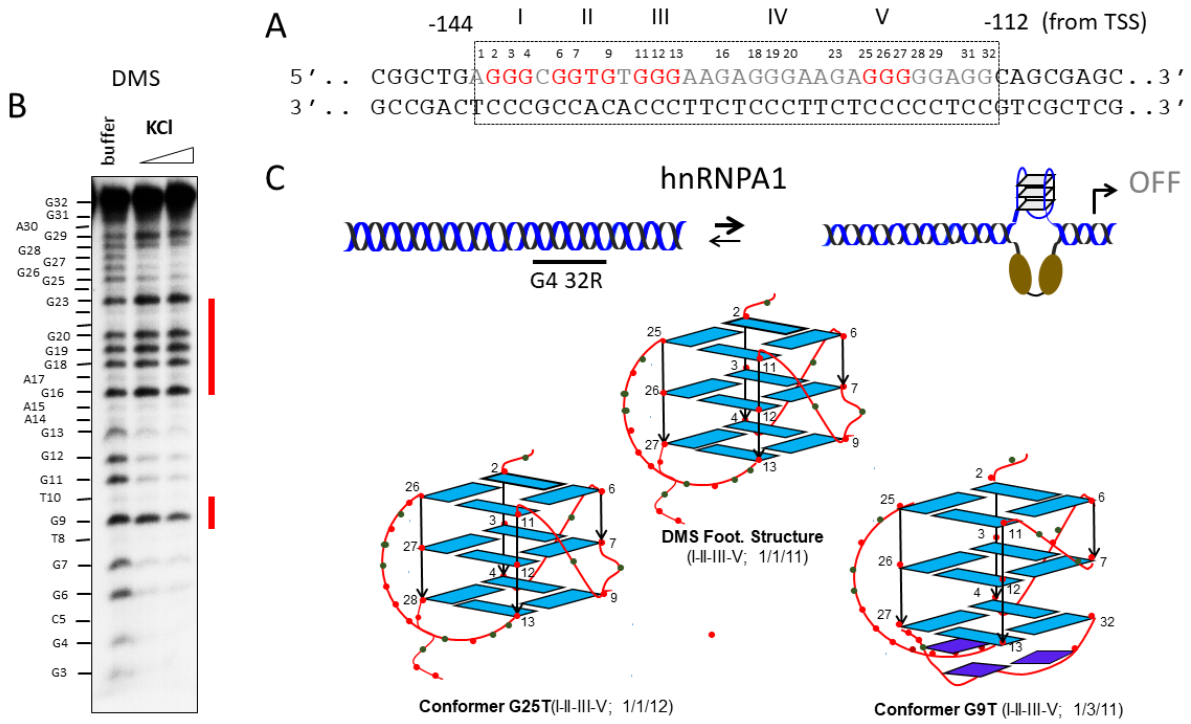

Figure 1: (A) Sequence of 32R. The five G-runs contained in the sequence are numbered I-V. The guanines are numbered from adenine at the 5'end of the G-rich strand; (B) DMS-footprinting of 32R at increasing KCl concentrations; (C) Structures of the G4 proposed on the basis of the DMS-footprinting profiles and of conformers G25T and G9T determined by NMR corresponding the two structured in equilibrium each other formed by 32R.

According to the proposed G4 structure (i) guanine G9 in G-run GGTG should have been expected protected from DMS, but the footprinting showed only a partial protection; (ii) G25 should be completely protected and G28 should not be partially protected. These features suggested that the folding of 32R is more complex than the one proposed. Recently we carried out a deep NMR analysis to gain insight into the folding of 32R.[7] We found that: (i) G→T mutations on G2 and G11 strongly disrupted the imino folding pattern suggesting that these guanines take part to the G-tetrad core; (ii)

mutations on G16 and G23, which are expected to be not implicated in the G-tetrad core did not have indeed much affect on the imino pattern; (iii) mutations on guanine expected to form the G-tetrad core such as G9 and G25 showed well resolved spectra. Two groups of imino patterns called G9T and G25T were distinguished: the first composed by G9, G18-G23, G29, the second by G25T, G25, G26, G27 and G28. The two groups of imino protons indicated that 32R forms two major conformations, the structures of which are reported in Figure 1C. One conformer, defined G25T has a structure substantially similar to that proposed for 32R on the basis of CD and DMS-footprinting. It is a tri-stacked G4 with a T-bulge in one strand, two 1-nt loops, an extended 12-nt loop and all guanines in the *anti* conformation. This structure is fully supported by the DMS footprinting profile except for the fact that G9 should not be reactive to DMS as it is instead observed. A behaviour that before the NMR analysis we could not rationalized. Now we know thanks to the NMR analysis that G9 is reactive because 32R folds in two conformers: G25T and G9T. The structure of G9T is singular showing a fold-back guanine in *syn* conformation (G32) and a triad (G28, A30 and G31) capping the 3′-end. The topology of G9T is 1/3/11 and G9 falls in the 3-nt loop. Reported structure for G9T implies that glycosidic bond between base and sugar G32 adopts *syn* conformation; despite predominance of *anti* conformation in DNA, guanines were found in the last decades to adopt *syn* conformation especially in non canonical DNA structure, i.e. DNA G4s. [8] As the DMS-footprinting reflects the folding of 32R in the two conformers it is to be expected that G9 appears only partially protected. Interestingly, the footprinting shows that in the G25-G29 run, guanines G26 and G27 are protected, while G25 and G28 are only partially protected while G29 is not protected. This is due to that fact that conformer G25T involves in the G-tetrad core the triad G26-G27-G29, while conformer G9T involves the triad G25-G26-G27.

In 2008 we found by pull-down experiments, with G4-oligonucleotide as baits, combined with mass spectrometry that the G4 structure of 32R is bound by several nuclear proteins including PARP1, Ku70 and hnRNP A1.[4] In addition, by means of a "Protein-DNA Binding" software we found that the MYC-associated zinc-finger protein (MAZ) should also bind to the 32R G4 motif. This was indeed confirmed by EMSA and chromatin immunoprecipitation assays.[9,10] Further studies supported the notion that G4 may form a sort of platform for the recruitment to the *KRAS* promoter of the transcription factors forming the transcription initiation complex. Indeed, by silencing PARP1 or MAZ with specific shRNA, we observed a clear downregulation of *KRAS* transcription.[11] Recently we reported that PARP1 on binding 32R undergoes auto-PARylation and thus we proposed that the net negative charge acquired by PARylated PARP1 should behave as a platform for the recruitment to the promoter of transcription factors with a pI > 7.4, i.e. with a net positive charge under physiological conditions. So, in the light of our recent NMR findings and on the putative pivotal role

played by PARP1 in recruiting the transcription factors, we asked whether both the G25T and G9T conformers are able to bind to PARP1 and contribute to the recruiting platform. To address this issue we carried out electrophoretic mobility shift assays (EMSA). We incubated for 30 min the two G4 conformers G25T an G9T and wild-type 32R G4, 5'-labeled with Cy5.5 (50 nM), with increasing amounts of PARP1 (protein/G4, *r*-value, of 0, 4, 8, 12, 16, 32, 48 [0, 0.25, 0.5, 0.75, 1, 2 and 3 µg] in 50 mM Tris-HCl, pH 8, 30 mM KCl, 1.5 mM $MgCl_2$, 1 mM DTT, 8% glycerol, 1% PIC, 50 µM ZnAc, 5 mM NaF, 1 mM Na_3VO_4, 2.5 ng/ml poly dI/dC (binding buffer) at room temperature. After incubation we loaded the samples in 5 % PAGE in Tris-borate. The results are shown in Figure 2. The interaction between PARP1 and the G4s appears rather strong, as a 4-fold excess of PARP1 over G4 is sufficient to show a retarded band in the gel with all three sequences. In contrast, three unstructured oligonucleotides (at PARP1/oligo of ~ 34) did not show any affinity for PARP1 (negative control, ref. [12]). It can be seen that at low protein/G4 ratios – i.e. at *r* values up to 12 for G25T, up to 8 for G9T and up to 4 for wild type 32R – a 1:1 complex is formed, whereas at higher *r*-values a 2:1 complex (2 PARP1 per G4) is observed.

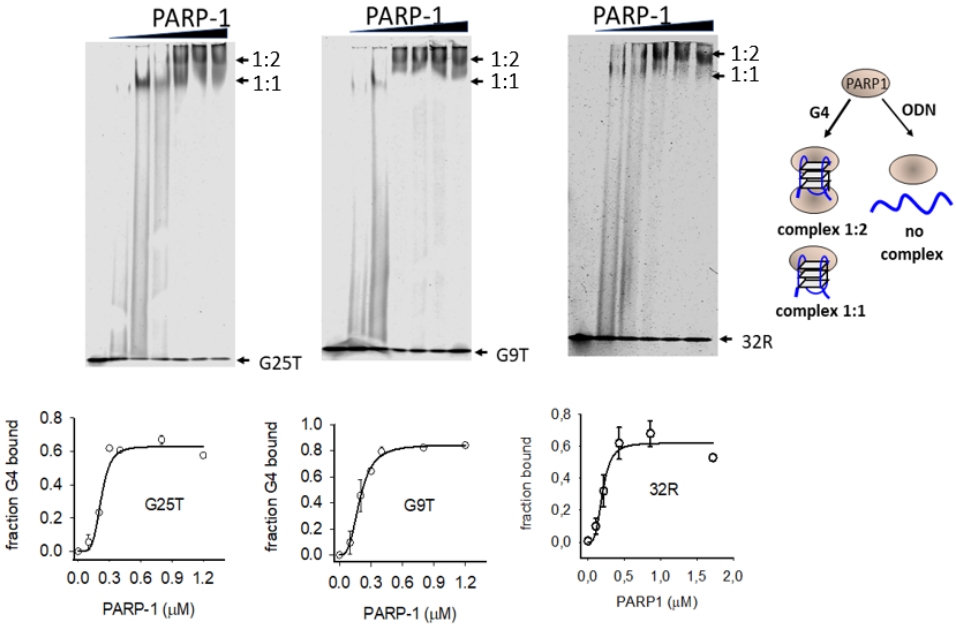

Figure 2. EMSA showing the binding of recombinant PARP1 to Cy5.5-labelled G25T, G9T, 32R G-quadruplexes (50 nM), with increasing amounts of PARP1. Reaction was carried out in 20 mM Tris–HCl pH 8, 30 mM KCl, 1.5 mM $MgCl_2$, 1 mM DTT, 8% glycerol, 1% Phosphatase Inhibitor Cocktail I (Sigma, Milan, Italy), 5 mM NaF, 1 mM Na_3VO_4, 2.5 ng/mL poly [dI-dC], 50 µM ZnAc for 30 min at RT. 50 nM Cy5.5-labelled G4 was incubated with protein/G4 [0, 0.25, 0.5, 0.75, 1.0, 2, and 3 µg PARP1 (Protein/G4 of 0, 4, 8, 12, 16, 32, 48).

For each EMSA we determined the fraction of bound G4 versus the concentration of PARP1. By plotting the data we obtained sigmoidal curves suggesting cooperative binding. We best-fitted the curves to the Hill equation and found K_D values of 0.22±0.012 for G25T (cooperative coefficient n=4.9), 0.18±0.06 for G9T (n=3.1); 0.25±0.03 for 32R (n=3).

As mentioned above, the G4 structures in the *KRAS* promoter are likely to behave as a platform for the recruiting of transcription factors to the promoter near TSS. So, we asked if both G4 conformers are able to form a multiprotein complex when they are incubated with a nuclear protein extract from Panc-1 cells. To address this point we used a streptavidin-biotin pulldown approach. We synthesized sequences G25T, G9T and 32R linked to biotin and let them to fold into G4 in a buffer containing 100 mM KCl. The biotinylated oligonucleotides in G4 conformation were used for the pulldown experiments (Figure 3A). Each biotinylated G4 was incubated with 80 μg of nuclear extract for 30 min and the proteins bound to the G4 bait were pulled down with streptavidin-coated magnetic beads. The pulled down proteins were eluted from the beads with Laemmli buffer and analysed by immunoblotting with antibodies specific for MAZ, hnRNP A1, Ku70 and PARP1. It can be seen that G4 32R pulled down all four transcription factors, suggesting that it forms a multi-protein complex upstream TSS that is expected to be the transcription pre-initiation complex. The eluates from the streptavidin-coated beads incubated with the nuclear extract in the absence of the G4 bait, contained a small amount of proteins due to unspecific interactions between the magnetic beads coated with streptavidin and the nuclear proteins (lane "coated beads"). By contrast, the eluates from the beads bound to the G4 bait pooled down an amount of target proteins higher than that present in the input. The result obtained with bait G25T is rather similar to that observed with bait 32R, while conformer G9T appears less efficient in pulling down the proteins. It can be seen that G9T binds tightly to PARP1. This may indicate that independently from the G4 conformation adopted by 32R under cellular conditions, a site of high affinity for PARP1 is constantly present in the *KRAS* promoter near TSS. The distribution of the transcription factors in the nucleus is dynamic and their recruitment to a specific region of the promoter is expected to be the result of the balance between protein-protein interactions and DNA binding. We therefore asked if some proteins recruited to the *KRAS* promoter behave independently or are somehow linked one another by weak interactions. To investigate this, we carried out immunoprecipitation assays (Figure 3C). We treated Panc-1 cells with 0.1 mM H_2O_2, to stimulate the machinery activating the expression of *KRAS*, then extracted the nuclear proteins. The extract was incubated one by one with the monoclonal antibodies (Abs) specific for the proteins binding to the *KRAS* promoter.

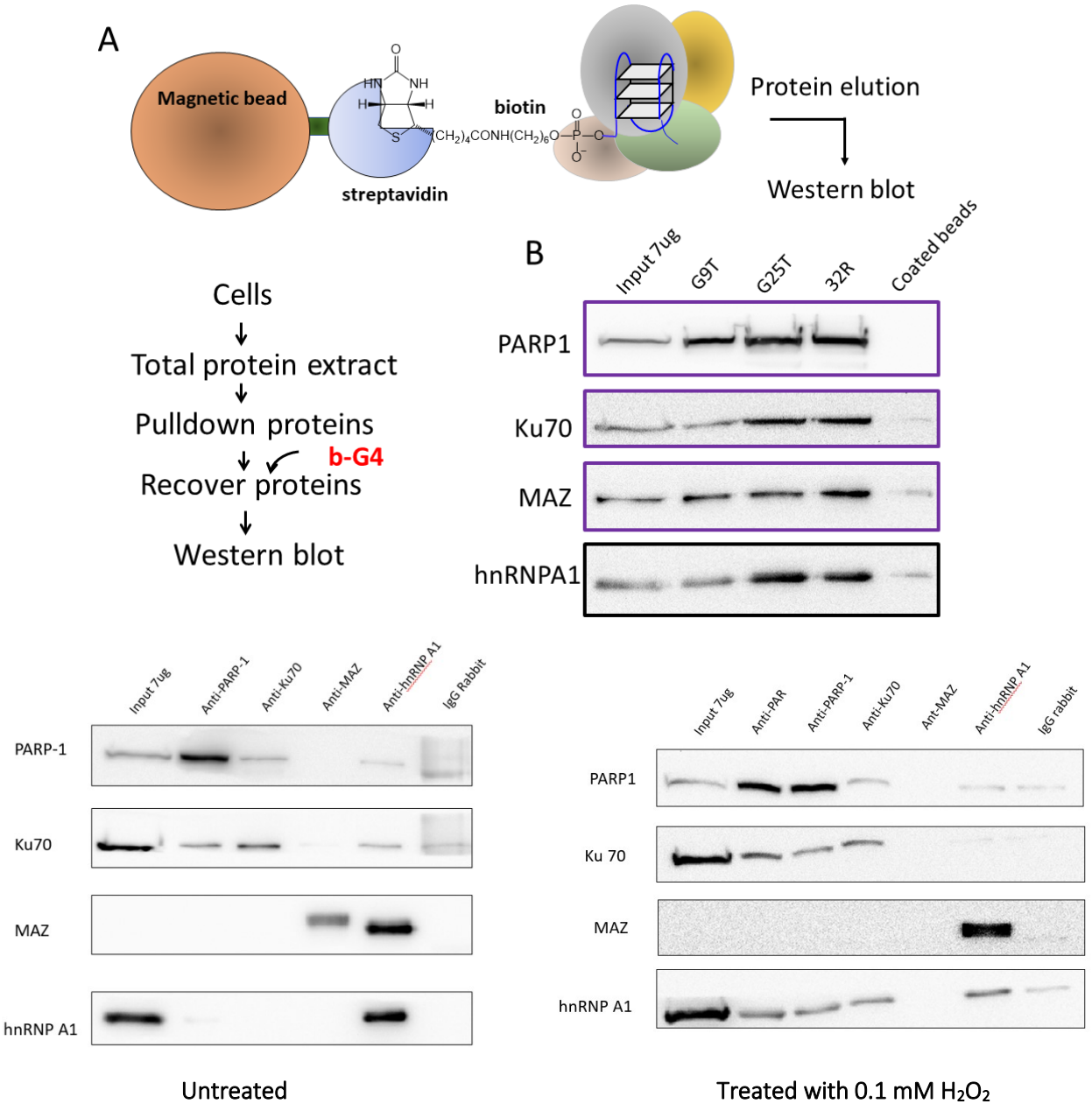

Figure 3. (**A**) Structure of the DNA baits used in the pull-down experiments. The scheme of the pull-down experiments is illustrated; (**B**) Pull-down with biotinylated G9T, G25T and 32RG-quadruplexes. The biotinylated G4 (80 nM) were incubated with 80 µg of nuclear extract for 30 min at RT. The DNA bait-protein complexes formed were pulled down with streptavidin magnetic beads. The pulled-down proteins were recovered and analyzed by Western blot with anti MAZ, anti PARP1 and anti hnRNP A1 primary antibodies and a secondary antibody conjugated to horseradish peroxidase; (**C**) Immunoprecipitation (IP) with antibodies specific for poly/mono-ADP ribose (PAR), PARP1, Ku70, MAZ and hnRNP A1. The recovered proteins from the pulldown were analysed by Western blots. Left: IP from Panc-1 nuclear extract; Right: IP from 0.1 mM H_2O_2 treated Panc-1 nuclear extract

The proteins binding directly and indirectly to the Abs were pulled down by magnetic beads coated with protein A and analysed by Western blots. It can be seen that Ab-PARP1 pulled down in addition to PARP1 also Ku70, suggesting that these two proteins are in contact one another.

Ab-Ku70 gave a similar result, i.e both Ku70 and PARP1 were pulled down by Ab-Ku70, confirming that the two proteins are associated one another. Ab-MAZ pulled down only MAZ, while Ab- hnRNP A1 pulled down MAZ and hnRNP A1 in large amount and PARP1 and Ku70 in lower amounts. Together, the data suggest that MAZ and hnRNP A1 are strongly associated each other. It's worth noting that, upon H_2O_2 treatment, Ab-MAZ did not pull down MAZ itself, this may be due to the fact that the association between MAZ and hnRNP A1 hides the epitope recognized by its own antibody. In Figure 4 we propose a mechanism for *KRAS* transcription activation. Under enhanced oxidative stress, typical of cancer cells, PARP1 and its associated Ku70 protein are recruited to the *KRAS* promoter where it binds to the G4 motif. [12,13] Upon binding to G4, PARP1 undergoes auto PARylation and acquires a negative net charge. Ku70, which is associated with PARP1, having a pI=6.23 is also anionic under physiological conditions. Despite the negative charge these two proteins display, caused either by PARylation or the anionic isoelectric point, they maintain a tight contact to the DNA. The explanation for PARP1 lies in the folding feature, as the Zn domains wraps tightly to the DNA thanks to their electrostatic interactions; in doing so, the protein changes its conformations shielding DNA phosphate groups, thus allowing auto- and etero-PARylation to occur. [14] On the other hand, Ku ring (made of the heterodimer Ku70/Ku80) binding to the DNA is kept by a polarization of positive electrostatic charge focused on the inner surface of the ring and along the DNA-binding cradle. [15] On the whole, the G4:PARP1:Ku70 complex forms an anionic platform capable to recruit cationic transcription factors such as hnRNP A1 (pI= 9.2). The recruitment of hnRNP A1 to the promoter driven by the electrostatic attraction should also affect MAZ that, being strictly in contact with hnRNP A1, follows the route of hnRNP A1 to the promoter. The enrichment of the transcription factors in the neighbouring of G4 should facilitate the formation of the multi-protein complex. Due to unfolding capacity of MAZ and hnRNP A1, [16,17] the DNA in the multi-protein complex should be in the double-stranded form, recognized by RNA polymerase II.

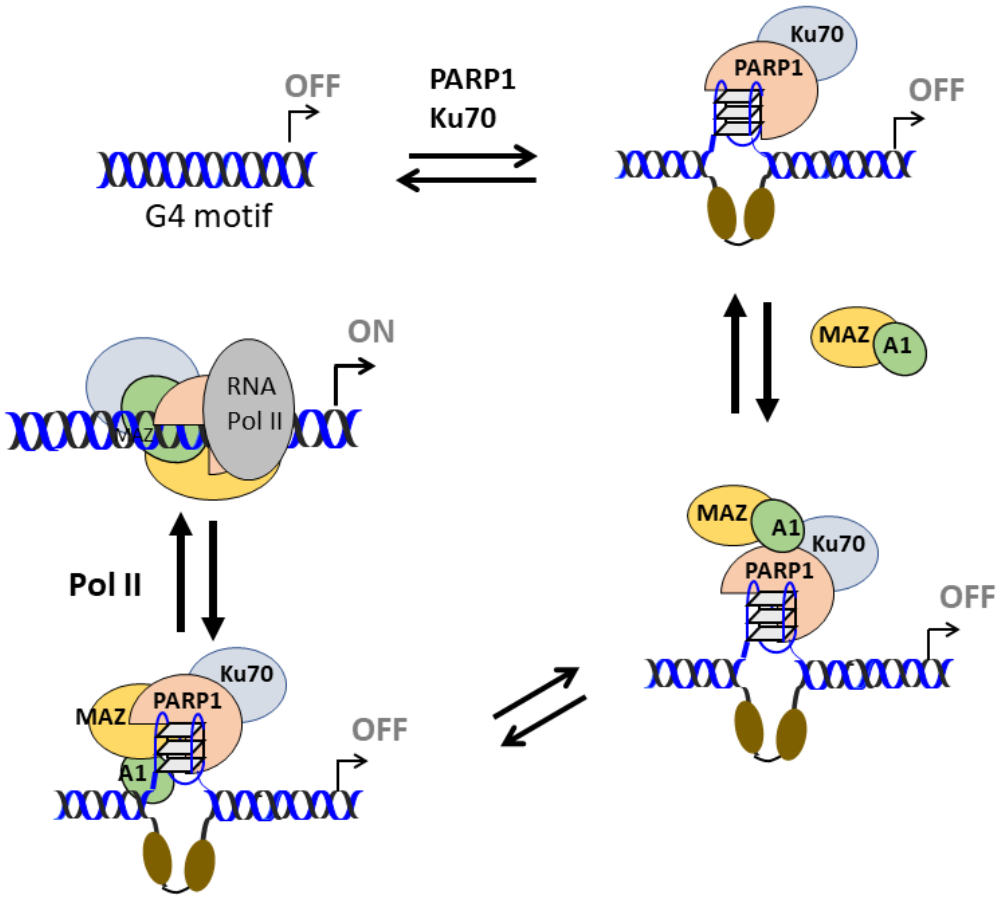

Figure 4. Proposed mechanism for the activation of KRAS transcription. First PARP1 binds to the KRAS promoter at the G4 motif. After binding the protein undergoes auto-PARylation becoming anionic. The G4:PARP1 complex behaves as a platform for the recruiting of the transcription factors. Protein hnRNP A1 should unfold the G4, thus promoting the G4 to duplex transformation at the promoter near TSS and the initiation of transcription.

Materials and methods

Oligonucleotides

The oligonucleotides have been purchased from Microsynth-AG, Balgach, Switzerland. Sequences are reported in Table 1.

Table 1. Oligonucleotides used in this study

Name	*Sequence 5' → 3'*
(1)b-32R	Biotin -TTTTTAGGGCGGTGTGGGAAGAGGGAAGAGGGGGAGG
(1)b-G9T	Biotin -TTTTTAGGGCGGTTTGGGAAGAGGGAAGAGGGGGAGG
(1)b-G25T	Biotin -TTTTTAGGGCGGTGTGGGAAGAGGGAAGATGGGGAGG
(2)Cy5.5-32R	Cy5.5 -TTTTTAGGGCGGTGTGGGAAGAGGGAAGAGGGGGAGG
(2)Cy5.5-G9T	Cy5.5 -TTTTTAGGGCGGTTTGGGAAGAGGGAAGAGGGGGAGG
(2)Cy5.5-G25T	Cy5.5 -TTTTTAGGGCGGTGTGGGAAGAGGGAAGATGGGGAGG

(1) = biotin; (2) = Cy5.5 fluorophore

Nuclear Extract and Biotin-Streptavidin Pull Down Assay

To obtain nuclear extracts, 6 plates of 15 cm diameter of Panc-1 cells at a given confluence were washed with PBS and treated with 0,1mM H_2O_2 in serum free DMEM-High Glucose for 30 min. The cells were collected in PBS buffer, centrifuged at 800 g for 10 min at 4 °C. Next, the cells were resuspended in hypotonic buffer (10 mM HEPES-KOH, pH 7.9, 1.5 mM MgCl2, 10 mM KCl, 0.2 mM PMSF, 0.5 mM DTT, 5 mM NaF, 1 mM Na_3VO_4) and kept in ice for 10 min. The swollen cells were homogenized with a Dounce homogenizer and the nuclei, pelleted by centrifugation and resuspended in low-salt buffer (20 mM HEPES-KOH, pH 7.9, 25 % glycerol, 1.5 mM $MgCl_2$, 20 mM KCl, 0.2 mM EDTA, 0.2 mM PMSF, 0.5 mM DTT). Release of nuclear proteins was obtained by the addition of a high-salt buffer (low-salt buffer containing 1.2 M KCl). Protein concentration was measured according to the Bradford method. Biotinylated 32R, G9T and G25T were folded in 50 mM Tris-HCl, pH 7.4 and 100 mM KCl by heating the solutions at 95 °C for 5 min and successive incubation at RT overnight. 80 μg of Panc-1 nuclear extract were incubated for 30 min at RT with 80 nM biotinylated 32R, G9T and G25T in 20 mM Tris–HCl, pH 7.4, 150 mM KCl, 8 % glycerol, 1 mM DTT, 0.1 mM ZnAc, 5 mM NaF, 1 mM Na_3VO_4 and 2.5 ng/μL poly[dI-dC]. Then 80 μg of Streptavidin MagneSphere Paramagnetic Particles (Promega Italia, Milano, Italy) were added and let to incubate for 30 min at RT. The beads were captured with a magnet and washed three times. The proteins were denatured and eluted with Laemmli buffer (4% SDS, 20% glycerol, 10% 2-mercaptoethanol, 0.004% bromophenol blue and 0.125 M Tris–HCl).

Mobility Shift Assays

Recombinant PARP1 was purchased by Antibodies-online GmbH, Germany and provided as powder; the lyophilized protein was reconstituted with dH2O following manufacturer instructions.

Before EMSA, 5'Cy5.5 G4 oligonucleotides (Cy5.5-32R, Cy5.5-G9T and Cy5.5-G25T) were allowed to form their structure in 50 mM Tris–HCl, pH 7.4, 100 mM KCl, heated at 95 °C for 5 min and incubated overnight at RT. Cy5.5-oligonucleotides (50 nM) were treated for 30 min at 25 °C with increasing amounts of PARP1 (0, 0.25, 0.5, 0.75, 1.0, 2 and 3 μg) in 20 mM Tris–HCl pH 8, 30 mM KCl, 1.5 mM MgCl2, 1 mM DTT, 8% glycerol, 1% Phosphatase Inhibitor Cocktail I (Merck Life Science, Milano, Italy), 5 mM NaF, 1 mM Na_3VO_4, 2.5 ng/mL poly [dI-dC], 50 μM ZnAc. After incubation, the reaction mixtures were loaded in 5% TB (1×) polyacrylamide gel and run at 300 V, 50 mA, 30 W for 2 h at 20 °C. After running, the gel was analyzed with Odyssey CLx Imaging System (Li-COR Biotechnology, Bad Homburg, Germany).

Immunoprecipitation Assay

Panc-1 cells were seeded onto 15 cm diameter plates. At a confluence of 80%, the cells were treated with 0.1 mM H_2O_2 in serum-free DMEM High Glucose medium for 30 min. Then the nuclear proteins were extracted and quantified as described in the "Nuclear extract and biotin-streptavidin pull down assay". For immunoprecipitation, 1.5 mg of Protein A-Dynabeads (ThermoFisher Scientific-Invitrogen, Waltham, MA, USA) were incubated with 3 μg of anti-PAR (Poly/Mono-ADP Ribose (E6F6A) Rabbit mAb #83732, Cell Signalling Technology, Leiden, The Netherlands), anti-PARP1 (46D11, Cell Signalling Technology, Leiden, The Netherlands), anti-Ku70 (D10A7, Cell Signalling Technology, Leiden, The Netherlands), anti-MAZ (clone 133.7, IgG mouse, Santa Cruz Biotechnology, Dallas, TX, USA), anti-hnRNP A1 (clone 9H10, IgG mouse, Merck Life Science, Milano, Italy) and IgG Rabbit (ThermoFisher Scientific-Invitrogen, Waltham, MA, USA) as negative control in 20 mM Tris-HCl, pH 7.4, 20 mM KCl, 8% glycerol, 1mM DTT and 0.1 mM ZnAc for 15 min at RT. After one wash with the same buffer, 80 μg of nuclear extracts were allowed to react with anti-PAR- and IgG rabbit-derivatized Dynabeads for 30 min at RT. The beads were captured with a magnet and washed three times with the same buffer. The proteins were denatured and eluted with Laemmli buffer (4% SDS, 20% glycerol, 10% 2-mercaptoethanol, 0.004% bromophenol blue and 0.125 M Tris–HCl).

Western Blots

Protein samples were separated in 10% SDS-PAGE and blotted onto nitrocellulose membrane at 70 V for 2 h. The nitrocellulose membrane was blocked for 1 h with 5 % fat dried milk in PBS and 0.1 % Tween (Merck Life Science, Milano, Italy) at room temperature. The primary antibodies used were: anti-MAZ (clone 133.7, IgG mouse, Santa Cruz Biotechnology, Dallas, TX, USA), anti-hnRNP A1 (clone 9H10, IgG mouse, Merck Life Science, Milano, Italy), anti-PARP1 (polyclonal antibody, IgG rabbit, Cell Signalling Technology, Leiden, The Netherlands), anti-PAR (Poly/Mono-ADP Ribose (E6F6A) Rabbit mAb #83732, Cell Signalling Technology, Leiden, The Netherlands) and anti-Ku70 (Cell Signalling Technology, Leiden, The Netherlands). The membranes were incubated overnight at 4 °C with the primary antibodies, then washed with 0.1% Tween in PBS and incubated for 1 h with the secondary antibodies conjugated to horseradish peroxidase: anti-mouse IgG (diluted 1:5000), anti-rabbit IgG (diluted 1:5000) and anti-mouse IgM (diluted 1:5000) (Merck Life Science, Milano, Italy). The signal was developed with Super Signal® West PICO, and FEMTO (Thermo Fisher Scientific, Waltham, MA, USA) and detected with ChemiDOC XRS, Quantity One 4.6.5 software (Bio-Rad Laboratories, Segrate, (Milano), Italy).

References

1. Cogoi S, Xodo LE. G4 DNA in ras genes and its potential in cancer therapy. Biochim Biophys Acta. 2016 Apr;1859(4):663-74. doi: 10.1016/j.bbagrm.2016.02.002. Epub 2016 Feb 4. PMID: 26855080.
2. Morgan RK, Batra H, Gaerig VC, Hockings J, Brooks TA. Identification and characterization of a new G-quadruplex forming region within the kRAS promoter as a transcriptional regulator. Biochim Biophys Acta. 2016 Feb;1859(2):235-45. doi: 10.1016/j.bbagrm.2015.11.004. Epub 2015 Nov 18. PMID: 26597160.
3. Kaiser CE, Van Ert NA, Agrawal P, Chawla R, Yang D, Hurley LH. Insight into the Complexity of the i-Motif and G-Quadruplex DNA Structures Formed in the KRAS Promoter and Subsequent Drug-Induced Gene Repression. J Am Chem Soc. 2017 Jun

28;139(25):8522-8536. doi: 10.1021/jacs.7b02046. Epub 2017 Jun 15. PMID: 28570076; PMCID: PMC5978000.

4. Cogoi S, Paramasivam M, Spolaore B, Xodo LE. Structural polymorphism within a regulatory element of the human KRAS promoter: formation of G4-DNA recognized by nuclear proteins. Nucleic Acids Res. 2008 Jun;36(11):3765-80. doi: 10.1093/nar/gkn120. Epub 2008 May 19. PMID: 18490377; PMCID: PMC2441797.
5. Cogoi S, Paramasivam M, Membrino A, Yokoyama KK, Xodo LE The KRAS promoter responds to MYC-associated zinc finger and poly(ADP-ribose) polymerase 1 proteins, which recognize a critical quadruplex-forming GA-element. J Biol Chem. 2010 Jul 16;285(29):22003-16.
6. Rafael Del Villar-Guerra, John O Trent, Jonathan B Chaires, G-Quadruplex Secondary Structure Obtained from Circular Dichroism Spectroscopy Angew Chem Int Ed Engl. 2018 Jun 11;57(24):7171-7175. doi: 10.1002/anie.201709184
7. Marquevielle J, Robert C, Lagrabette O, Wahid M, Bourdoncle A, Xodo LE, Mergny JL, Salgado GF. Structure of two G-quadruplexes in equilibrium in the KRAS promoter. Nucleic Acids Res. 2020 Sep 18;48(16):9336-9345.
8. Foloppe N, Hartmann B, Nilsson L, MacKerell AD Jr. Intrinsic conformational energetics associated with the glycosyl torsion in DNA: a quantum mechanical study. Biophys J. 2002;82(3):1554-1569. doi:10.1016/S0006-3495(02)75507-0
9. Cogoi S, Zorzet S, Rapozzi V, Géci I, Pedersen EB, Xodo LE.MAZ-binding G4-decoy with locked nucleic acid and twisted intercalating nucleic acid modifications suppresses KRAS in pancreatic cancer cells and delays tumour growth in mice. Nucleic Acids Res. 2013 Apr;41(7):4049-64.

10. Cogoi S, Shchekotikhin AE, Xodo LE HRAS is silenced by two neighboring G-quadruplexes and activated by MAZ, a zinc-finger transcription factor with DNA unfolding property. Nucleic Acids Res. 2014 Jul;42(13):8379-88. doi: 10.1093/nar/gku574.
11. Cogoi S, Paramasivam M, Membrino A, Yokoyama KK, Xodo LE. The KRAS promoter responds to MYC-associated zinc finger and poly(ADP-ribose) polymerase 1 proteins, which recognize a critical quadruplex-forming GA-element. J Biol Chem. 2010 Jul 16;285(29):22003-16. doi: 10.1074/jbc.M110.101923. Epub 2010 May 10. PMID: 20457603; PMCID: PMC2903372.
12. Cinque G, Ferino A, Pedersen EB, Xodo LE. Role of Poly [ADP-ribose] Polymerase 1 in Activating the *Kirsten ras* (*KRAS*) Gene in Response to Oxidative Stress. Int J Mol Sci. 2020 Aug 28;21(17):6237. doi: 10.3390/ijms21176237.
13. Cogoi S, Ferino A, Miglietta G, Pedersen EB, Xodo LE. The regulatory G4 motif of the Kirsten ras (KRAS) gene is sensitive to guanine oxidation: implications on transcription. Nucleic Acids Res 2018 Jan 25;46(2):661-676.
14. Langelier MF, Planck JL, Roy S, Pascal JM. Structural basis for DNA damage-dependent poly(ADP-ribosyl)ation by human PARP1. Science. 2012 May 11;336(6082):728-32. doi: 10.1126/science.1216338. PMID: 22582261; PMCID: PMC3532513.
15. Walker JR, Corpina RA, Goldberg J. Structure of the Ku heterodimer bound to DNA and its implications for double-strand break repair. Nature. 2001 Aug 9;412(6847):607-14. doi: 10.1038/35088000. PMID: 11493912.
16. Paramasivam M, Membrino A, Cogoi S, Fukuda H, Nakagama H, Xodo LE. Protein hnRNP A1 and its derivative Up1 unfold quadruplex DNA in the human KRAS promoter: implications for transcription. Nucleic Acids Res. 2009 May;37(9):2841-53.
17. Cogoi S, Shchekotikhin AE, Xodo LE. HRAS is silenced by two neighboring G-quadruplexes and activated by MAZ, a zinc-finger transcription factor with DNA unfolding property. Nucleic Acids Res. 2014 Jul;42(13):8379-88.

9 Conclusions

Over 90% of pancreatic tumours display a mutant of form of KRAS where it promotes initiation and progress of the disease. Despite the important goals achieved over the last decades, several aspects on KRAS biology are not yet clear and further studies are needed to develop targeted strategies against this oncogene for the treatment of PDAC. Previous work from our laboratory showed that the KRAS promoter contains a G- rich region located upstream of the transcription start site (TSS). This sequence being composed by runs of guanines (G4 motif) folds into a G-quadruplex (or G4) structure that, despite some scepticism, studies revealed to be present in the cell. This unusual conformation is recognized by several transcription factors such as MAZ, PARP1 and hnRNP A1: our hypothesis is that G4 serves as a recruitment platform for these proteins that, once bound, they unwind G4 and promote KRAS transcription. Recent studies have reported that pancreatic cancer cells are addicted to KRAS because it reprograms the metabolism (in particular glutamine and serine breakdown) in order to fuel a high metabolic rate, typical of cancer. A detrimental by-product of the metabolism are the so-called ROS species, indeed free radical reactive oxygen species that, if not readily tackled, they may cause severe damage to cells. Because of the rapid metabolism of cancer cells, their level of ROS rises above the one of their physiological counterpart. ROS are strong oxidizing agents and may affect the cellular biomolecules including DNA. It is worth noting that guanine is the nucleobases that displays the lowest redox potential, thus being more susceptible to oxidation, turning into 8-oxoguanine; moreover, when guanines stuck one upon others (i.e. in G4s), redox potential decreases furtherly.

By the way, level of ROS must be kept under a threshold over which cells trigger apoptosis. The major cellular response to oxidative stress is the activation of Nrf2 (nuclear factor erythroid 2-related factor 2), a redox-sensitive transcription factor that regulates the expression of antioxidant response element (ARE)-regulated genes. Our lab previously demonstrated that KRAS expression is controlled by Nrf2, which brings down ROS level resulting in the upregulation of pro-survival Snail and the downregulation of pro-apoptotic RKIP [104]. Together with this paper, my work brought additional evidence that ROS induce KRAS expression in a concentration dependant manner.

PARP1 is a nuclear enzyme that catalyses the transfer of mono or poly ADP-ribose units onto itself and/or other target proteins. PARP1 is also known to take part in almost all DNA repair pathways: in this context, base excision repair (BER) accounts for recognition and removal of oxidized bases and repair of ensuing DNA lesions. It has been established that PARP1 plays a key role in BER by sensing DNA nicks and recruiting factors required for repair [137]. ChIP experiments carried out in this lab confirmed this trend in PDAC: when Panc-1 cells were treated with H_2O_2, PARP1 recruitment onto KRAS promoter increases in a concentration dependent manner. As reported in literature, PARP1 is involved in oncogene recognition at their G4 forming sites (i.e. *CKIT*, *CMYC*, telomeres); together with hnRNP A1 and MAZ, we established that PARP1 is recruited at KRAS G4-near and G4-middle sites under oxidative stress. Despite *in vitro* experiments clearly indicate that 8OG in KRAS promoter G4 region enhances proteins recruitment, this trend is not reflected by pull down assays. According to our data, recruitment in pull down assays seems to be affected by different elements: (i) in G4 near region it's the position of 8OG in the 12-nt loop (i.e. MAZ and hnRNP A1 display less affinity toward b-96); (ii) in G4 mid the length of the bait is the key element (54-nt long bait pulls down a reduced amount of proteins). Further analysis would be desirable to shed light to this aspect. Upon DNA recognition, PARP1 undergoes conformational exchange that turns this enzyme into its active form promoting either MARylation or PARylation. These post-translational modification have been receiving greater and greater attention over the last decades, given their involvement in a huge number of cellular processes i.e. including DNA repair, genomic stability, chromatin remodelling, apoptosis, aging and transcription regulation. In our hypothesis, when PARP1 binds to G4 motifs, it gets self-PARylated, so negatively charged: this favours the recruitment of those nuclear factors which display a cationic pI under physiological conditions like MAZ (pI = 8.1) and hnRNP A1 (pI = 9.2); once this multiprotein complex gets assembled onto G4s, it resolves this non canonical structure restoring DNA duplex conformation that allows KRAS transcription.

FDA and EMA approved some PARP inhibitors for tackling tumours progression, with ovarian carcinoma and breast cancer on the top of the list (reviewed in [191]). Common in these tumours are mutations either on BRCA1/2 genes or in homologous recombination mechanism, which account for PARP inhibition efficacy in the context of synthetic lethality. None of the four driver genes that promote malignant transformation in pancreas are used as therapeutic target (*KRAS, Tp53, SMAD4, CDKN2A*). Nonetheless, PDCA can be tackled by targeting downstream

genes involved in SSBR including BRCA1/2, PALB and ATM, the last of which is a known PARylation target. In our experimental settings we confirmed this trend: silencing PARP1 by siRNA-mediated treatment or blocking its activity by the use of validated inhibitors (Veliparib and Olaparib) we found that KRAS expression was dramatically reduced. Taken together, these results furtherly prove that PARP inhibition is a validated strategy to arrest PDAC cell proliferation.

10 References

[1] Betts, J. G., Young, K. A., Wise, J. A., Johnson, E., Poe, B., Kruse, D. H., … De Saix, P. (2013). The endocrine pancreas. In Anatomy and Physiology. OpenStax.

[2] Q. Zhou and D. A. Melton, "Pancreas regeneration," *Nature*, vol. 557, no. 7705, pp. 351–358, May 2018, doi: 10.1038/s41586-018-0088-0.

[3] S. Lanfredini, A. Thapa, and E. O'Neill, "RAS in pancreatic cancer," *Biochem. Soc. Trans.*, vol. 47, no. 4, pp. 961–972, Jul. 2019, doi: 10.1042/BST20170521.

[4] J. Y. Kim and S. M. Hong, "Precursor Lesions of Pancreatic Cancer," *Oncol. Res. Treat.*, vol. 41, no. 10, pp. 603–610, 2018, doi: 10.1159/000493554.

[5] P. Storz, "Acinar cell plasticity and development of pancreatic ductal adenocarcinoma," *Nat. Rev. Gastroenterol. Hepatol.*, vol. 14, no. 5, pp. 296–304, May 2017, doi: 10.1038/nrgastro.2017.12.

[6] R. L. Siegel, K. D. Miller, and A. Jemal, "Cancer statistics, 2018," *CA. Cancer J. Clin.*, vol. 68, no. 1, pp. 7–30, Jan. 2018, doi: 10.3322/caac.21442.

[7] C. Torres and P. J. Grippo, "Pancreatic cancer subtypes: a roadmap for precision medicine," *Ann. Med.*, vol. 50, no. 4, pp. 277–287, Jun. 2018, doi: 10.1080/07853890.2018.1453168.

[8] P. Bailey *et al.*, "Genomic analyses identify molecular subtypes of pancreatic cancer," *Nature*, vol. 531, no. 7592, pp. 47–52, 2016, doi: 10.1038/nature16965.

[9] E. Pelosi, G. Castelli, and U. Testa, "Pancreatic cancer: Molecular characterization, clonal evolution and cancer stem cells," *Biomedicines*, vol. 5, no. 4, p. 65, Nov. 2017, doi: 10.3390/biomedicines5040065.

[10] K. Wennerberg, K. L. Rossman, and C. J. Der, "The Ras superfamily at a glance," *J. Cell Sci.*, vol. 118, no. 5, pp. 843–846, Mar. 2005, doi: 10.1242/jcs.01660.

[11] A. D. Cox and C. J. Der, "Ras history: The saga continues," *Small GTPases*, vol. 1, no. 1, pp. 2–27, Jul. 2010, doi: 10.4161/sgtp.1.1.12178.

[12] J. J. Harvey, "An unidentified virus which causes the rapid production of tumours in mice [33]," *Nature*, vol. 204, no. 4963, pp. 1104–1105, 1964, doi: 10.1038/2041104b0.

[13] W. H. Kirsten and L. A. Mayer, "Morphologic responses to a murine erythroblastosis virus," *J. Natl. Cancer Inst.*, vol. 39, no. 2, pp. 311–335, Aug. 1967, doi: 10.1093/jnci/39.2.311.

[14] E. M. Scolnick and W. P. Parks, "Harvey Sarcoma Virus: A Second Murine Type C Sarcoma Virus with

Rat Genetic Information," *J. Virol.*, vol. 13, no. 6, pp. 1211–1219, Jun. 1974, doi: 10.1128/jvi.13.6.1211-1219.1974.

[15] C. J. Der, T. G. Krontiris, and G. M. Cooper, "Transforming genes of human bladder and lung carcinoma cell lines are homologous to the ras genes of Harvey and Kristen sarcoma viruses," *Proc. Natl. Acad. Sci. U. S. A.*, vol. 79, no. 11 I, pp. 3637–3640, Jun. 1982, doi: 10.1073/pnas.79.11.3637.

[16] C. W. Han, M. S. Jeong, and S. B. Jang, "Structure, signaling and the drug discovery of the Ras oncogene protein," *BMB Rep.*, vol. 50, no. 7, pp. 355–360, Jul. 2017, doi: 10.5483/BMBRep.2017.50.7.062.

[17] T. Pantsar, "The current understanding of KRAS protein structure and dynamics," *Comput. Struct. Biotechnol. J.*, vol. 18, pp. 189–198, 2020, doi: 10.1016/j.csbj.2019.12.004.

[18] A. D. Cox, C. J. Der, and M. R. Philips, "Targeting RAS membrane association: Back to the future for anti-RAS drug discovery?," *Clin. Cancer Res.*, vol. 21, no. 8, pp. 1819–1827, Apr. 2015, doi: 10.1158/1078-0432.CCR-14-3214.

[19] M. V. Milburn *et al.*, "Molecular switch for signal transduction: Structural differences between active and inactive forms of protooncogenic ras proteins," *Science (80-.).*, vol. 247, no. 4945, pp. 939–945, Feb. 1990, doi: 10.1126/science.2406906.

[20] B. E. Hall, D. Bar-Sagi, and N. Nassar, "The structural basis for the transition from Ras-GTP to Ras-GDP," *Proc. Natl. Acad. Sci. U. S. A.*, vol. 99, no. 19, pp. 12138–12142, Sep. 2002, doi: 10.1073/pnas.192453199.

[21] J. E. Walker, M. Saraste, M. J. Runswick, and N. J. Gay, "Distantly related sequences in the alpha- and beta-subunits of ATP synthase, myosin, kinases and other ATP-requiring enzymes and a common nucleotide binding fold.," *EMBO J.*, vol. 1, no. 8, pp. 945–951, Aug. 1982, doi: 10.1002/j.1460-2075.1982.tb01276.x.

[22] M. Saraste, P. R. Sibbald, and A. Wittinghofer, "The P-loop - a common motif in ATP- and GTP-binding proteins," *Trends Biochem. Sci.*, vol. 15, no. 11, pp. 430–434, 1990, doi: 10.1016/0968-0004(90)90281-F.

[23] B. Klockow, M. R. Ahmadia, C. Block, and A. Wittinghofer, "Oncogenic insertional mutations in the P-loop of Ras are overactive in MAP kinase signaling," *Oncogene*, vol. 19, no. 47, pp. 5367–5376, 2000, doi: 10.1038/sj.onc.1203909.

[24] Y. Pylayeva-Gupta, E. Grabocka, and D. Bar-Sagi, "RAS oncogenes: Weaving a tumorigenic web," *Nat. Rev. Cancer*, vol. 11, no. 11, pp. 761–774, 2011, doi: 10.1038/nrc3106.

[25] K. M. Mann, H. Ying, J. Juan, N. A. Jenkins, and N. G. Copeland, "KRAS-related proteins in pancreatic

cancer," *Pharmacol. Ther.*, vol. 168, pp. 29–42, 2016, doi: 10.1016/j.pharmthera.2016.09.003.

[26] S. Eser *et al.*, "Selective requirement of PI3K/PDK1 signaling for kras oncogene-driven pancreatic cell plasticity and cancer," *Cancer Cell*, vol. 23, no. 3, pp. 406–420, 2013, doi: 10.1016/j.ccr.2013.01.023.

[27] R. B. Blasco *et al.*, "C-Raf, but Not B-Raf, Is Essential for Development of K-Ras Oncogene-Driven Non-Small Cell Lung Carcinoma," *Cancer Cell*, vol. 19, no. 5, pp. 652–663, May 2011, doi: 10.1016/j.ccr.2011.04.002.

[28] E. A. Collisson *et al.*, "A Central role for RAF→MEK→ERK signaling in the genesis of pancreatic ductal adenocarcinoma," *Cancer Discov.*, vol. 2, no. 8, pp. 685–693, Aug. 2012, doi: 10.1158/2159-8290.CD-11-0347.

[29] T. Maehama and J. E. Dixon, "The tumor suppressor, PTEN/MMAC1, dephosphorylates the lipid second messenger, phosphatidylinositol 3,4,5-trisphosphate," *J. Biol. Chem.*, vol. 273, no. 22, pp. 13375–13378, May 1998, doi: 10.1074/jbc.273.22.13375.

[30] P. Chardin and A. Tavitian, "The ral gene: a new ras related gene isolated by the use of a synthetic probe.," *EMBO J.*, vol. 5, no. 9, pp. 2203–2208, Sep. 1986, doi: 10.1002/j.1460-2075.1986.tb04485.x.

[31] K. H. Lim *et al.*, "Activation of RalA is critical for Ras-induced tumorigenesis of human cells," *Cancer Cell*, vol. 7, no. 6, pp. 533–545, Jun. 2005, doi: 10.1016/j.ccr.2005.04.030.

[32] K. H. Lim *et al.*, "Divergent Roles for RalA and RalB in Malignant Growth of Human Pancreatic Carcinoma Cells," *Curr. Biol.*, vol. 16, no. 24, pp. 2385–2394, Dec. 2006, doi: 10.1016/j.cub.2006.10.023.

[33] M. A. Collins *et al.*, "Oncogenic Kras is required for both the initiation and maintenance of pancreatic cancer in mice," *J. Clin. Invest.*, vol. 122, no. 2, pp. 639–653, Feb. 2012, doi: 10.1172/JCI59227.

[34] H. Ying *et al.*, "Oncogenic kras maintains pancreatic tumors through regulation of anabolic glucose metabolism," *Cell*, vol. 149, no. 3, pp. 656–670, 2012, doi: 10.1016/j.cell.2012.01.058.

[35] J. Son *et al.*, "Erratum: Glutamine supports pancreatic cancer growth through a KRAS-regulated metabolic pathway (Nature (2013) 496 (101-105) DOI: 10.1038/nature12040)," *Nature*, vol. 499, no. 7459, p. 504, Mar. 2013, doi: 10.1038/nature12317.

[36] I. B. Weinstein and A. K. Joe, "Mechanisms of Disease: Oncogene addiction - A rationale for molecular targeting in cancer therapy," *Nat. Clin. Pract. Oncol.*, vol. 3, no. 8, pp. 448–457, Aug. 2006, doi: 10.1038/ncponc0558.

[37] R. Pagliarini, W. Shao, and W. R. Sellers, "Oncogene addiction: pathways of therapeutic response, resistance, and road maps toward a cure," *EMBO Rep.*, vol. 16, no. 3, pp. 280–296, Mar. 2015, doi:

10.15252/embr.201439949.

[38] E. Pupo, D. Avanzato, E. Middonti, F. Bussolino, and L. Lanzetti, “KRAS-driven metabolic rewiring reveals novel actionable targets in cancer,” *Frontiers in Oncology*, vol. 9, no. AUG. p. 848, 2019, doi: 10.3389/fonc.2019.00848.

[39] L. Yan, P. Raj, W. Yao, and H. Ying, “Glucose Metabolism in Pancreatic Cancer,” *Cancers (Basel).*, vol. 11, no. 10, p. 1460, Sep. 2019, doi: 10.3390/cancers11101460.

[40] K. Nyíri, G. Koppány, and B. G. Vértessy, “Structure-based inhibitor design of mutant RAS proteins—a paradigm shift,” *Cancer Metastasis Rev.*, 2020, doi: 10.1007/s10555-020-09914-6.

[41] P. Liu, Y. Wang, and X. Li, “Targeting the untargetable KRAS in cancer therapy,” *Acta Pharm. Sin. B*, vol. 9, no. 5, pp. 871–879, 2019, doi: 10.1016/j.apsb.2019.03.002.

[42] M. S. Padanad *et al.*, “Fatty Acid Oxidation Mediated by Acyl-CoA Synthetase Long Chain 3 Is Required for Mutant KRAS Lung Tumorigenesis,” *Cell Rep.*, vol. 16, no. 6, pp. 1614–1628, 2016, doi: 10.1016/j.celrep.2016.07.009.

[43] A. Singh *et al.*, “De novo lipogenesis represents a therapeutic target in mutant Kras non-small cell lung cancer,” *FASEB J.*, vol. 32, no. 12, pp. 7018–7027, Jun. 2018, doi: 10.1096/fj.201800204.

[44] R. R. Singh, J. Goldberg, A. M. Varghese, K. H. Yu, W. Park, and E. M. O’Reilly, “Genomic profiling in pancreatic ductal adenocarcinoma and a pathway towards therapy individualization: A scoping review,” *Cancer Treat. Rev.*, vol. 75, pp. 27–38, 2019, doi: 10.1016/j.ctrv.2019.03.003.

[45] D. D. Waller, J. Park, and Y. S. Tsantrizos, “Inhibition of farnesyl pyrophosphate (FPP) and/or geranylgeranyl pyrophosphate (GGPP) biosynthesis and its implication in the treatment of cancers,” *Crit. Rev. Biochem. Mol. Biol.*, vol. 54, no. 1, pp. 41–60, Jan. 2019, doi: 10.1080/10409238.2019.1568964.

[46] H. Adderley, F. H. Blackhall, and C. R. Lindsay, “KRAS-mutant non-small cell lung cancer: Converging small molecules and immune checkpoint inhibition,” *EBioMedicine*, vol. 41, pp. 711–716, Mar. 2019, doi: 10.1016/j.ebiom.2019.02.049.

[47] S. R. Chandana, H. M. Babiker, and D. Mahadevan, “Therapeutic trends in pancreatic ductal adenocarcinoma (PDAC),” *Expert Opin. Investig. Drugs*, vol. 28, no. 2, pp. 161–177, Feb. 2019, doi: 10.1080/13543784.2019.1557145.

[48] T. Maurer *et al.*, “Small-molecule ligands bind to a distinct pocket in Ras and inhibit SOS-mediated nucleotide exchange activity,” *Proc. Natl. Acad. Sci. U. S. A.*, vol. 109, no. 14, pp. 5299–5304, Apr. 2012, doi: 10.1073/pnas.1116510109.

[49] Q. Sun *et al.*, "Discovery of small molecules that bind to K-Ras and inhibit Sos-mediated activation," *Angew. Chemie - Int. Ed.*, vol. 51, no. 25, pp. 6140–6143, Jun. 2012, doi: 10.1002/anie.201201358.

[50] C. Xie *et al.*, "Identification of a new potent inhibitor targeting KRAS in non-small cell lung cancer cells," *Front. Pharmacol.*, vol. 8, no. NOV, p. 823, 2017, doi: 10.3389/fphar.2017.00823.

[51] A. Ferino, G. Miglietta, R. Picco, S. Vogel, J. Wengel, and L. E. Xodo, "MicroRNA therapeutics: design of single-stranded miR-216b mimics to target KRAS in pancreatic cancer cells," *RNA Biol.*, vol. 15, no. 10, pp. 1273–1285, 2018, doi: 10.1080/15476286.2018.1526536.

[52] S. Kumari, A. Bugaut, J. L. Huppert, and S. Balasubramanian, "An RNA G-quadruplex in the 5′ UTR of the NRAS proto-oncogene modulates translation," *Nat. Chem. Biol.*, vol. 3, no. 4, pp. 218–221, 2007, doi: 10.1038/nchembio864.

[53] A. Bugaut and S. Balasubramanian, "5′-UTR RNA G-quadruplexes: Translation regulation and targeting," *Nucleic Acids Res.*, vol. 40, no. 11, pp. 4727–4741, Jun. 2012, doi: 10.1093/nar/gks068.

[54] G. Miglietta *et al.*, "RNA G-Quadruplexes in Kirsten Ras (KRAS) Oncogene as Targets for Small Molecules Inhibiting Translation," *J. Med. Chem.*, vol. 60, no. 23, pp. 9448–9461, Dec. 2017, doi: 10.1021/acs.jmedchem.7b00622.

[55] A. Ferino *et al.*, "Photodynamic Therapy for ras-Driven Cancers: Targeting G-Quadruplex RNA Structures with Bifunctional Alkyl-Modified Porphyrins," *J. Med. Chem.*, vol. 63, no. 3, pp. 1245–1260, Feb. 2020, doi: 10.1021/acs.jmedchem.9b01577.

[56] J. Jordano and M. Perucho, "Chromatin structure of the promoter region of the human c-K-ras gene," *Nucleic Acids Res.*, vol. 14, no. 18, pp. 7361–7378, Sep. 1986, doi: 10.1093/nar/14.18.7361.

[57] J. Jordano and M. Perucho, "Initial characterization of a potential transcriptional enhancer for the human c-K-ras gene," *Oncogene*, vol. 2, no. 4, pp. 359–366, Apr. 1988, doi: 10.13039/100000002.

[58] S. Cogoi, M. Paramasivam, B. Spolaore, and L. E. Xodo, "Structural polymorphism within a regulatory element of the human KRAS promoter: Formation of G4-DNA recognized by nuclear proteins," *Nucleic Acids Res.*, vol. 36, no. 11, pp. 3765–3780, 2008, doi: 10.1093/nar/gkn120.

[59] S. Cogoi, S. Zorzet, V. Rapozzi, I. Géci, E. B. Pedersen, and L. E. Xodo, "MAZ-binding G4-decoy with locked nucleic acid and twisted intercalating nucleic acid modifications suppresses KRAS in pancreatic cancer cells and delays tumor growth in mice," *Nucleic Acids Res.*, vol. 41, no. 7, pp. 4049–4064, Apr. 2013, doi: 10.1093/nar/gkt127.

[60] J. D. Watson and F. H. C. Crick, "Molecular structure of nucleic acids: A structure for deoxyribose nucleic acid," *Nature*, vol. 171, no. 4356, pp. 737–738, 1953, doi: 10.1038/171737a0.

[61] H. Tateishi-Karimata and N. Sugimoto, “Chemical biology of non-canonical structures of nucleic acids for therapeutic applications,” *Chem. Commun.*, vol. 56, no. 16, pp. 2379–2390, 2020, doi: 10.1039/c9cc09771f.

[62] I. Bang, “Untersuchungen über die Guanylsäure,” *Biochem. Z*, vol. 26, pp. 293–311, 1910.

[63] M. GELLERT, M. N. LIPSETT, and D. R. DAVIES, “Helix formation by guanylic acid,” *Proc. Natl. Acad. Sci. U. S. A.*, vol. 48, no. 12, pp. 2013–2018, Dec. 1962, doi: 10.1073/pnas.48.12.2013.

[64] W. I. Sundquist and A. Klug, “Telomeric DNA dimerizes by formation of guanine tetrads between hairpin loops,” *Nature*, vol. 342, no. 6251, pp. 825–829, 1989, doi: 10.1038/342825a0.

[65] H. J. Lipps, W. Gruissem, and D. M. Prescott, “Higher order DNA structure in macronuclear chromatin of the hypotrichous ciliate Oxytricha nova,” *Proc. Natl. Acad. Sci. U. S. A.*, vol. 79, no. 8 I, pp. 2495–2499, Apr. 1982, doi: 10.1073/pnas.79.8.2495.

[66] P. Majee *et al.*, “Identification and characterization of two conserved G-quadruplex forming motifs in the Nipah virus genome and their interaction with G-quadruplex specific ligands,” *Sci. Rep.*, vol. 10, no. 1, p. 1477, 2020, doi: 10.1038/s41598-020-58406-8.

[67] S. Burge, G. N. Parkinson, P. Hazel, A. K. Todd, and S. Neidle, “Quadruplex DNA: Sequence, topology and structure,” *Nucleic Acids Res.*, vol. 34, no. 19, pp. 5402–5415, Sep. 2006, doi: 10.1093/nar/gkl655.

[68] E. Ruggiero and S. N. Richter, “Survey and summary G-quadruplexes and G-quadruplex ligands: Targets and tools in antiviral therapy,” *Nucleic Acids Res.*, vol. 46, no. 7, pp. 3270–3283, 2018, doi: 10.1093/nar/gky187.

[69] V. Brázda *et al.*, “G4Hunter web application: A web server for G-quadruplex prediction,” *Bioinformatics*, vol. 35, no. 18, pp. 3493–3495, Feb. 2019, doi: 10.1093/bioinformatics/btz087.

[70] O. Kikin, L. D’Antonio, and P. S. Bagga, “QGRS Mapper: A web-based server for predicting G-quadruplexes in nucleotide sequences,” *Nucleic Acids Res.*, vol. 34, no. WEB. SERV. ISS., pp. W676–W682, Jul. 2006, doi: 10.1093/nar/gkl253.

[71] J. L. Huppert and S. Balasubramanian, “G-quadruplexes in promoters throughout the human genome,” *Nucleic Acids Res.*, vol. 35, no. 2, pp. 406–413, 2007, doi: 10.1093/nar/gkl1057.

[72] V. Yadav, Hemansi, N. Kim, N. Tuteja, and P. Yadav, “G quadruplex in plants: A ubiquitous regulatory element and its biological relevance,” *Front. Plant Sci.*, vol. 8, p. 1163, Jul. 2017, doi: 10.3389/fpls.2017.01163.

[73] D. J. Patel, A. T. Phan, and V. Kuryavyi, “Human telomere, oncogenic promoter and 5’-UTR G-quadruplexes: Diverse higher order DNA and RNA targets for cancer therapeutics,” *Nucleic Acids Res.*,

vol. 35, no. 22, pp. 7429–7455, Oct. 2007, doi: 10.1093/nar/gkm711.

[74] P. Yadav, V. Harcy, J. L. Argueso, M. Dominska, S. Jinks-Robertson, and N. Kim, "Topoisomerase I Plays a Critical Role in Suppressing Genome Instability at a Highly Transcribed G-Quadruplex-Forming Sequence," *PLoS Genet.*, vol. 10, no. 12, pp. e1004839–e1004839, Dec. 2014, doi: 10.1371/journal.pgen.1004839.

[75] G. Biffi, D. Tannahill, J. McCafferty, and S. Balasubramanian, "Quantitative visualization of DNA G-quadruplex structures in human cells," *Nat. Chem.*, vol. 5, no. 3, pp. 182–186, Mar. 2013, doi: 10.1038/nchem.1548.

[76] G. Biffi, M. Di Antonio, D. Tannahill, and S. Balasubramanian, "Visualization and selective chemical targeting of RNA G-quadruplex structures in the cytoplasm of human cells," *Nat. Chem.*, vol. 6, no. 1, pp. 75–80, Jan. 2014, doi: 10.1038/nchem.1805.

[77] V. S. Chambers, G. Marsico, J. M. Boutell, M. Di Antonio, G. P. Smith, and S. Balasubramanian, "High-throughput sequencing of DNA G-quadruplex structures in the human genome," *Nat. Biotechnol.*, vol. 33, no. 8, pp. 877–881, Aug. 2015, doi: 10.1038/nbt.3295.

[78] R. Hänsel-Hertsch *et al.*, "G-quadruplex structures mark human regulatory chromatin," *Nat. Genet.*, vol. 48, no. 10, pp. 1267–1272, Oct. 2016, doi: 10.1038/ng.3662.

[79] J. L. Huppert, "Four-stranded nucleic acids: Structure, function and targeting of G-quadruplexes," *Chem. Soc. Rev.*, vol. 37, no. 7, pp. 1375–1384, 2008, doi: 10.1039/b702491f.

[80] S. Neidle, "Quadruplex nucleic acids as targets for anticancer therapeutics," *Nat. Rev. Chem.*, vol. 1, no. 5, p. 41, 2017, doi: 10.1038/s41570-017-0041.

[81] X. H. Zheng, X. Nie, H. Y. Liu, Y. M. Fang, Y. Zhao, and L. X. Xia, "TMPyP4 promotes cancer cell migration at low doses, but induces cell death at high doses," *Sci. Rep.*, vol. 6, no. 1, p. 26592, May 2016, doi: 10.1038/srep26592.

[82] R. Hänsel-Hertsch, M. Di Antonio, and S. Balasubramanian, "DNA G-quadruplexes in the human genome: Detection, functions and therapeutic potential," *Nat. Rev. Mol. Cell Biol.*, vol. 18, no. 5, pp. 279–284, 2017, doi: 10.1038/nrm.2017.3.

[83] M. Aggarwal, J. A. Sommers, R. H. Shoemaker, and R. M. Brosh, "Inhibition of helicase activity by a small molecule impairs Werner syndrome helicase (WRN) function in the cellular response to DNA damage or replication stress," *Proc. Natl. Acad. Sci. U. S. A.*, vol. 108, no. 4, pp. 1525–1530, 2011, doi: 10.1073/pnas.1006423108.

[84] E. Salvati *et al.*, "PARP1 is activated at telomeres upon G4 stabilization: Possible target for telomere-

based therapy," *Oncogene*, vol. 29, no. 47, pp. 6280–6293, 2010, doi: 10.1038/onc.2010.344.

[85] S. A. Ohnmacht *et al.*, "A G-quadruplex-binding compound showing anti-tumour activity in an in vivo model for pancreatic cancer," *Sci. Rep.*, vol. 5, no. 1, p. 11385, 2015, doi: 10.1038/srep11385.

[86] C. Marchetti *et al.*, "Targeting Multiple Effector Pathways in Pancreatic Ductal Adenocarcinoma with a G-Quadruplex-Binding Small Molecule," *J. Med. Chem.*, vol. 61, no. 6, pp. 2500–2517, Mar. 2018, doi: 10.1021/acs.jmedchem.7b01781.

[87] J. P. Kehrer, J. D. Robertson, and C. V. Smith, "Free Radicals and Reactive Oxygen Species," in *Comprehensive Toxicology: Second Edition*, vol. 1–14, C. A. B. T.-C. T. (Second E. McQueen, Ed. Oxford: Elsevier, 2010, pp. 277–307.

[88] A. M. Fleming and C. J. Burrows, "Interplay of Guanine Oxidation and G-Quadruplex Folding in Gene Promoters," *J. Am. Chem. Soc.*, vol. 142, no. 3, pp. 1115–1136, 2020, doi: 10.1021/jacs.9b11050.

[89] G. Aviello and U. G. Knaus, "NADPH oxidases and ROS signaling in the gastrointestinal tract review-article," *Mucosal Immunol.*, vol. 11, no. 4, pp. 1011–1023, Jul. 2018, doi: 10.1038/s41385-018-0021-8.

[90] Y. Tang, J. Long, and J. Liu, "Hyperglycemia-Associated Oxidative Stress Induces Autophagy: Involvement of the ROS-ERK/JNK-p53 Pathway," in *Autophagy: Cancer, Other Pathologies, Inflammation, Immunity, Infection, and Aging*, vol. 1, M. A. B. T.-A. C. Hayat Other Pathologies, Inflammation, Immunity, Infection, and Aging, Ed. Amsterdam: Academic Press, 2014, pp. 105–115.

[91] J. Korbecki, I. Baranowska-Bosiacka, I. Gutowska, and D. Chlubek, "Cyclooxygenase pathways," *Acta Biochim. Pol.*, vol. 61, no. 4, pp. 639–649, 2014, doi: 10.18388/abp.2014_1825.

[92] R. Radi, "Oxygen radicals, nitric oxide, and peroxynitrite: Redox pathways in molecular medicine," *Proc. Natl. Acad. Sci. U. S. A.*, vol. 115, no. 23, pp. 5839–5848, Jun. 2018, doi: 10.1073/pnas.1804932115.

[93] J. Vásquez-Vivar, B. Kalyanaraman, and M. C. Kennedy, "Mitochondrial aconitase is a source of hydroxyl radical. An electron spin resonance investigation," *J. Biol. Chem.*, vol. 275, no. 19, pp. 14064–14069, May 2000, doi: 10.1074/jbc.275.19.14064.

[94] M. Redza-Dutordoir and D. A. Averill-Bates, "Activation of apoptosis signalling pathways by reactive oxygen species," *Biochim. Biophys. Acta - Mol. Cell Res.*, vol. 1863, no. 12, pp. 2977–2992, 2016, doi: 10.1016/j.bbamcr.2016.09.012.

[95] C. Peng *et al.*, "Biology of ageing and role of dietary antioxidants," *Biomed Res. Int.*, vol. 2014, p. 831841, 2014, doi: 10.1155/2014/831841.

[96] L. Covarrubias, D. Hernández-García, D. Schnabel, E. Salas-Vidal, and S. Castro-Obregón, "Function of reactive oxygen species during animal development: Passive or active?," *Dev. Biol.*, vol. 320, no. 1, pp. 1–11, 2008, doi: 10.1016/j.ydbio.2008.04.041.

[97] J. N. Moloney and T. G. Cotter, "ROS signalling in the biology of cancer," *Semin. Cell Dev. Biol.*, vol. 80, pp. 50–64, 2018, doi: 10.1016/j.semcdb.2017.05.023.

[98] A. Sznarkowska, A. Kostecka, K. Meller, and K. P. Bielawski, "Inhibition of cancer antioxidant defense by natural compounds," *Oncotarget*, vol. 8, no. 9, pp. 15996–16016, Feb. 2017, doi: 10.18632/oncotarget.13723.

[99] G. M. Denicola *et al.*, "Oncogene-induced Nrf2 transcription promotes ROS detoxification and tumorigenesis," *Nature*, vol. 475, no. 7354, pp. 106–110, Jul. 2011, doi: 10.1038/nature10189.

[100] I. S. Harris *et al.*, "Glutathione and Thioredoxin Antioxidant Pathways Synergize to Drive Cancer Initiation and Progression," *Cancer Cell*, vol. 27, no. 2, pp. 211–222, Feb. 2015, doi: 10.1016/j.ccell.2014.11.019.

[101] H. Kitamura and H. Motohashi, "NRF2 addiction in cancer cells," *Cancer Sci.*, vol. 109, no. 4, pp. 900–911, Apr. 2018, doi: 10.1111/cas.13537.

[102] S. Sajadimajd and M. Khazaei, "Oxidative Stress and Cancer: The Role of Nrf2," *Curr. Cancer Drug Targets*, vol. 18, no. 6, pp. 538–557, 2017, doi: 10.2174/1568009617666171002144228.

[103] M. Rojo de la Vega, E. Chapman, and D. D. Zhang, "NRF2 and the Hallmarks of Cancer," *Cancer Cell*, vol. 34, no. 1, pp. 21–43, Jul. 2018, doi: 10.1016/j.ccell.2018.03.022.

[104] A. Ferino, V. Rapozzi, and L. E. Xodo, "The ROS-KRAS-Nrf2 axis in the control of the redox homeostasis and the intersection with survival-apoptosis pathways: Implications for photodynamic therapy," *J. Photochem. Photobiol. B Biol.*, vol. 202, p. 111672, 2020, doi: 10.1016/j.jphotobiol.2019.111672.

[105] B. Kong, C. Qia, M. Erkan, J. Kleeff, and C. W. Michalski, "Overview on how oncogenic Kras promotes pancreatic carcinogenesis by inducing low intracellular ROS levels," *Front. Physiol.*, vol. 4 SEP, p. 246, Sep. 2013, doi: 10.3389/fphys.2013.00246.

[106] E. Markkanen, "Not breathing is not an option: How to deal with oxidative DNA damage," *DNA Repair (Amst).*, vol. 59, pp. 82–105, 2017, doi: 10.1016/j.dnarep.2017.09.007.

[107] S. Steenken and S. V. Jovanovic, "How easily oxidizable is DNA? One-electron reduction potentials of adenosine and guanosine radicals in aqueous solution," *J. Am. Chem. Soc.*, vol. 119, no. 3, pp. 617–618, Jan. 1997, doi: 10.1021/ja962255b.

[108] T. Lindahl and D. E. Barnes, "Repair of endogenous DNA damage," *Cold Spring Harb. Symp. Quant.*

Biol., vol. 65, pp. 127–133, 2000, doi: 10.1101/sqb.2000.65.127.

[109] S. S. David, V. L. O'Shea, and S. Kundu, "Base-excision repair of oxidative DNA damage," *Nature*, vol. 447, no. 7147, pp. 941–950, Jun. 2007, doi: 10.1038/nature05978.

[110] A. M. Fleming and C. J. Burrows, "8-Oxo-7,8-dihydroguanine, friend and foe: Epigenetic-like regulator versus initiator of mutagenesis," *DNA Repair (Amst).*, vol. 56, pp. 75–83, Aug. 2017, doi: 10.1016/j.dnarep.2017.06.009.

[111] S. Cogoi, A. Ferino, G. Miglietta, E. B. Pedersen, and L. E. Xodo, "The regulatory G4 motif of the Kirsten ras (KRAS) gene is sensitive to guanine oxidation: Implications on transcription," *Nucleic Acids Res.*, vol. 46, no. 2, pp. 661–676, Jan. 2018, doi: 10.1093/nar/gkx1142.

[112] A. M. Fleming, J. Zhou, S. S. Wallace, and C. J. Burrows, "A role for the fifth G-track in G-quadruplex forming oncogene promoter sequences during oxidative stress: Do these 'spare tires' have an evolved function?," *ACS Cent. Sci.*, vol. 1, no. 5, pp. 226–233, Aug. 2015, doi: 10.1021/acscentsci.5b00202.

[113] J. Zhou, A. M. Fleming, A. M. Averill, C. J. Burrows, and S. S. Wallace, "The NEIL glycosylases remove oxidized guanine lesions from telomeric and promoter quadruplex DNA structures," *Nucleic Acids Res.*, vol. 43, no. 8, pp. 4039–4054, Apr. 2015, doi: 10.1093/nar/gkv252.

[114] T. Honjo, Y. Nishizuka, and O. Hayaishi, "Diphtheria toxin-dependent adenosine diphosphate ribosylation of aminoacyl transferase II and inhibition of protein synthesis.," *J. Biol. Chem.*, vol. 243, no. 12, pp. 3553–3555, Jun. 1968.

[115] R. J. COLLIER and A. M. PAPPENHEIMER, "Studies on the Mode of Action of Diphtheria Toxin. Ii. Effect of Toxin on Amino Acid Incorporation in Cell-Free Systems.," *J. Exp. Med.*, vol. 120, no. 6, pp. 1019–1039, Dec. 1964, doi: 10.1084/jem.120.6.1019.

[116] R. J. Collier, "Effect of diphtheria toxin on protein synthesis: Inactivation of one of the transfer factors," *J. Mol. Biol.*, vol. 25, no. 1, pp. 83–98, Apr. 1967, doi: 10.1016/0022-2836(67)90280-X.

[117] P. Chambon, J. D. Weill, and P. Mandel, "Nicotinamide mononucleotide activation of a new DNA-dependent polyadenylic acid synthesizing nuclear enzyme," *Biochem. Biophys. Res. Commun.*, vol. 11, no. 1, pp. 39–43, 1963, doi: 10.1016/0006-291X(63)90024-X.

[118] M. O. Hottiger, P. O. Hassa, B. Lüscher, H. Schüler, and F. Koch-Nolte, "Toward a unified nomenclature for mammalian ADP-ribosyltransferases," *Trends Biochem. Sci.*, vol. 35, no. 4, pp. 208–219, Apr. 2010, doi: 10.1016/j.tibs.2009.12.003.

[119] W. H. Hou, S. H. Chen, and X. Yu, "Poly-ADP ribosylation in DNA damage response and cancer therapy," *Mutat. Res. - Rev. Mutat. Res.*, vol. 780, pp. 82–91, 2019, doi: 10.1016/j.mrrev.2017.09.004.

[120] D. Perina, A. Mikoč, J. Ahel, H. Ćetković, R. Žaja, and I. Ahel, “Distribution of protein poly(ADP-ribosyl)ation systems across all domains of life,” *DNA Repair (Amst).*, vol. 23, pp. 4–16, Nov. 2014, doi: 10.1016/j.dnarep.2014.05.003.

[121] M. Faraone Mennella, “The Dichotomy of the Poly(ADP-Ribose) Polymerase-Like Thermozyme from Sulfolobus solfataricus,” *Challenges*, vol. 9, no. 1, p. 5, 2018, doi: 10.3390/challe9010005.

[122] M. Citarelli, S. Teotia, and R. S. Lamb, “Evolutionary history of the poly(ADP-ribose) polymerase gene family in eukaryotes,” *BMC Evol. Biol.*, vol. 10, no. 1, p. 308, 2010, doi: 10.1186/1471-2148-10-308.

[123] B. A. Gibson and W. L. Kraus, “New insights into the molecular and cellular functions of poly(ADP-ribose) and PARPs,” *Nat. Rev. Mol. Cell Biol.*, vol. 13, no. 7, pp. 411–424, Jun. 2012, doi: 10.1038/nrm3376.

[124] C. Beck, I. Robert, B. Reina-San-Martin, V. Schreiber, and F. Dantzer, “Poly(ADP-ribose) polymerases in double-strand break repair: Focus on PARP1, PARP2 and PARP3,” *Exp. Cell Res.*, vol. 329, no. 1, pp. 18–25, Nov. 2014, doi: 10.1016/j.yexcr.2014.07.003.

[125] M. S. Cohen and P. Chang, “Insights into the biogenesis, function, and regulation of ADP-ribosylation,” *Nat. Chem. Biol.*, vol. 14, no. 3, pp. 236–243, Feb. 2018, doi: 10.1038/nchembio.2568.

[126] E. E. Alemasova and O. I. Lavrik, “Poly(ADP-ribosyl)ation by PARP1: Reaction mechanism and regulatory proteins,” *Nucleic Acids Res.*, vol. 47, no. 8, pp. 3811–3827, 2019, doi: 10.1093/nar/gkz120.

[127] M. Y. Kim, T. Zhang, and W. L. Kraus, “Poly(ADP-ribosyl)ation by PARP-1: ‘PAR-laying’ NAD^+ into a nuclear signal,” *Genes Dev.*, vol. 19, no. 17, pp. 1951–1967, 2005, doi: 10.1101/gad.1331805.

[128] S. ichi Tanuma, Y. Shibui, T. Oyama, F. Uchiumi, and H. Abe, “Targeting poly(ADP-ribose) glycohydrolase to draw apoptosis codes in cancer,” *Biochem. Pharmacol.*, vol. 167, no. April, pp. 163–172, 2019, doi: 10.1016/j.bcp.2019.06.004.

[129] M. F. Langelier, J. L. Planck, S. Roy, and J. M. Pascal, “Structural basis for DNA damage-dependent poly(ADP-ribosyl)ation by human PARP-1,” *Science (80-.).*, vol. 336, no. 6082, pp. 728–732, 2012, doi: 10.1126/science.1216338.

[130] M. F. Langelier, J. L. Planck, S. Roy, and J. M. Pascal, “Crystal structures of poly(ADP-ribose) polymerase-1 (PARP-1) zinc fingers bound to DNA: Structural and functional insights into DNA-dependent PARP-1 activity,” *J. Biol. Chem.*, vol. 286, no. 12, pp. 10690–10701, Mar. 2011, doi: 10.1074/jbc.M110.202507.

[131] M. F. Langelier, K. M. Servent, E. E. Rogers, and J. M. Pascal, “A third zinc-binding domain of human poly(ADP-ribose) polymerase-1 coordinates DNA-dependent enzyme activation,” *J. Biol. Chem.*, vol.

283, no. 7, pp. 4105–4114, 2008, doi: 10.1074/jbc.M708558200.

[132] M. F. Langelier, D. D. Ruhl, J. L. Planck, W. L. Kraus, and J. M. Pascal, “The Zn3 domain of human poly(ADP-ribose) polymerase-1 (PARP-1) functions in both DNA-dependent poly(ADP-ribose) synthesis activity and chromatin compaction,” *J. Biol. Chem.*, vol. 285, no. 24, pp. 18877–18887, 2010, doi: 10.1074/jbc.M110.105668.

[133] D. D’Amours, S. Desnoyers, I. D’Silva, and G. G. Poirier, “Poly(ADP-ribosyl)ation reactions in the regulation of nuclear functions,” *Biochem. J.*, vol. 342, no. 2, pp. 249–268, Sep. 1999, doi: 10.1042/0264-6021:3420249.

[134] J. Rudolph, J. Mahadevan, P. Dyer, and K. Luger, “Poly(ADP-ribose) polymerase 1 searches DNA via a ‘monkey bar’ mechanism,” *Elife*, vol. 7, p. e37818, Aug. 2018, doi: 10.7554/eLife.37818.

[135] M. F. Langelier, L. Zandarashvili, P. M. Aguiar, B. E. Black, and J. M. Pascal, “NAD^+ analog reveals PARP-1 substrate-blocking mechanism and allosteric communication from catalytic center to DNA-binding domains,” *Nat. Commun.*, vol. 9, no. 1, p. 844, Feb. 2018, doi: 10.1038/s41467-018-03234-8.

[136] S. Eustermann *et al.*, “Structural Basis of Detection and Signaling of DNA Single-Strand Breaks by Human PARP-1,” *Mol. Cell*, vol. 60, no. 5, pp. 742–754, Dec. 2015, doi: 10.1016/j.molcel.2015.10.032.

[137] J. M. Pascal, “The comings and goings of PARP-1 in response to DNA damage,” *DNA Repair (Amst).*, vol. 71, no. August, pp. 177–182, 2018, doi: 10.1016/j.dnarep.2018.08.022.

[138] H. Wei and X. Yu, “Functions of PARylation in DNA Damage Repair Pathways,” *Genomics, Proteomics Bioinforma.*, vol. 14, no. 3, pp. 131–139, Jun. 2016, doi: 10.1016/j.gpb.2016.05.001.

[139] N. Noren Hooten, K. Kompaniez, J. Barnes, A. Lohani, and M. K. Evans, “Poly(ADP-ribose) polymerase 1 (PARP-1) binds to 8-oxoguanine-DNA glycosylase (OGG1),” *J. Biol. Chem.*, vol. 286, no. 52, pp. 44679–44690, 2011, doi: 10.1074/jbc.M111.255869.

[140] A. Ray Chaudhuri and A. Nussenzweig, “The multifaceted roles of PARP1 in DNA repair and chromatin remodelling,” *Nat. Rev. Mol. Cell Biol.*, vol. 18, no. 10, pp. 610–621, Oct. 2017, doi: 10.1038/nrm.2017.53.

[141] E. Matveeva *et al.*, “Involvement of PARP1 in the regulation of alternative splicing,” *Cell Discov.*, vol. 2, p. 15046, 2016, doi: 10.1038/celldisc.2015.46.

[142] D. C. Di Giammartino, Y. Shi, and J. L. Manley, “PARP1 Represses PAP and Inhibits Polyadenylation during Heat Shock,” *Mol. Cell*, vol. 49, no. 1, pp. 7–17, Jan. 2013, doi: 10.1016/j.molcel.2012.11.005.

[143] J. M. Rodríguez-Vargas *et al.*, “Autophagy requires poly(adp-ribosyl)ation-dependent AMPK nuclear export,” *Cell Death Differ.*, vol. 23, no. 12, pp. 2007–2018, Dec. 2016, doi: 10.1038/cdd.2016.80.

[144] S. N. Chand *et al.*, "Posttranscriptional regulation of PARG mRNA by HuR facilitates DNA repair and resistance to PARP inhibitors," *Cancer Res.*, vol. 77, no. 18, pp. 5011–5025, Sep. 2017, doi: 10.1158/0008-5472.CAN-16-2704.

[145] P. O. Hassa, M. Covic, M. T. Bedford, and M. O. Hottiger, "Protein Arginine Methyltransferase 1 Coactivates NF-κB-Dependent Gene Expression Synergistically with CARM1 and PARP1," *J. Mol. Biol.*, vol. 377, no. 3, pp. 668–678, Mar. 2008, doi: 10.1016/j.jmb.2008.01.044.

[146] D. Hanahan and R. A. Weinberg, "Hallmarks of cancer: The next generation," *Cell*, vol. 144, no. 5, pp. 646–674, Mar. 2011, doi: 10.1016/j.cell.2011.02.013.

[147] N. V. Malyuchenko, E. Y. Kotova, O. I. Kulaeva, M. P. Kirpichnikov, and V. M. Studitskiy, "PARP1 Inhibitors: Antitumor drug design," *Acta Naturae*, vol. 7, no. 3, pp. 27–37, 2015, doi: 10.32607/20758251-2015-7-3-27-37.

[148] A. D. D'Andrea, "Mechanisms of PARP inhibitor sensitivity and resistance," *DNA Repair (Amst).*, vol. 71, pp. 172–176, 2018, doi: 10.1016/j.dnarep.2018.08.021.

[149] E. Sachdev, R. Tabatabai, V. Roy, B. J. Rimel, and M. M. Mita, "PARP Inhibition in Cancer: An Update on Clinical Development," *Target. Oncol.*, vol. 14, no. 6, pp. 657–679, 2019, doi: 10.1007/s11523-019-00680-2.

[150] W. L. Kraus and J. T. Lis, "PARP goes transcription," *Cell*, vol. 113, no. 6, pp. 677–683, Jun. 2003, doi: 10.1016/S0092-8674(03)00433-1.

[151] M. A. Babaei, B. Kamalidehghan, M. Saleem, H. Z. Huri, and F. Ahmadipour, "Receptor tyrosine kinase (c-Kit) inhibitors: A potential therapeutic target in cancer cells," *Drug Des. Devel. Ther.*, vol. 10, pp. 2443–2459, Aug. 2016, doi: 10.2147/DDDT.S89114.

[152] C. Bellio *et al.*, "PARP inhibition induces enrichment of DNA repair-proficient CD133 and CD117 positive ovarian cancer stem cells," *Mol. Cancer Res.*, vol. 17, no. 2, pp. 431–445, Feb. 2019, doi: 10.1158/1541-7786.MCR-18-0594.

[153] M. Nieborowska-Skorska *et al.*, "Inhibition of the mutated c-KIT kinase in AML1-ETO–positive leukemia cells restores sensitivity to PARP inhibitor," *Blood Adv.*, vol. 3, no. 23, pp. 4050–4054, Dec. 2019, doi: 10.1182/bloodadvances.2019000756.

[154] V. A. Soldatenkov, A. A. Vetcher, T. Duka, and S. Ladame, "First evidence of a functional interaction between DNA quadruplexes and poly(ADP-ribose) polymerase-1," *ACS Chem. Biol.*, vol. 3, no. 4, pp. 214–219, 2008, doi: 10.1021/cb700234f.

[155] Y. Xu, L. Liu, Z. Wang, and Z. Dai, "Stable and Reusable Electrochemical Biosensor for Poly(ADP-ribose)

Polymerase and Its Inhibitor Based on Enzyme-Initiated Auto-PARylation," *ACS Appl. Mater. Interfaces*, vol. 8, no. 29, pp. 18669–18674, 2016, doi: 10.1021/acsami.6b01883.

[156] Z. Wang, L. Liu, Y. Xu, L. Sun, and G. Li, "Simulation and assay of protein biotinylation with electrochemical technique," *Biosens. Bioelectron.*, vol. 26, no. 11, pp. 4610–4613, 2011, doi: 10.1016/j.bios.2011.04.052.

[157] D. M. Miller, S. D. Thomas, A. Islam, D. Muench, and K. Sedoris, "c-Myc and cancer metabolism," *Clin. Cancer Res.*, vol. 18, no. 20, pp. 5546–5553, Oct. 2012, doi: 10.1158/1078-0432.CCR-12-0977.

[158] J. P. W. Carey *et al.*, "Synthetic lethality of PARP inhibitors in combination with MYC blockade is independent of BRCA status in triple-negative breast cancer," *Cancer Res.*, vol. 78, no. 3, pp. 742–757, Feb. 2018, doi: 10.1158/0008-5472.CAN-17-1494.

[159] J. F. Ning *et al.*, "Myc targeted CDK18 promotes ATR and homologous recombination to mediate PARP inhibitor resistance in glioblastoma," *Nat. Commun.*, vol. 10, no. 1, p. 2910, Jul. 2019, doi: 10.1038/s41467-019-10993-5.

[160] M. Mann *et al.*, "PARP-1 inhibitor modulate β-catenin signaling to enhance cisplatin sensitivity in cancer cervix," *Oncotarget*, vol. 10, no. 42, pp. 4262–4275, Jul. 2019, doi: 10.18632/oncotarget.27008.

[161] C. Mostocotto, M. Carbone, C. Battistelli, A. Ciotti, P. Amati, and R. Maione, "Poly(ADP-Ribosyl)ation is required to modulate chromatin changes at c-MYC promoter during emergence from quiescence," *PLoS One*, vol. 9, no. 7, pp. e102575–e102575, Jul. 2014, doi: 10.1371/journal.pone.0102575.

[162] A. Fekete *et al.*, "The guanine-quadruplex structure in the human c-myc gene's promoter is converted into B-DNA form by the human poly(ADP-ribose)polymerase-1," *PLoS One*, vol. 7, no. 8, pp. 19–22, 2012, doi: 10.1371/journal.pone.0042690.

[163] K. C. Sedoris *et al.*, "Genomic c-Myc quadruplex DNA selectively kills leukemia," *Mol. Cancer Ther.*, vol. 11, no. 1, pp. 66–76, Jan. 2012, doi: 10.1158/1535-7163.MCT-11-0515.

[164] R. V. Brown, F. L. Danford, V. Gokhale, L. H. Hurley, and T. A. Brooks, "Demonstration that drug-targeted down-regulation of MYC in non-Hodgkins lymphoma is directly mediated through the promoter G-quadruplex," *J. Biol. Chem.*, vol. 286, no. 47, pp. 41018–41027, Nov. 2011, doi: 10.1074/jbc.M111.274720.

[165] D. Sun and L. H. Hurley, "The importance of negative superhelicity in inducing the formation of G-quadruplex and i-motif structures in the c-Myc promoter: Implications for drug targeting and control of gene expression," *J. Med. Chem.*, vol. 52, no. 9, pp. 2863–2874, May 2009, doi: 10.1021/jm900055s.

[166] K. Cleal, K. Norris, and D. Baird, "Telomere length dynamics and the evolution of cancer genome

architecture," *International Journal of Molecular Sciences*, vol. 19, no. 2. 2018, doi: 10.3390/ijms19020482.

[167] S. Schoeftner and M. A. Blasco, "Developmentally regulated transcription of mammalian telomeres by DNA-dependent RNA polymerase II," *Nat. Cell Biol.*, vol. 10, no. 2, pp. 228–236, 2008, doi: 10.1038/ncb1685.

[168] J. Maciejowski and T. De Lange, "Telomeres in cancer: Tumour suppression and genome instability," *Nat. Rev. Mol. Cell Biol.*, vol. 18, no. 3, pp. 175–186, 2017, doi: 10.1038/nrm.2016.171.

[169] I. Schmutz and T. De Lange, "Shelterin," *Curr. Biol.*, vol. 26, no. 10, pp. R397–R399, May 2016, doi: 10.1016/j.cub.2016.01.056.

[170] K. Okamoto and H. Seimiya, "Revisiting Telomere Shortening in Cancer," *Cells*, vol. 8, no. 2. p. 107, 2019, doi: 10.3390/cells8020107.

[171] F. P. Barthel *et al.*, "Systematic analysis of telomere length and somatic alterations in 31 cancer types," *Nat. Genet.*, vol. 49, no. 3, pp. 349–357, 2017, doi: 10.1038/ng.3781.

[172] H. Seimiya, "The telomeric PARP, tankyrases, as targets for cancer therapy," *Br. J. Cancer*, vol. 94, no. 3, pp. 341–345, Feb. 2006, doi: 10.1038/sj.bjc.6602951.

[173] G. Ngo *et al.*, "PARP inhibition prevents escape from a telomere-driven crisis and inhibits cell immortalisation," *Oncotarget*, vol. 9, no. 101, pp. 37549–37563, Dec. 2018, doi: 10.18632/oncotarget.26499.

[174] F. D. A. Di Fagagna, M. P. Hande, W. M. Tong, P. M. Lansdorp, Z. Q. Wang, and S. P. Jackson, "Functions of poly(ADP-ribose) polymerase in controlling telomere length and chromosomal stability," *Nat. Genet.*, vol. 23, no. 1, pp. 76–80, 1999, doi: 10.1038/12680.

[175] F. Dantzer *et al.*, "Functional Interaction between Poly(ADP-Ribose) Polymerase 2 (PARP-2) and TRF2: PARP Activity Negatively Regulates TRF2," *Mol. Cell. Biol.*, vol. 24, no. 4, pp. 1595–1607, Feb. 2004, doi: 10.1128/mcb.24.4.1595-1607.2004.

[176] S. A. Juranek and K. Paeschke, "Cell Cycle Regulation of G-Quadruplex DNA Structures at Telomeres," *Current Pharmaceutical Design*, vol. 18, no. 14. pp. 1867–1872, 2012, doi: 10.2174/138161212799958404.

[177] S. Gilbert-Girard *et al.*, "Stabilization of Telomere G-Quadruplexes Interferes with Human Herpesvirus 6A Chromosomal Integration," *J. Virol.*, vol. 91, no. 14, pp. e00402-17, Jul. 2017, doi: 10.1128/jvi.00402-17.

[178] A. J. Zaug, E. R. Podell, and T. R. Cech, "Human POT1 disrupts telomeric G-quadruplexes allowing

telomerase extension in vitro," *Proc. Natl. Acad. Sci. U. S. A.*, vol. 102, no. 31, pp. 10864–10869, Aug. 2005, doi: 10.1073/pnas.0504744102.

[179] M. Ghosh and M. Singh, "RGG-box in hnRNPA1 specifically recognizes the telomere G-quadruplex DNA and enhances the G-quadruplex unfolding ability of UP1 domain," *Nucleic Acids Res.*, vol. 46, no. 19, pp. 10246–10261, 2018, doi: 10.1093/nar/gky854.

[180] H. Izumi and K. Funa, "Telomere Function and the G-Quadruplex Formation are Regulated by hnRNP U," *Cells*, vol. 8, no. 5, p. 390, Apr. 2019, doi: 10.3390/cells8050390.

[181] J. Amato *et al.*, "Insights into telomeric G-quadruplex DNA recognition by HMGB1 protein," *Nucleic Acids Res.*, vol. 47, no. 18, pp. 9950–9966, Oct. 2019, doi: 10.1093/nar/gkz727.

[182] S. Arena *et al.*, "A subset of colorectal cancers with cross-sensitivity to olaparib and oxaliplatin," *Clin. Cancer Res.*, vol. 26, no. 6, pp. 1372–1384, Mar. 2020, doi: 10.1158/1078-0432.CCR-19-2409.

[183] P. P. Vitiello *et al.*, "Combination treatment with the PARP inhibitor niraparib and chemotherapeutics in a preclinical model of KRAS/BRAF mutated colorectal cancer cell lines across the four consensus molecular subtypes," *Ann. Oncol.*, vol. 29, no. suppl_8, p. viii5, Oct. 2018, doi: 10.1093/annonc/mdy268.017.

[184] L. A. Parsels *et al.*, "PARP1 Trapping and DNA Replication Stress Enhance Radiosensitization with Combined WEE1 and PARP Inhibitors," *Mol. Cancer Res.*, vol. 16, no. 2, pp. 222–232, Feb. 2018, doi: 10.1158/1541-7786.MCR-17-0455.

[185] S. Cogoi, M. Paramasivam, B. Spolaore, and L. E. Xodo, "Structural polymorphism within a regulatory element of the human KRAS promoter: Formation of G4-DNA recognized by nuclear proteins," *Nucleic Acids Res.*, vol. 36, no. 11, pp. 3765–3780, Jun. 2008, doi: 10.1093/nar/gkn120.

[186] S. Cogoi, M. Paramasivam, A. Membrino, K. K. Yokoyama, and L. E. Xodo, "The KRAS promoter responds to Myc-associated zinc finger and poly(ADP-ribose) polymerase 1 proteins, which recognize a critical quadruplex-forming GA-element," *J. Biol. Chem.*, vol. 285, no. 29, pp. 22003–22016, 2010, doi: 10.1074/jbc.M110.101923.

[187] N. Nalabothula *et al.*, "Genome-wide profiling of PARP1 reveals an interplay with gene regulatory regions and DNA methylation," *PLoS One*, vol. 10, no. 8, p. e0135410, Aug. 2015, doi: 10.1371/journal.pone.0135410.

[188] N. S. Benabdallah *et al.*, "Decreased Enhancer-Promoter Proximity Accompanying Enhancer Activation," *Mol. Cell*, vol. 76, no. 3, pp. 473-484.e7, 2019, doi: 10.1016/j.molcel.2019.07.038.

[189] S. J. Roper *et al.*, "ADP-ribosyltransferases Parp1 and Parp7 safeguard pluripotency of ES cells," *Nucleic*

Acids Res., vol. 42, no. 14, pp. 8914–8927, Jul. 2014, doi: 10.1093/nar/gku591.

[190] G. Cinque, A. Ferino, E. B. Pedersen, and L. E. Xodo, "Role of Poly [ADP-ribose] Polymerase 1 in Activating the Kirsten ras (KRAS) Gene in Response to Oxidative Stress.," *Int. J. Mol. Sci.*, vol. 21, no. 17, Aug. 2020, doi: 10.3390/ijms21176237.

[191] M. Rose, J. T. Burgess, K. O'Byrne, D. J. Richard, and E. Bolderson, "PARP Inhibitors: Clinical Relevance, Mechanisms of Action and Tumor Resistance," *Frontiers in Cell and Developmental Biology*, vol. 8. p. 879, 2020, doi: 10.3389/fcell.2020.564601.

11 Acknowledgments

Firstly, I would like to express my deepest gratitude to my supervisor, professor Luigi E. Xodo, who drove me into this period with his knowledge and helped me throughout these years to implement my formation as a mature PhD student.

Beside my tutor, I'd like to thank professor Valentina Rapozzi for her contribute that supported me under both a scientific and a human point of view.

A sincere thank goes to the colleagues I met in this 3-year period, especially PhD Annalisa Ferino, who proved herself not only as a valuable scientist and a dependable colleague, but also a trusted friend I could rely on especially during the most difficult moments. My thankfulness goes also to Giulia Nicoletto, a person I had the privilege to share with not only our mutual love for science but also an impressive number of interests. I would like to express a great encouragement to Himanshi with the hope that she will always manage to find the best way out of all the challenges and the difficulties.

My thought goes to PhD Susanna Cogoi who left us so soon. I've known her for little, but the first impression I had was her to be a woman with an incredible strength within who put an immense passion on everything she did. I feel I missed the opportunity to know an extraordinary and talented person.

Lastly, PhD period turned out to be also a great opportunity to meet and know closer splendid companions I shared this adventure with. For this and more, I would like to thank all of you from the deep of my heart, with the promise that we'll see back again!